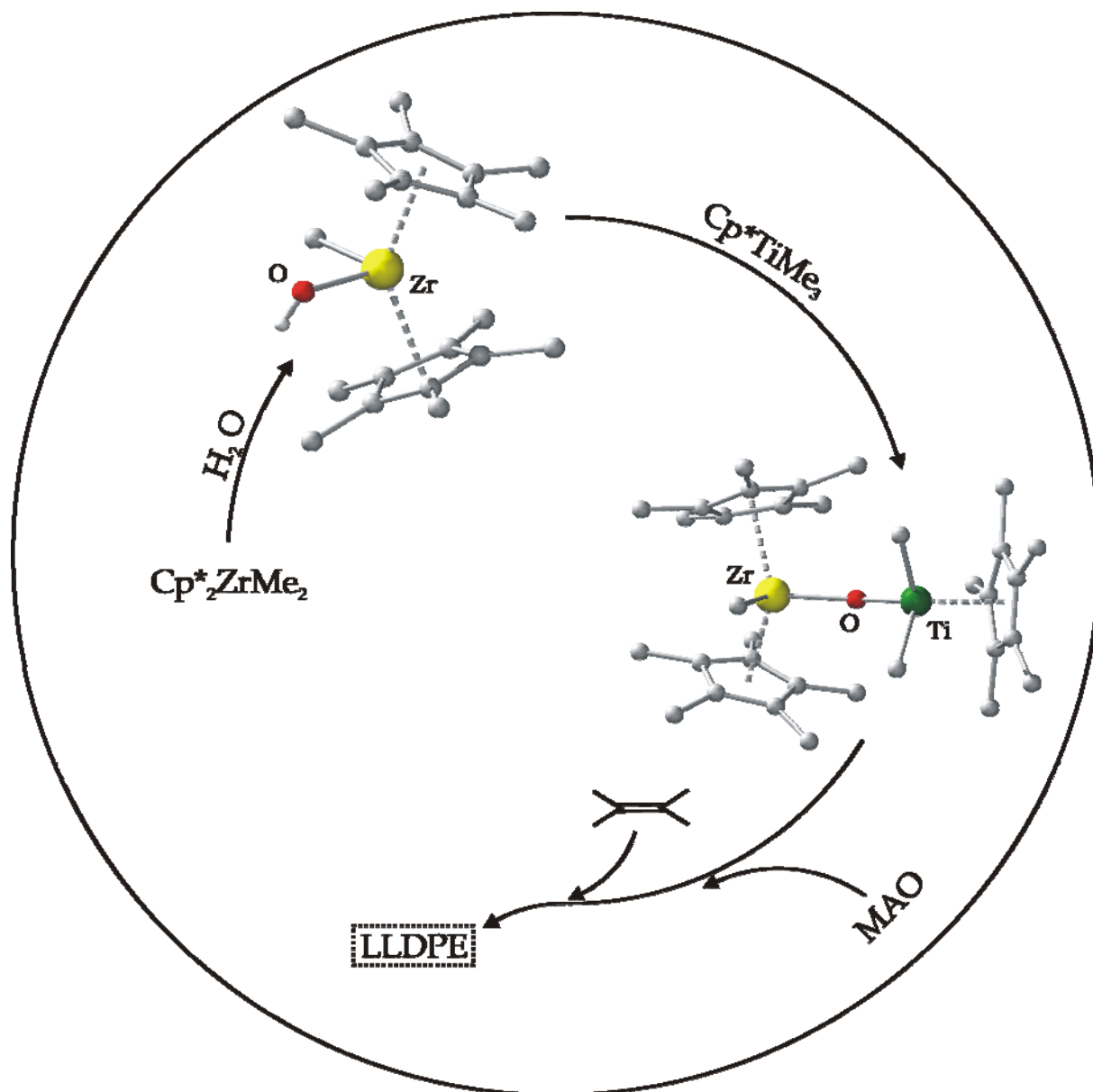**Prabhuodeyara Matada Gurubasavaraj**

Synthesis and X-ray Structural Characterization of Oxygen Bridged Complexes for Olefin Polymerization: A Theoretical Interpretation of Structure and Activity Relationship

Göttingen 2007

Synthesis and X-ray Structural Characterization of Oxygen Bridged Complexes for Olefin Polymerization: A Theoretical Interpretation of Structure and Activity Relationship

Dissertation

zur Erlangung des Doktorgrades

der Mathematisch-Naturwissenschaftlichen Fakultäten

der Georg-August-Universität zu Göttingen

vorgelegt von

Prabhuodeyara Matada Gurubasavaraj

aus Kottur

(INDIA)

Göttingen 2007

D 7

Referent: Prof. Dr. Dr. h.c. mult. Herbert W. Roesky
Koreferent: Prof. Dr. Dietmar Stalke

Tag der mündlichem Prüfung:

Dedicated to my parents
For their love and affection

Acknowledgement

The work described in this doctoral thesis has been carried out under the guidance and supervision of Professor Dr. Dr. h.c. mult. Herbert W. Roesky at the Institute of Inorganic Chemistry of the Georg-August-Universität Göttingen between May 2004 and August 2007.

My sincere thanks and gratitude are due to

Prof. Dr. Dr. h.c. mult. Herbert W. Roesky

for his constant guidance, motivation, suggestions, and discussions throughout this work.

My sincere thanks to Dr. Rainer Oswald for his help in DFT calculation studies. I would like to express my special thanks to Dr. Swadhin K. Mandal, Radoslaw Kaminski, Dr. S. Nagendran, Ying Yang, for numerous fruitful discussions and their help during this work.

I take this opportunity to sincerely thank my former supervisor, Prof. A. Venkataraman, for his constant motivation throughout my studies.

I thank Aritra Pal, Prof. Dietmar Stalke, G. Schwab, and Dr. Regine Herbst-Irmer for their help in the X-ray crystal structural investigations and refinement of disordered molecules and twinned crystals. I thank Mr. W. Zolke, Mr. R. Schöne and Dr. M. John (NMR spectra), Dr. D. Böhler, Mr. T. Schuchardt and Mr. J. Schöne (mass spectra), Mr. M. Hesse (IR spectra), Mr. J. Schimkowiak, Mr. M. Schlote and the staff of the Analytical Laboratories and Werkstatt for their timely support during this research work. My special thanks to Frau K. Gehrke and Dr. V. Dolle (Basell R&D, Frankfurt) for their help in performing and analyzing DSC and GPC measurements.

I would like to thank the Göttinger Akademie der Wissenschaften, Deutsche Forschungsgemeinschaft and the Fonds der Chemischen Industrie for their financial support which I was receiving during my PhD studies.

I thank all my colleagues in our research lab for the good and motivating working atmosphere. I would like to express my special thanks to Dr. L. W. P. Cedeño, Dr. V. Jancik,

Abbreviations

δ	chemical shift
λ	wavelength
μ	bridging
ν	wave number
A	activity
Ar	aryl
atm	atmoshphere
av	average
br	broad
*t*Bu	*tert*-butyl
C	Celsius
calcd.	calculated
Cp	cyclopentadienyl
Cp*	pentamethly cyclopentadienyl
d	doublet
decomp.	decomposition
DFT	density functional theory
DSC	differential Scanning Calorimetry
EI	electron impact ionization
Et	ethyl
eqivs.	equivalents
eV	electron volt
g	grams
GPC	gel permeation chromatography
HOMO	highest occupied molecular orbital

Hz   Hertz

*i*Pr   isopropyl

IR   infrared

J   coupling constant

K   Kelvin

L   ligand

LPE   linear polyethylene

LUMO   lowest unoccupied molecular orbital

M   metal

m   multiplet

MAO   methylaluminoxane

m/*z*   mass/charge

M.p.   melting point

M^+ molecular ion

Me   methyl

min.   minutes

MS   mass spectrometry, mass spectra

NMR   nuclear magnetic resonance

PE   polyethylene

Ph   phenyl

ppm   parts per million

PS   polystyrene

q   quartet

R, R', R''   organic substituent

s   singlet

sept   septet

t   triplet

T_g glass transition temperature of polymers

THF   tetrahydrofuran

T_m melting points of polymers

TMS   tetramethylsilane

UV   ultraviolet

V   volume

Z   number of molecules in the unit cell

1. Introduction

1.1. Heterobi- and Heterotrimetallic Oxygen Bridged Complexes as Polymerization Catalysts

Transition metal oxides, which are used as polyfunctional catalysts and precursors for the preparation of bi- and trimetallic heterogeneous catalysts, have been the topic of various academic and industrial studies,[1] since the discovery of the catalytic olefin polymerization by Ziegler and Natta. These oxides can also act as catalysts themselves and can serve as models for the catalyst-substrate interaction.[2-5] In this context, the study of transition metal oxides is not only an attractive subject of academic research but also relevant to the applied aspects of their chemistry. The immense research interest in this field of organometallic oxides is initiated by the remarkable properties of methylaluminoxane (MAO) as activator for metallocene catalysts in olefin polymerization[6,7] and the valuable catalytic properties of organorhenium oxides.[8]

The main disadvantage of these heterogeneous transition metal oxides is that they have complicated structural features and are insoluble in solvents advantageous for polymerization reactions. Investigations by Sinn and Kaminsky[9] revealed that soluble metallocene catalysts in combination with methylaluminoxane achieve extremely high activities in the polymerization of olefins leading to the new developments in this field. These investigations are accompanied by an increased understanding of the factors that are important for stabilizing polymerization-active metal centers and controlling their activity and selectivity. The design and synthesis of new transition metal precursors and main group organometallic cocatalysts is a very important subject which can provide high catalytic activity with low cocatalyst to catalyst precursor ratio and allows unprecedented control over the polymer microstructure generating new polymers with improved properties. The well-defined single-site metallocene catalysts are slowly replacing the conventional heterogeneous Ziegler-Natta catalysts.

Polymerization of olefins catalyzed by soluble, well-defined transition metal complexes has been one of the most attractive subjects in organometallic chemistry.[10-25] Particularly, there has been immense interest in the synthesis of multinuclear complexes for olefin polymerization which exhibit cooperative effects between their active metal centers. For example Marks *et al.*[26] reported that the binuclear compounds exhibit higher catalytic activity than the mononuclear complexes. Another approach for olefin polymerization is using "tandem catalysis".[27-38] In this type of catalysis, two separate single site olefin polymerization catalysts of zirconium and later transition metals were used in the same system to catalyze the polymerization reaction. The first single site catalytic center produces oligomers, which are subsequently incorporated into high molecular weight polymers by the second metallic center. Since this type of polymerization requires intermolecular processes, it was speculated that the spatial proximity between two metallic centers might perform such functions more efficiently.[26] For single site olefin polymerization catalysts two connectivity strategies (electrostatic and covalent) have been pursued to achieve cooperative effects via multinuclear complexes.[39] It was assumed that the dicationic bimetallic framework exhibits enhanced comonomer binding affinity. Therefore the attractive possibility of bringing two catalytic centers in close constrained proximity offers the potential for significantly enhanced catalytic efficiency. Stereoregularity and molecular weight of the polymers can be controlled by changing the environment on the ligand surrounding the metal centers (e.g. by introducing the bulky substituents on the Cp ring or by an intraanular bridge) which in turn leads to the different specifications of the active species.[40] There are some examples of olefin polymerization known, using heterobimetallic complexes where bis(cyclopentadienyl) M (M = Zr, Hf) moieties are connected to other transition metals via cyclopentadienyl,[41] phosphido,[42] nitrogen ligands,[43] and some alkoxide groups[44] (Chart 1). However, significant enhancement in catalytic activity has rarely been observed even at high temperatures and pressure. Recently H. W. Roesky *et al.* reported a class of oxygen bridged heterobimetallic

complexes containing Al–O–M moiety (M = Zr, Ti, Hf) which are highly active in olefin polymerization.[45]
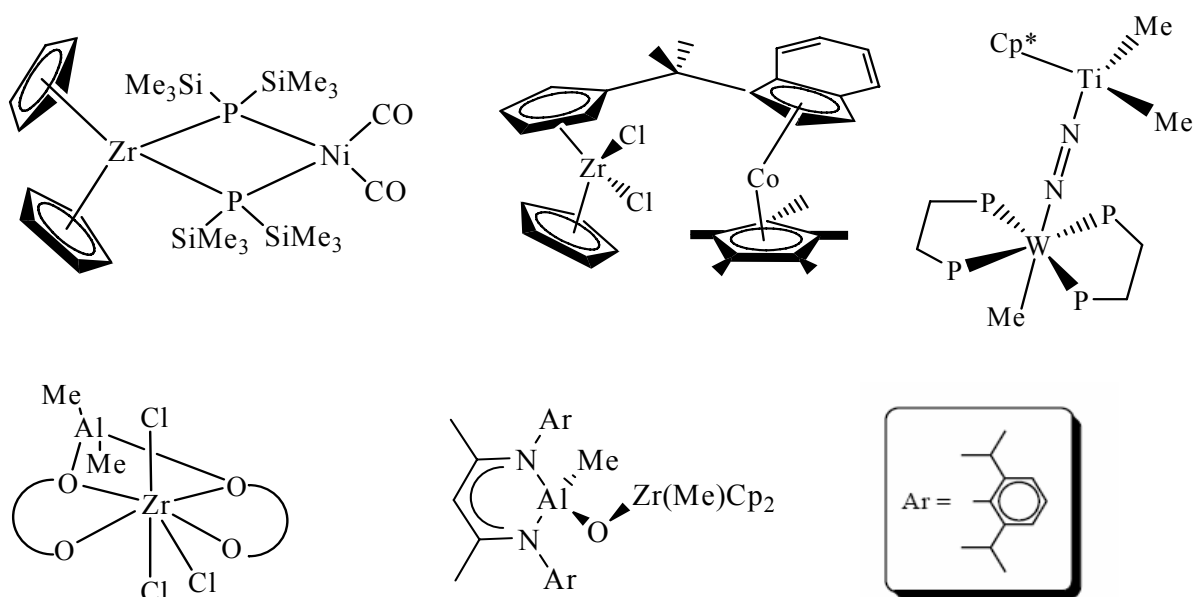
Chart 1. Some bridged heterobimetallic complexes.

The oxide bridged complexes prepared by H. W. Roesky *et al.* were rationally prepared by using the metal-hydroxide precursors.[46,47]

1.2. Metal Hydroxides

The study on hydroxo complexes of transition metals is one of the most challenging fields in chemistry because these complexes have been postulated as critical intermediates in a number of catalytic reactions involving water as a substrate.[48-55] These hydroxo-complexes can be used as the building blocks for the bi- or trimetallic complexes which can find application in catalysts, cocatalysts and models for fixation of the catalysts on oxide surfaces.[56-59]

Recently, H. W. Roesky *et al.* have successfully synthesized several unique molecular hydroxides bearing β-diketiminato ligands e.g. on aluminum (LMeAl(OH),[45] LAl(OH)$_2$,[60] and

[LAl(OH)]$_2$O)[61]) and gallium (LMeGa(OH),[46] and LGa(OH)$_2$ [62]) or germanium (LGe(OH)[63]) (Chart 2).
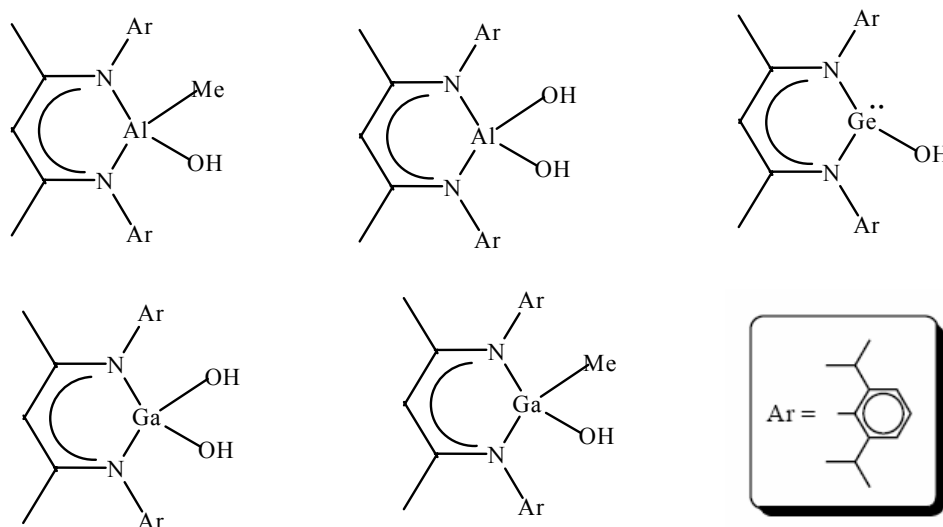
Chart 2. Some β-diketiminato ligands based metal hydroxides prepared by H. W. Roesky *et al.*

Using these unprecedented hydroxide precursors H. W. Roesky *et al.* reported a series of bimetallic complexes[46,47] and some of them were tested as catalysts for the polymerization reactions. These oxygen bridged bimetallic complexes exhibit high activity in presence of cocatalysts to give polymer with tunable microstructure.[45]

1.3. Cocatalysts

1.3.1. Trialkylaluminum

Aluminum alkyls, including trialkylaluminum and alkylaluminum chlorides, are important components in classical heterogeneous Ziegler-Natta coordination polymerization catalysis.[64,65] A wide variety of homogeneous Ziegler-Natta catalysts based on aluminum alkyls as cocatalysts were also reported in the early literature for the polymerization of

olefins.[66,67] Although as the temperature of the polymerization increases, the polymerization becomes nonstereospecific in these systems, they can be used to prepare a variety of homo, block, random, and alternating polyolefins. Cr- and Ni- based homogeneous catalysts,[68,69] when activated by aluminum alkyls, are also known as diene polymerization and ethylene oligomerization catalysts, respectively. The Ti- or Zr- based metallocene/alkylaluminum catalysts usually exhibit low-to-medium activities for ethylene polymerization,[70] and only for ethylene, narrow product molecular weight distributions. This is because of rapid catalyst deactivation leading to the formation of an inactive species, presumably due to side reactions such as alkyl exchange and H-exchange, as well as reduction to lower Ti oxidation states.[7,71] Overall, the inability of metallocenes activated by alkylaluminum halides to polymerize propylene and higher α-olefins has limited their utility in this field. A number of attempts were made to improve the performance of these catalyst systems.[72]

By addition of water to the halogen-free, polymerization-inactive Cp_2ZrMe_2/$AlMe_3$ system, Sinn and Kaminsky observed a surprisingly high activity for ethylene polymerization, which led to the discovery of a highly efficient activator, an oligomeric methylaluminoxane (MAO).[73] This discovery, a result of research efforts seeking more effective cocatalysts, rejuvenated Ziegler-Natta catalysis.[74] The major advances achieved in controlling polymer stereochemistry and architecture began the metallocene and single-site polymerization catalysis era.[75-80]

1.3.2. Methylaluminoxane (MAO)

Alkylaluminoxanes, oligomeric compounds consisting of -Al(R)-O- subunits, have been known to be active for the polymerization of monomers such as oxiranes since the early 1960s.[81] Methylaluminoxane [-Al(Me)-O-]$_n$ (MAO), prepared by controlled hydrolysis of $AlMe_3$ and typically having $n \approx$ 5-20, affords highly active catalysts for polymerizing ethylene, propylene, and higher α-olefins when combined with group 4 metallocenes.[75] Since

these discoveries, MAO has become a very important cocatalyst for metal-catalyzed olefin polymerization. Although very extensive research has been carried out in both academia and industry, the exact composition and structure of MAO are still not entirely clear or well understood.[82,83] The proposed structures for MAO include one-dimensional linear chains (**I**) or cyclic rings (**II**) which contain three-coordinate Al centers, two-dimensional structures (**III**), and three dimensional clusters (**IV**) (Chart 3).

1.3.2.1 Proposed Structures of MAO

The three dimensional structure **IV** recently proposed by Sinn[84] is based on structural similarities with *tert*-butylaluminoxanes, which form isolable and X-ray crystallographically characterizable cage structures (**V**).[85] Structure **IV** has the basic formula $[Al_4O_3(Me)_6]_4$ with a Me:Al ratio of ≈ 1.5, which is in agreement with the general formula $[AlO_{0.8-0.75}(Me)_{1.4-1.5}]_n$, recently reported by Albemarle researchers from ^1H NMR measurements.[86] Sinn et al.[87] recently presented additional evidence for hexamethyl-tetraaluminoxane, $[Al_4O(Me)_6]_4$, as a major component of MAO, and have proposed an alternative structural model (similar to **IV** but having a more rigid structure with four-, six-, and eight-membered rings) for this tetramer.

Multinuclear NMR investigations of MAO also indicate a possible cage structure under ambient conditions.[88] Most aluminum centers in structure **IV**, except for the peripheral ones, are tetracoordinated. Characterization of MAO by ^{27}Al NMR spectroscopy has shown that four coordinate Al centers predominate in MAO solutions,[89] although three coordinate Al sites are also present.[90] Chemical evidence that MAO contains three coordinate aluminum was also demonstrated by Siedle et al.,[91] who showed that MAO undergoes facile ($\Delta G^* = 13.9$ kcal/mol at 22 °C in dichloromethane) reversible methyl exchange with $Cp_2Zr(^{13}CH_3)_2$.
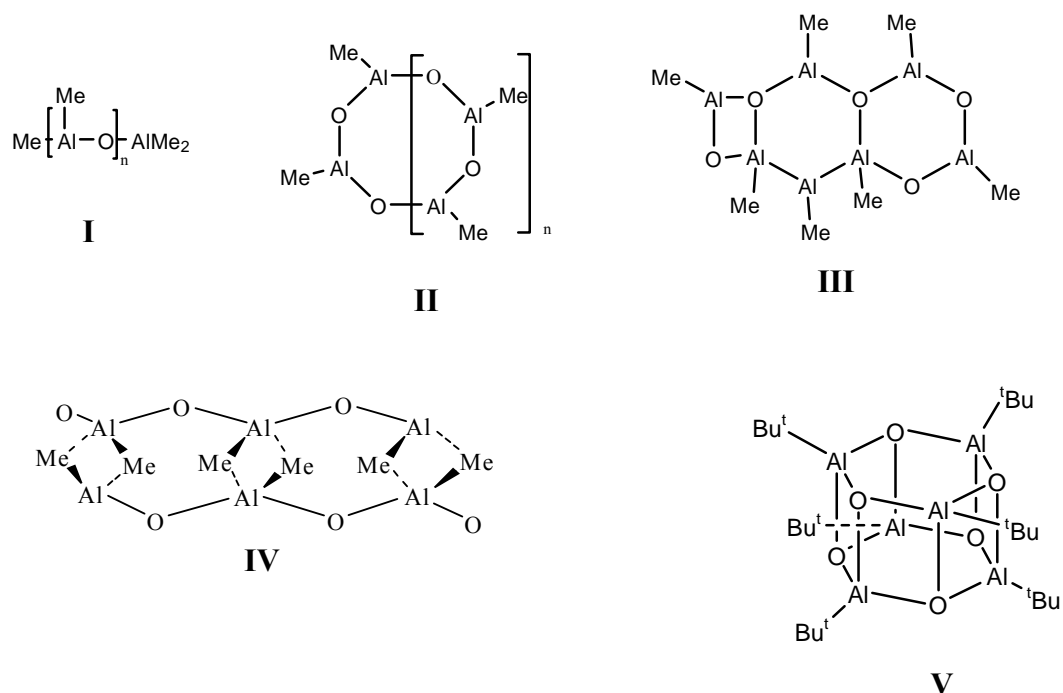
Chart 3. Proposed structures of methylaluminoxane (MAO)

Despite its unique effectiveness as a cocatalyst, MAO still remains a "black box".[87] Depending on the nature of the hydrated salt (the H_2O source) used for the MAO synthesis and the exact MAO synthetic reaction conditions, MAO-activated metallocenes may exhibit widely differing activities in olefin polymerization. The MAO structure can hardly be elucidated directly because of the multiple equilibria present in MAO solutions, and residual trimethylaluminum in MAO solutions appears to participate in equilibria that interconvert various MAO oligomers.[92-94] Nevertheless, in light of its complicated, unresolved structural features, MAO is usually represented for the sake of simplicity as having linear chain or cyclic ring structures [-Al(Me)-O-]*n*, containing three coordinate aluminum centers.[72]

1.4. Microstructure of Polymer Products

As mentioned earlier well-defined single-site metallocene catalysts have been the study of high research interest over conventional Ziegler-Natta heterogeneous catalysts.[95] This is mainly due to that these metallocene catalysts in combination with cocatalysts exhibit higher steroselectivity, narrower molecular weight distribution, and high catalytic activity in ethylene, propylene, and styrene polymerization.[75,96] Other advantages include that these systems produce structurally well-defined single-site active catalytic species,[72] which leads to a variety of high performance polyolefin products including isotactic,[96] syndiotactic,[97] and atactic polypropylenes,[98] high-density polyethylene (HDPE),[99] linear low-density polyethylene (LLDPE),[100] syndiotactic polystyrene,[101] and cyclo-olefin copolymers[102] with uniform and tunable microstructure.

In recent years there has been immense research interest in preparing catalysts to produce linear low density polyethylene (LLDPE). This is due to the following significant rheological and mechanical properties of LLDPE compared to the conventional polymers of ethylene: high tensile strength, higher impact and puncture resistance, superior toughness, good organoleptics and low blocking, excellent clarity and gloss, and easy blends with other polyolefins.[103-111] LLDPE can be obtained from the polymerization of ethylene by using Ziegler-Natta catalysts or by metallocene catalysts, which are formed by the reaction of group 4 metallocene with a coactivator, of which methylaluminoxane (MAO) is most typical.[8,112] In the case of conventional Ziegler-Natta catalysts, LLDPE suffers in terms of clarity or stiffness, but by using metallocene catalysts, some long chain branching is introduced, which improves clarity and stiffness.

1.5. Scope and Aim of the Present Work

The Sections 1.2.−1.4. describe the importance of bimetallic and trimetallic oxygen bridged compounds as catalysts for the polymerization reactions to produce the polymers of tunable microstructure. Furthermore, there are no rationally prepared oxygen bridged heterobimetallic complexes known which are used as the catalysts for the polymerization reactions. Based on these premises, the objectives of the present work are:

1. to develop new synthetic strategies for the preparation of oxygen bridged heterobi- and trimetallic complexes.

2. to use these complexes as catalysts in the ethylene, styrene polymerization, and copolymerization reactions.

3. to use spectral methods such as NMR spectroscopy, IR spectroscopy and X-Ray structural analysis to characterize the obtained products.

4. to characterize the polymer products by using NMR, GPC, DSC measurements to elucidate their properties.

5. DFT calculation studies to understand the mechanism of the polymerization process.

2. Results and Discussion

2.1. Synthesis and Structural Characterization of the Oxygen Bridged Heterobimetallic Complex Cp*$_2$MeZr(μ-O)TiMe$_2$Cp*(3) for Ethylene Polymerization Including Theoretical Interpretation of the "Oxygen Effect"

2.1.1. Synthesis of Zirconium and Hafnium Hydroxides Cp*$_2$MeZr(OH) (1) and Cp*$_2$Hf(OH)$_2$ (2).

Organotransition metal hydroxides have been known for a long time, and there has been interest in them for many years, primarily because of their role in catalysis.[113] However, this class of compounds has taken on increased importance with the growth of activity in materials-related chemistry. As organometallic precursors are now being used for the synthesis of oxide materials by sol-gel and related hydrothermal syntheses, an understanding of organometallic hydroxides, which occur as intermediates or themselves function as precursors, becomes important.[114] These hydroxides can also serve as building blocks to the polymetallic oxides. On this basis we became interested in the preparation of group 4 metal hydroxides and use them as the precursors for the bi- and trimetallic oxides.

The controlled hydrolysis of Cp*$_2$ZrMe$_2$ with one equivalent of water resulted in the formation of Cp*$_2$MeZr(OH) (**1**) in high yield with the elimination of methane (Scheme 1).

Scheme 1

$$\text{Cp*}_2\text{ZrMe}_2 \quad + \quad \text{H}_2\text{O} \quad \xrightarrow[\substack{n\text{-hexane} \\ -\ \text{CH}_4}]{-30\,^{\circ}\text{C to RT}} \quad \text{Cp*}_2\text{MeZr(OH)}$$

$$\text{Cp*} = \text{C}_5\text{Me}_5 \qquad\qquad\qquad\qquad\qquad \mathbf{1}$$
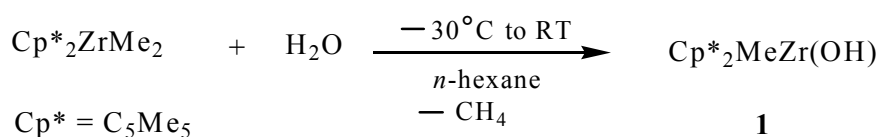
The hafnium dimethyl compound (Cp*$_2$HfMe$_2$) reacts with water in 1:2 stoichiometry to yield Cp*$_2$Hf(OH)$_2$ (Scheme 2). Even controlled hydrolysis resulted in the formation of dihydroxide rather than monohydroxide (Cp*$_2$HfMe(OH)).

Scheme 2

$$Cp*_2HfMe_2 \quad + \quad 2H_2O \xrightarrow[\substack{n\text{-hexane} \\ -\ 2CH_4}]{-30°C \text{ to RT}} \quad Cp*_2Hf(OH)_2$$

$$Cp* = C_5Me_5 \qquad\qquad\qquad\qquad\qquad\qquad\qquad \mathbf{2}$$
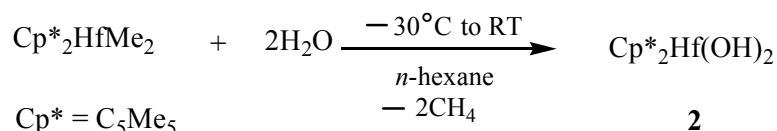
Compound **1** is the first zirconium compound which is bonded to a methyl and OH group at the same zirconium atom. Interestingly, **1** is monomeric in the solid state and even more striking the Me and OH group are not involved in any kind of hydrogen bonding as shown by X-ray structural analysis and IR spectroscopy. Surprisingly compound **1** is unexpectedly stable and does not eliminate methane even at elevated temperatures to form an oxo-bridged complex unlike Cp*$_2$ZrH$_2$, which gives an oxo-bridged complex under elimination of H$_2$ when treated with water in a 2:1 stoichiometry.[115] A reaction of **1** with one equivalent of Cp*$_2$ZrMe$_2$ did not occur. This may be due to the fact that the zirconium center is surrounded by sterically bulky Cp* ligands, which avoid complex **1** from reacting under elimination of methane.

Compounds **1** and **2** are sensitive to air. Complex **1** hydrolyses to dihydroxide on exposing to moisture. Compounds **1** and **2** are soluble in hexane, toluene, ether, tetrahydrofuran, and dichloromethane. Complex **1** was characterized by EI mass spectrometry, elemental analysis, ^{1}H and ^{13}C NMR, and IR spectroscopy. The ^{1}H NMR spectrum of **1** reveals a singlet for Me protons (–0.2 ppm), which appears at remarkably low field as compared with the Me protons (–0.62 ppm) of Cp*$_2$ZrMe$_2$. This can be explained by considering the electron affinity of the oxygen in the OH group attached to the Zr center. A

single resonance (1.8 ppm) is observed for the methyl protons of the Cp* rings. The presence of the hydroxyl group is confirmed by a resonance of the OH proton (4.2 ppm) in ^{1}H NMR and an O–H stretching mode (3680 cm^{-1}) in the IR spectrum. The MS spectrum of compound **1** is interesting when compared to that of Cp*$_2$Zr(OH)$_2$,[116] which gives an intense peak at *m/z* 376 (^{90}Zr) corresponding to the oxozirconium cation [Cp*$_2$ZrO]$^+$, whereas compound **1** shows an intense peak at *m/z* 377 (^{90}Zr) corresponding to [M^+–Me]. This indicates the low acidic character of the proton attached to oxygen, obviously due to the strong electron donating nature of the methyl groups. ^{1}H NMR spectral data for compound **2** is in good agreement with the literature data.[115]
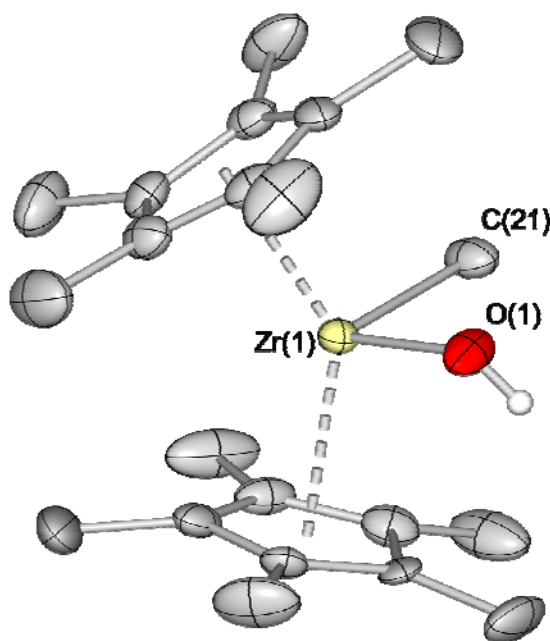
Figure 1. Molecular structure of Cp*$_2$MeZr(OH) (**1).** Thermal ellipsoids are set at 50% probability level. H atoms, except for the OH group, are omitted for clarity.
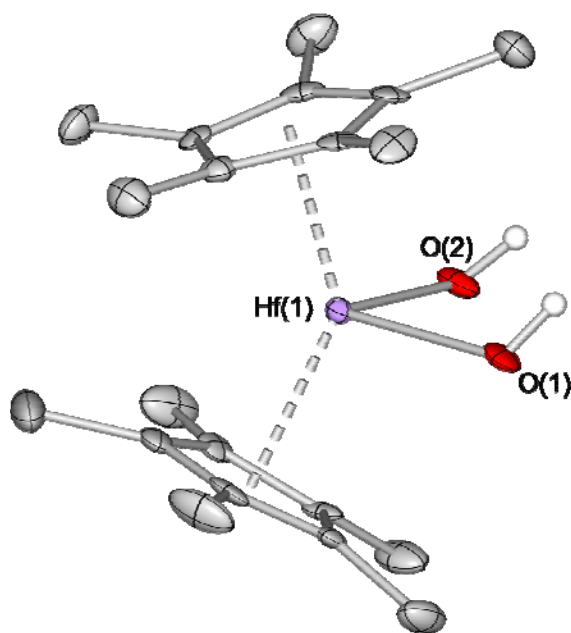
Figure 2. Molecular structure of Cp*$_2$Hf(OH)$_2$ (**2**). Thermal ellipsoids are set at 50% probability level. H atoms, except for the OH groups, are omitted for clarity.

2.1.2. Molecular Structures of Cp*$_2$MeZr(OH) (1) and Cp*$_2$Hf(OH)$_2$ (2)

Crystals of **1** suitable for X-ray structural analysis were obtained from *n*-hexane at –20 ºC. Compound **1** crystallizes in the orthorhombic space group $P2_12_12_1$. The Zr center is bonded to two Cp* groups and to two ancillary ligands (Me and OH) adopting a distorted tetrahedral geometry around the metal (Figure 1). The OH, methyl positions and also one Cp* ring are disordered. The O(1)–Zr(1)–C(21) bond angle (95.5(2)º) and the angle involving the centroids of the Cp* rings (137.6º) (Table 1) are comparable to those of the corresponding Cp*$_2$Zr(OH)$_2$[116] (O–Zr–O, av 98.9(2)º and Cp* angle av 137.7(5)º) suggesting a steric interaction between the methyl-methyl groups of the Cp* ligands.

Table 1. Selected Bond Distances (Å) and Angles (deg) for Compounds **1** and **2**

Compound **1**			
Zr(1)–O(1)	2.040(4)	O(1)–Zr(1)–C(21)	95.5(2)
Zr(1)–C(21)	2.302(7)	X_{Cp*1}–Zr–X_{Cp*2}	137.6
Compound **2**			
Hf(1)–O(1)	2.345(3)	O(1)–Hf(1)–O(2)	93.3º
Hf(1)–O(2)	2.351(3)	X_{Cp*1}–Hf–X_{Cp*2}	131.7

X_{Cp*} = Centroid of the Cp ring

To the best of our knowledge compound **2** is the first structurally characterized hafnium hydroxide. The X-ray quality crystals were obtained from *n*-hexane by cooling **2** at –20 ºC. Molecular structure of **2** is shown in Figure 2. Compound **2** crystallizes in the orthorhombic space group $P2_12_12_1$. The Hf center is bonded to two Cp* groups and to two ancillary ligands (OH) adopting a distorted tetrahedral geometry around the metal (Figure 2). The O(1)–Hf(1)–O(2) bond angle (93.3º) and the angle involving the centroids of the Cp* rings (138.7º) (Table 1) are narrower when compared to those of the corresponding $Cp*_2Zr(OH)_2$[116] (O–Zr–O, av 98.9(2)º and Cp* angle av 137.7(5)º) suggesting a steric interaction between the methyl-methyl groups of the Cp* ligands. The Hf(1)-O(1) and Hf(2)-O(2) bond lengths are similar to each other (2.345(3) and 2.351(3) Å) but are longer when compared to those (Hf–O, av 1.943 Å), in the homobimetallic compound ($Cp_2ClHf(\mu$-O)HfClCp_2$).[117]

2.1.3. Theoretical Study on Compound Cp*₂MeZr(OH) (1)

To further investigate the bonding situation around the zirconium atom and to know the reason for the unusual stability of compound **1** compared to $Cp*_2HZr(OH)$ which could not be isolated, a NBO analysis including donor and acceptor interactions has been performed for the molecules. This analysis shows that the compounds vary significantly in the charge on

the central atom. For compound **1** the charge is 1.82, and for Cp*$_2$HZr(OH), it is 1.58. Compound **1** containing a Zr-C bond which can best be described as polar covalent. The small charge value of 1.58 for compound Cp*$_2$HZr(OH) is a result of the hydrogen atom which carries a small negative charge of –0.30 thus leading to a hydridic character.

The weak acid-strength of these compounds can be put into an order by taking into account the two electron stabilization interactions of the O-H bond with other molecular orbitals which can be described as a donor acceptor interaction. Summing up all the contributions the ordering is **1** (33.3 kcal/mol) > Cp*$_2$HZr(OH) (29.6 kcal/mol) with **1** being the weakest acid. As a consequence, the stability of complex **1** can be attributed to the weak acidic character of the proton in OH and steric bulkiness of the Cp* ligands.

2.1.4. Reactivity of Compound Cp*$_2$MeZr(OH) (1): Synthesis of Cp*$_2$MeZr(μ-O)TiMe$_2$Cp*(3).

The unusual kinetic stability of **1** allows its further reactions with a variety of titanium complexes. It reacts under elimination of only one molecule of methane. Complex **1** does not react with CpTiMe$_3$ in ether at –30 ºC and at room temperature, CpTiMe$_3$ decomposes to a black precipitate due to its thermal instability. Similar reaction of complex **1** with CpTiMeCl$_2$ at room temperature yielded (CpTiMeO)$_3$ (**A**), and Cp*$_2$ZrCl$_2$ (**B**) (Scheme 3). The data of **B** is in good agreement with the literature.[118]

Complex **1** reacts cleanly with Cp*TiMe$_3$ at room temperature under elimination of methane to form the heterobimetallic compound **3** with a Zr(μ-O)Ti moiety (Scheme 3) in good yield. The reaction of **1** with two equivalents of Cp*TiMe$_3$ resulted in the formation of the bimetallic compound **3**. This may be due to the steric crowd of Cp* which hinders the further reaction to yield a trimetallic compound. When a solution of Cp*TiMe$_3$ in ether was added drop by drop to the solution of **1** in ether (–30 ºC) a precipitate was formed. After

stirring at room temperature for 12 h the solvent was removed in vacuum and the crude product was washed with *n*-hexane.

Scheme 3

$$\text{decomp. of CpTiMe}_3 \xleftarrow[\substack{-30°C \text{ to RT} \\ \text{ether}}]{\text{CpTiMe}_3} \text{Cp*}_2\text{MeZr(OH)} \xrightarrow[\substack{-30°C \text{ to RT} \\ \text{ether}}]{\text{Cp*TiMe}_3} \text{Cp*}_2\text{MeZr(}\mu\text{–O)TiMe}_2\text{Cp*}$$

1

3

$$\downarrow \substack{\text{RT} \\ \text{ether}} \quad \text{CpTiMeCl}_2$$

$$\text{(CpTiMeO)}_3 \ + \ \text{Cp*}_2\text{ZrCl}_2$$

A   **B**
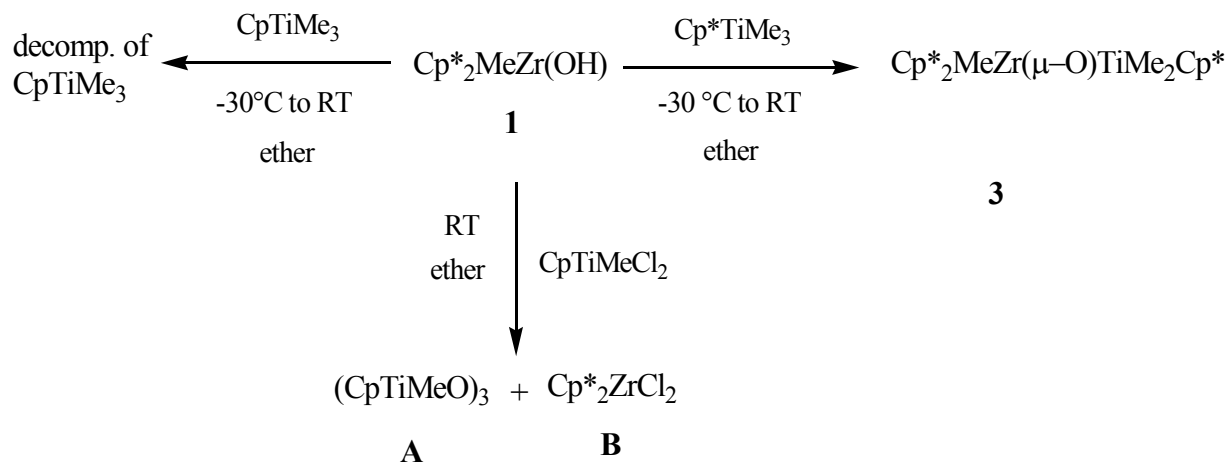
Compound **3** forms Cp*$_2$ZrMe(OH) (**1**) and an unidentified side product, when exposed to moisture. Complex **3** is insoluble in *n*-hexane, and pentane but sparingly soluble in toluene, diethyl ether, and THF at room temperature, whereas it dissolves in hot toluene. Compound **3** was thoroughly characterized by ^{1}H and ^{13}C NMR spectroscopy, EI mass spectrometry, and elemental analysis. The ^{1}H NMR spectrum of **3** shows two singlets (0.22 and 0.40 ppm) which can be assigned to the Me protons of TiMe$_2$ and ZrMe respectively, whereas the methyl protons on Cp* of Zr and Ti resonate as two different singlets (1.8 and 2.2 ppm) respectively. The EI mass spectrum (^{90}Zr) exhibits an intense peak at *m/z* 574 [M – 2Me]$^+$, and the peak at *m/z* 589 (6%) was assigned to [M – Me]$^+$.

2.1.5. Molecular Structure Description of Cp*₂MeZr(μ-O)TiMe₂Cp* (3)

Suitable crystals for X-ray structural analysis were obtained by cooling the hot toluene solution of **3**. Complex **3** crystallizes as a non-merohedral twin in the monoclinic space group *Pc* with two nearly identical molecules in the asymmetric unit. The molecular structure is shown in Figure 3.
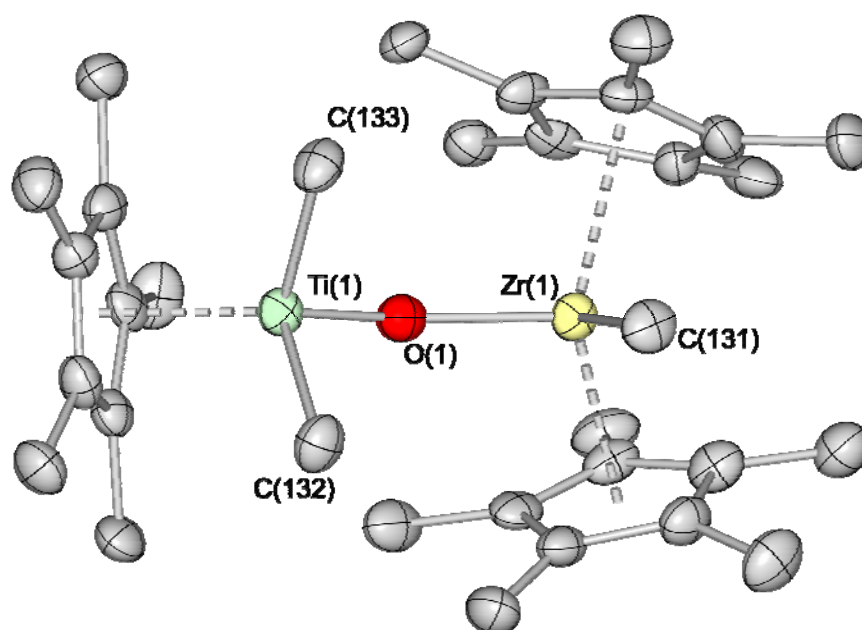
Figure 3. Molecular structure of Cp*₂MeZr(μ-O)TiMe₂Cp* (**3**). Thermal ellipsoids are set at 50% probability level. H atoms are omitted for clarity.

Compound **3** exhibits a bent Zr(μ-O)Ti core. Table 2 exhibits the selected bond distances and bond angles for complex **3**. The Zr and Ti show highly distorted tetrahedral geometry. The coordination sphere of the Zr center consists of two Cp* ligands, one Me group, and one (μ-O) unit, while that of the Ti has a Cp* ligand, two Me groups, and one (μ-O) unit. The Me groups on Ti and Zr are in staggered conformation. The Zr–C(131) bond distance (2.295(6) Å) is comparable to the average Zr–C bond length in the complex Cp₂Zr-[CH₂SiMe₃]₂[119] (av 2.284 Å) but is longer than the (av 2.251 Å) value found for (η^5-

$C_9H_7)_2ZrMe_2$.[119] The Zr(1)–O(1)–Ti(1) bond angle (av 155.9º) is significantly narrower when compared with the homobimetallic angles M(μ-O)M (M = Zr, Ti) in compounds (Cp$_2$ZrMe)$_2$(μ-O) (174.1(3)º)[119] and [Cp$_2$Ti(CF$_3$C=C(H)CF$_3$)]$_2$(μ-O) (170.0(2)º).[120] The angle between the centroids of Cp* and the Zr center (134.1º) is also smaller when compared with that of compound **1** (137.6º) and the zirconium dihydroxide (137.7(5)º).[116] But these angles are much wider than those of highly sterically congested alkoxide bridged clusters (Ti$_4$Zr$_2$O$_4$(OBu)$_n$(OMc)$_{10}$ (OMc = methacrylate, n = 2,4,6) (98.8(2)º to 108.61(8)º).[121] The Zr(1)–O(1) (2.022(4) Å) bond distance is slightly longer when compared with the corresponding oxygen-bridged (μ-O) compounds (Cp$_2$ZrL)$_2$(μ-O) (L = Me, SC$_6$H$_5$) (1.945(1) and 1.966(5) Å)[119] but shorter than those of heterobimetallic alkoxide bridged clusters ((Ti$_4$Zr$_2$O$_4$(OBu)$_n$(OMc)$_{10}$ (n=2,4,6) Zr–O, av 2.189(2) Å).[121] The Ti(1)–O(1) (1.816(4)Å) bond distance is slightly shorter than those in the (μ-O) compound [Cp$_2$Ti(CF$_3$C=C(H)CF$_3$)]$_2$(μ-O) (av Ti–O, 1.856(6)Å)[120] and alkoxide bridged cluster ((Ti$_4$Zr$_2$O$_4$(OBu)$_n$(OMc)$_{10}$ (n = 2,4,6), Ti–O, av 2.041(5) Å).[121]

Table 2. Selected Bond Distances (Å) and Angles (deg) for Compound **3**

Zr(1)–O(1)	2.022(4)	Zr(1)–O(1)–Ti(1)	156.1(2)
Ti(1)–O(1)	1.816(4)	X$_{Cp*1}$–Zr(1)–X$_{Cp*2}$	134.1
Zr(1)–X$_{Cp*1}$	2.289	O(1)–Zr(1)–C(131)	94.8(2)
Zr(1)–X$_{Cp*2}$	2.269	O(1)–Ti(1)–C(132)	106.3(2)
Ti(1)–X$_{Cp*}$	2.092	O(1)–Ti(1)–C(133)	105.3(2)
Zr(1)–C(131)	2.295(6)		
Ti(1)–C(132)	2.120(6)		
Ti(1)–C(133)	2.123(6)		

X$_{Cp}$ = Centroid of the Cp ring

2.1.6. Reactivity of Compound Cp*₂MeZr(μ-O)TiMe₂Cp* (3)

To study the reactivity of compound **3**, we carried out a further reaction of **3** with LMeAl(OH) (**7**) [L = CH(N(Ar)(CMe))₂, Ar = 2,6-iPr₂C₆H₃] at room temperature. However, the reaction did not occur even at refluxing the reaction mixture for 24 hours. Only the decomposition of LMeAl(OH) to β-diketiminate ligand has been observed (Scheme 4).

Scheme 4

[L = CH(N(Ar)(CMe))₂, Ar = 2,6-iPr₂C₆H₃]
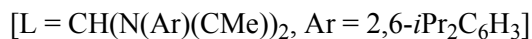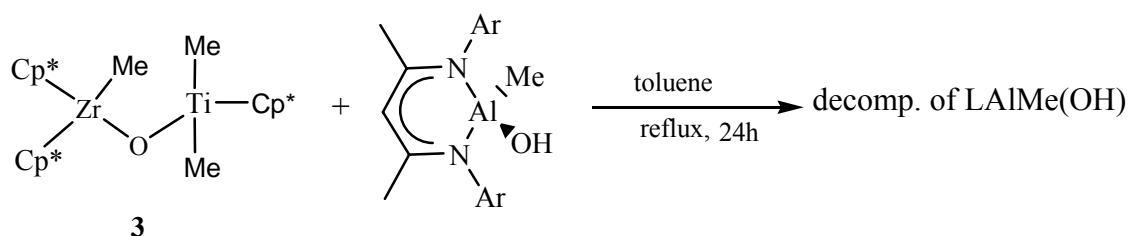
2.1.7. Polymerization of Ethylene by Cp*₂MeZr(μ-O)TiMe₂Cp* (3)

Compound **3** catalyzes the polymerization of ethylene in toluene when activated with MAO. All polymeric materials were isolated as white powders. Table 3 represents the results of ethylene polymerization data. Figure 4 exhibits a graph of activity against MAO to catalyst ratio of **3**. The polymerization data exhibits that the complex **3** is very active even at low (86:1) MAO to catalyst ratio. This high activity in **3** may be due to the bridging oxygen which enhances the Lewis acidity at the metal centers.

Table 3. Ethylene Polymerization Data for **3**[a]

catalyst	MAO: catalyst	t(min)	T(°C)	PE(g)	A×10^6	M_w	M_w/M_n	T_m[b] (°C)
3	86	20	25	1.6	0.25	178523	4.17	124.0
3	172	20	25	2.4	0.37	105149	3.42	120.0
3	345	20	25	3.1	0.48			124.5
3	461	20	25	5.5	0.85			124.9
3	518	20	25	6.3	0.97			122.2
3[c]	172	10	83	1.5	0.69			124.1

[a] polymerization condition; **3** = 19.8 μmol, 100 mL of toluene at 25 °C, at 1 atm ethylene pressure. Activity (A) = g PE/mol cat·h. [b]DSC. [c]polymerization condition; **3** = 13.2 μmol, 83 °C, at 1 atm ethylene pressure.
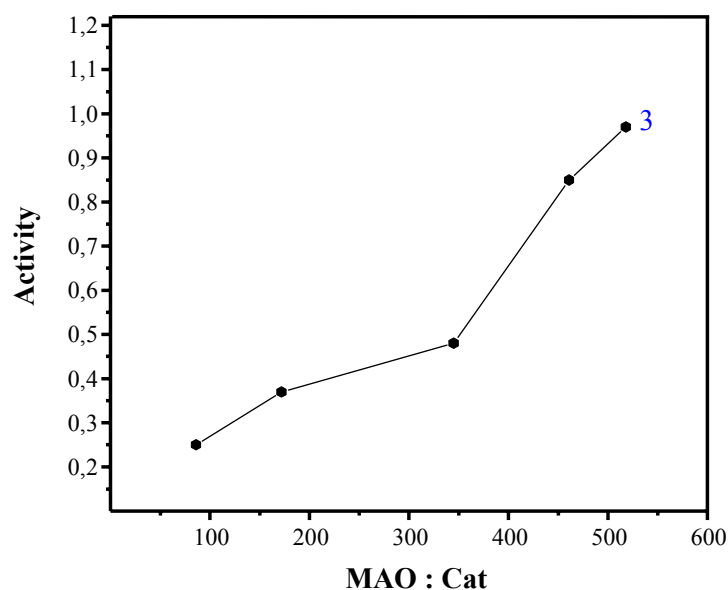
Figure 4. Plots of activity against MAO to catalyst ratios of **3**.

2.1.8. Polymer Properties

DSC measurements show that the melting points (T_m) of the polyethylene produced by **3** are in the range of 120 to 125 °C, which is in the typical range for the LLDPE.[95] The

resonances of ^{13}C NMR spectral data are assigned according to the literature.[95] The GPC measurements are monomodal for measured polyethylene samples. The M_w values are low and PDI are broad, which may be due to the fact that a good amount of the products coming from the titanium site are not incorporated into the growing polyethylene chain governed by the zirconium site. Polymerization data of complex **3** indicates high activity but less incorporation of ethylene to growing polyethylene chain. It can be assumed that two active sites compete for ethylene leading to the formation of lower molecular weight polyethylene, which makes PDI broad.

2.1.9. Results of Computational Studies on Complex Cp*$_2$MeZr(μ-O)TiMe$_2$Cp* (3)

It is evident from the crystal structure data that the M–O (M = Zr, Ti) bond length is short. Polymerization data shows that the compound exhibits high activity in ethylene polymerization. This may be due to the bridging oxygen, which causes short Zr–O and Ti–O bonds, indicative for high electron density within these bonds. As a consequence the electron density at the active metal sites is decreasing exhibiting enhanced Lewis acidic character. To support our findings from the experimental data, ab initio calculations were carried out aiming at the determination of the electronic density between Zr–O and Ti–O bonds.

As shown in Table 4, the resulting structure compares very well with the data obtained by X-ray diffraction, thus giving a solid foundation for the following bond analysis to describe the bonding situation quite well.

Table 4. Selected Calculated and X-ray Bond Distances (Å) and Bond Angles (deg)

Bond length	Calcd	X-ray	Bond angles	Calcd	X-ray
Zr(1)–O(1)	2.039	2.022	Zr(1)–O(1)–Ti(1)	157.37	156.90
Ti(1)–O(1)	1.820	1.816	O(1)–Zr(1)–C(131)	94.89	94.80
Zr(1)–C(131)	2.289	2.295	O(1)–Ti(1)–C(132)	104.69	106.30
Ti(1)–C(132)	2.122	2.120	O(1)–Ti(1)–C(133)	104.74	105.3

The NBO-analysis shows that the bonds formed between the metal atoms and the oxygen lead to a significant build-up of electron density on the oxygen atom. The distribution of electrons can be best described as locating 90% in a p-rich orbital of oxygen and leaving only 10% in a d-orbital of the metal. Figures 5 and 6 of the corresponding bonds show that electron density on the Zr atom is more depleted compared with that of the Ti atom.
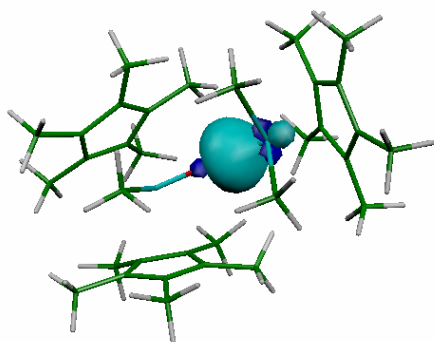
Figure 5. Shape of the bonding orbital between zirconium and oxygen.
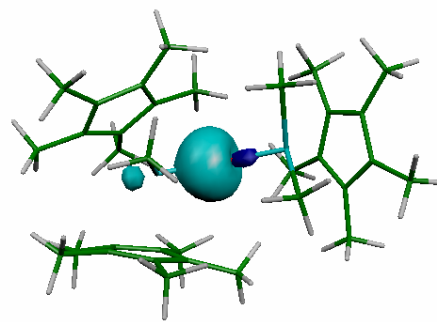
Figure 6. Shape of the bonding orbital between titanium and oxygen.

2.2. Oxygen Bridged Hybrid Metallocene-Nonmetallocene Heterobi- and Heterotrimetallic Catalysts of Group 4 Metals for Bimodal Activity in Olefin Polymerization: Synthesis, Characterization, and Catalytic Activity

Poly- and heterometallic complexes in general have enormous potential to revolutionize homogeneous catalytic processes. They can simultaneously activate both components of a bimolecular reaction, overcome entropy barriers associated with bringing the two reagents together, and minimize the energy barrier that arises from solvent–shell rearrangements during the reaction by virtue of the cooperative interaction between the two different metal centers. Continuing our research on heterobimetallic oxygen bridged complexes we became interested in preparing oxygen bridged hybrid metallocene-nonmetallocene polymetallic catalysts of group 4 metals and study their catalytic properties in the polymerization reactions.

2.2.1. Synthesis and Reactivity of Oxygen Bridged Metallocene-Nonmetallocene Hybrid Bi- and Trimetallic Catalysts

Synthesis of Cp*$_2$MeZr(μ-O)Ti(NMe$_2$)$_3$ (**4**) containing the Zr(μ-O)Ti motif (Scheme 5) was accomplished by reacting the monometallic hydroxide precursor, Cp*$_2$MeZr(OH) (**1**) with Ti(NMe$_2$)$_4$ under the elimination of Me$_2$NH in high yield. The solution of Cp*$_2$MeZr(OH) in toluene was added drop by drop to the solution of Ti(NMe$_2$)$_4$ in a 1:1 stoichiometric ratio in toluene and stirred at 25 ºC for 14 h to yield the yellow complex **4**. The ^{1}H NMR spectrum of the reaction mixture reveals almost quantitative conversion of the reactants to product as revealed by the absence of any characteristic Zr–OH resonance at 4.2 ppm in C$_6$D$_6$. Complex **4** is insoluble in *n*-hexane or pentane, but readily soluble in toluene

and benzene at room temperature. Complex **4** was characterized by ^{1}H and ^{13}C NMR spectroscopy, analytical data, EI mass spectrometry, and single crystal X-ray diffraction studies. The ^{1}H NMR spectrum of **4** in C_6D_6 exhibits three singlets at 0.01, 1.89, and 3.14 ppm, attributed to the proton resonances arising from Zr–Me, η^5-C_5Me_5, and NMe_2 groups respectively. The singlet at 0.01 ppm integrates one-sixth against the singlet at 3.14 ppm revealing the formation of a bimetallic complex **4** as formulated in Scheme 5. The ^{13}C NMR spectrum of compound **4** reveals a resonance at 29.1 ppm assigned to the zirconium bound methyl-carbon resonance. The six methyl-carbon nuclei arising from the three dimethylamino groups attached to the Ti center resonate at 45.4 ppm. Additionally, the peaks at 11.3 and 117.7 ppm are assigned to the carbon resonances of the methyl groups and the carbon resonances of η^5-cyclopentadienyl arising from zirconium bound Zr–C_5Me_5 group respectively. Analytically pure crystals of **4** were obtained from cold toluene at –20 ^{o}C and finally the structure of **4** was unambiguously determined by single crystal X-ray crystallography.

Scheme 5

$$Cp^*_2MeZr(OH) \quad + \quad Ti(NMe_2)_4 \quad \xrightarrow{\text{toluene, 25 }^o\text{C}}$$

1

$$Cp^* = \eta^5\text{-}C_5Me_5$$

4
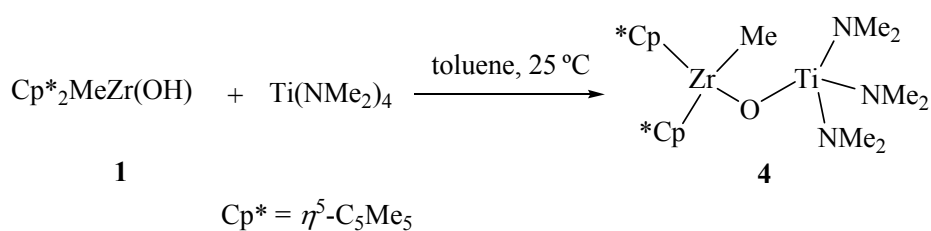
Compound **4** breaks up to the monohydroxide **1**, and an unidentified product, when exposed to moisture as revealed by the characteristic Zr–OH resonance in the ^{1}H NMR spectrum (4.2 ppm in C_6D_6). The reaction of **4** with Me_2SiCl_2 leads to the cleavage of Zr(μ-O)Ti bond and chlorine transfer reaction forming $Cp^*_2ZrCl_2$ and other unidentified products. However, compound **4** was found to be remarkably stable for several months under an inert

atmosphere. Further reaction of **4** with one equivalent of Cp*$_2$MeZr(OH) (**1**) in toluene does not lead to the formation of the expected heterotrimetallic complex bearing the Zr(μ–O)Ti(μ–O)Zr moiety. Compound **4** does not undergo further reaction with **1** to form a heterotrimetallic complex that can probably be attributed to the steric demand imposed by the bulky Cp* ligands of **1** hindering further transformation of **4** into a trimetallic complex.

Scheme 6
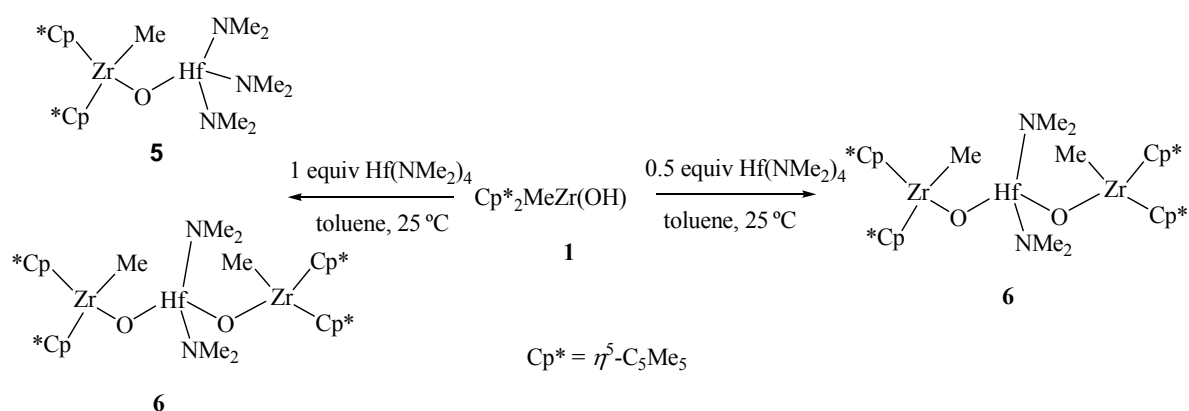
However, Hf(NMe$_2$)$_4$ reacts in a different way with Cp*$_2$MeZr(OH) (**1**) than Ti(NMe$_2$)$_4$. The solution of Cp*$_2$MeZr(OH) in toluene was added drop by drop to the solution of Hf(NMe$_2$)$_4$ in a 1:1 stoichiometric ratio in toluene and stirred at 25 ºC for 24 h to yield a colorless heterobimetallic compound Cp*$_2$MeZr(μ-O)Hf(NMe$_2$)$_3$ (**5**) along with another minor product in a 4:1 molar ratio. Complex **5** could not be isolated in a pure form, but it was formulated as a heterobimetallic complex shown in Scheme 6 by its characteristic ^{1}H NMR pattern. The ^{1}H NMR spectrum of **5** reveals a 1:6 relative intensity ratio of Zr–Me to NMe$_2$ protons indicating a heterobimetallic formulation of **5**. The structure of the minor compound was established as the heterotrimetallic Cp*$_2$MeZr(μ-O)Hf(NMe$_2$)$_2$(μ-O)ZrMeCp*$_2$ (**6**) complex. This compound was prepared in higher yield using different stoichiometry of the reactants. A toluene solution of Cp*$_2$MeZr(OH) was added to the solution of Hf(NMe$_2$)$_4$ in

toluene in a 2:1 stoichiometric ratio and stirred at 25 ºC for 24 h yielding almost quantitatively the heterotrimetallic complex **6** as revealed by the ^{1}H NMR spectrum of the reaction mixture. Complex **6** is soluble in toluene and benzene at room temperature. Compound **6** was characterized by ^{1}H and ^{13}C NMR spectroscopy, analytical data, EI mass spectrometry, and single crystal X-ray diffraction studies. Analytically pure crystals of **6** were obtained from cold toluene at –20 ºC. The ^{1}H NMR spectrum of **6** exhibits three singlets at –0.05, 1.92, and 2.99 ppm, assigned to the proton resonances arising from Zr–Me, η^5-C$_5$Me$_5$ ligand, and two NMe$_2$ groups respectively. The singlet at 2.99 ppm integrates twice against the singlet at –0.05 ppm clearly suggesting the formation of a trimetallic complex **6** as formulated in Scheme 6. The ^{13}C NMR spectrum is almost similar to that observed for the heterobimetallic complex **4**, exhibiting singlets at 27.9 and 43.5 ppm assigned to the carbon resonances arising from Zr–Me and Hf–NMe$_2$ groups respectively.

The EI mass spectral data for both **4** and **6** are in accord with the assigned structures. Neither of them exhibits a molecular ion. Compound **4** shows a peak at *m/z* 556.2 corresponding to $[M - Me]^+$. The next fragment for compound **4** is observed at *m/z* 526.2 corresponding to $[M – NMe_2]^+$. Compound **6** exhibits an ion at *m/z* 1037.3 corresponding to $[M - Me]^+$.

2.2.2. 2D NMR Experimental Results for Complexes 4 and 6

To get to know the more insight into the molecules of **4** and **6** in solution state 2D ^{1}H,^{1}H NOESY NMR experiments were carried out. The experiments reveal that **4** and **6** are indeed heterometallic complexes. The data of complex **4** exhibits the methyl resonances from the Zr-Me (δ 0.01 ppm) and Ti-NMe$_2$ (δ 3.14 ppm) moieties have cross-peaks, and also the methyl signals on Cp* (δ 1.89 ppm) and methyl signals on Ti-NMe$_2$ (δ 3.14 ppm) shows the cross peaks which can be expected considering the bulky Cp* ligands. This data indicates that

the Zr and Ti moieties are present within the same molecule (Figure 7) which is further confirmed by the crystal structure of **4** (Figure 9).
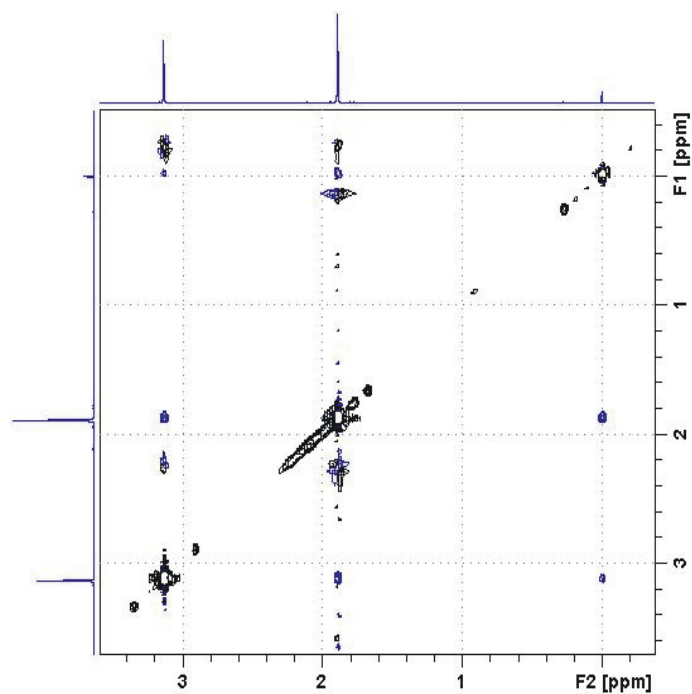
Figure 7. 2D (^{1}H,^{1}H NOESY) spectrum of Cp*$_2$MeZr(μ-O)Ti(NMe$_2$)$_3$ (**4**).
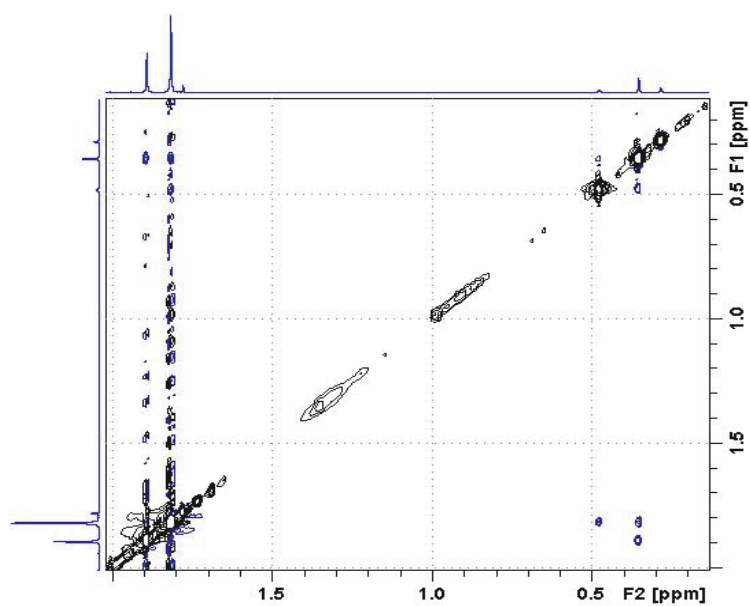
Figure 8. 2D (^{1}H,^{1}H NOESY) spectrum of Cp*$_2$MeZr(μ-O)Hf(NMe$_2$)$_2$(μ-O)ZrMeCp*$_2$ (**6**).

The ^{1}H,^{1}H NOESY spectrum for complex **6** is shown in Figure 8. The spectrum is similar to that of **4** exhibiting the cross peaks between the methyl resonances of Zr-Me (δ -0.05 ppm) and methyl resonances of Hf-NMe$_2$ (δ 2.99 ppm). The cross peaks between methyl signals of Hf-NMe$_2$ (δ 2.99 ppm) and methyl signals of Cp* (δ 1.92 ppm) has also been seen indicating the presence of Zr and Hf in the same molecule. In both 2D spectra of compounds **4** and **6** the cross peaks between corresponding methyl resonances of Zr-Me (δ 0.01 ppm, for **4**, and δ -0.05 ppm for **6**) and methyl resonances of Cp* (δ 1.89 ppm for **4**, and δ 1.92 ppm for **6**) has been observed. This may be attributed to the steric interaction between the methyl-methyl groups of the bulky Cp* ligands.

2.2.3. Crystal Structures of Compounds 4 and 6

Suitable crystals for X-ray structural analysis were obtained by cooling a toluene solution of **4** at –20 ^{o}C for several days. Compound **4** crystallizes in the triclinic space group $P\bar{1}$. The molecular structure of **4** is shown in Figure 9. The Zr and Ti centers in compound **4** adopt distorted tetrahedral geometry. The coordination sphere of the Zr center consists of two Cp* ligands, one methyl group, and one (μ-O) unit, while that of the Ti has three dimethylamino groups and one (μ-O) unit. Table 5 compiles the selected bond distances and angles for compound **4**. The bonding parameters compare well with the related oxygen bridged heterobimetallic complex, Cp*$_2$MeZr(μ-O)TiMe$_2$Cp* (**3**). Compound **4** exhibits a slightly bent Zr(μ–O)Ti core. The Zr(1)–O(1)–Ti(1) bond angle in **4** is 169.73(6)^o which is considerably wider than the Zr(μ–O)Ti bond angle (156.1(2)^o) observed in Cp*$_2$MeZr(μ-O)TiMe$_2$Cp* but comparable to the homobimetallic M(μ–O)M (M = Zr, Ti) angles in compounds (Cp$_2$Zr(Me))$_2$(μ-O) (174.1(3)^o)[119] and (Cp$_2$Ti(CF$_3$C=C(H)CF$_3$))$_2$(μ-O) (170.0(2)^o).[120] The Zr–C(50) bond distance (2.2950(15) Å) is comparable to the average Zr–C bond length in Cp$_2$Zr(CH$_2$SiMe$_3$)$_2$ (av 2.284 Å) but is slightly longer than the value (av 2.251

Å) found for $(\eta^5\text{-}C_9H_7)_2Zr(Me)_2$.[119] The Zr(1)–O(1) (2.0016(10) Å) bond distance is comparable to the Zr–O bond distance (2.022(4) Å) observed in Cp*$_2$MeZr(μ-O)TiMe$_2$Cp* (**3**) but shorter than the heterobimetallic alkoxide bridged clusters Ti$_4$Zr$_4$O$_6$(OBu)$_4$(OMc)$_{16}$ (OMc = methacrylate, av Zr–O 2.17 Å).[121] The angle between the centroids of Cp* and the Zr center (136.0°) is slightly wider when compared with that of Cp*$_2$MeZr(μ-O)TiMe$_2$Cp* (**3**) (134.1º).
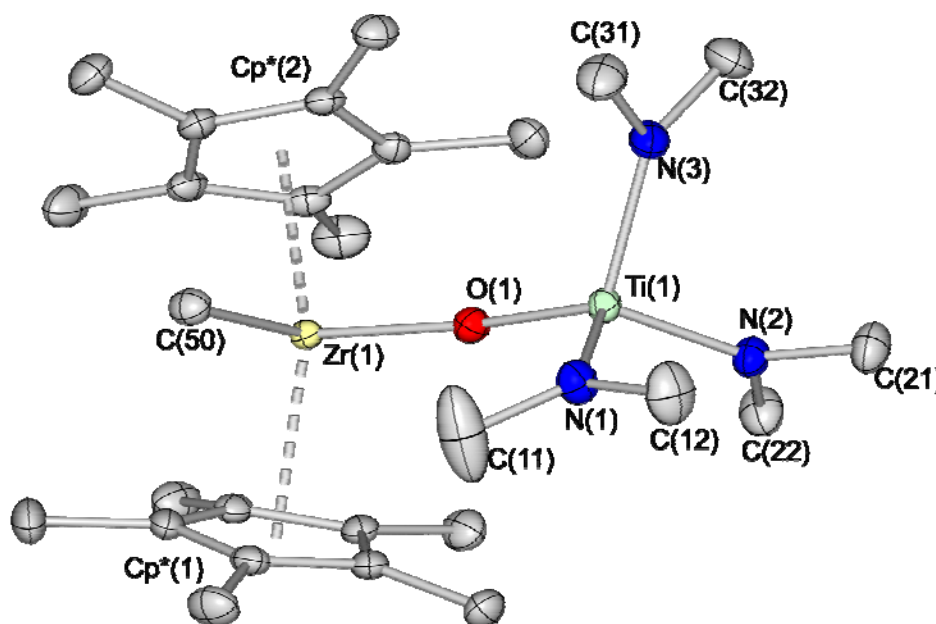
Figure 9. Molecular structure of Cp*$_2$MeZr(μ-O)Ti(NMe$_2$)$_3$ (**4**). Thermal ellipsoids are set at 50% probability level. H atoms are omitted for clarity.

Table 5. Selected Bond Distances (Å) and Angles (deg) for **4**

Ti(1)–O(1)	1.8028(10)	Ti(1)–N(1)	1.9088(14)
Ti(1)–N(2)	1.9129(13)	Ti(1)–N(3)	1.9316(13)
Zr(1)–O(1)	2.0016(10)	Zr(1)–C(50)	2.2950(15)
Cp*(1)–Zr(1)	2.278(8)	Cp*(2)–Zr(1)	2.263(7)
O(1)–Ti(1)–N(1)	109.73(5)	O(1)–Ti(1)–N(2)	111.19(5)
N(1)–Ti(1)–N(2)	114.82(6)	O(1)–Ti(1)–N(3)	118.21(5)
N(1)–Ti(1)–N(3)	101.44(6)	N(2)–Ti(1)–N(3)	101.16(6)
Ti(1)–O(1)–Zr(1)	169.73(6)	O(1)–Zr(1)–C(50)	96.92(5)
Cp*(1)–Zr(1)–Cp*(2)	136.0(3)	Cp*(1)–Zr(1)–C(50)	103.2(2)
Cp*(2)–Zr(1)–C(50)	102.3(2)	Cp*(1)–Zr(1)–O(1)	106.0(2)
Cp*(2)–Zr(1)–O(1)	105.8(2)		

Cp* = Centroid of the Cp* ring

Colorless crystals of **6** suitable for X-ray structural analysis were obtained from toluene at –20 ºC. Compound **6** crystallizes in the monoclinic space group $P2_1/n$. The molecular structure is shown in Figure 10. It shows the Hf atom is bonded through two bridging oxygen atoms to two zirconium centers establishing a trimetallic core with Zr(μ–O)Hf(μ–O)Zr backbone. The Hf atom exhibits a distorted tetrahedral geometry with two nitrogen atoms of two dimethylamino ligands, and two (μ-O) units. Each Zr center is bonded to two Cp* groups and to two ancillary ligands (Me and (μ-O)) adopting a distorted tetrahedral geometry around the metal (Figure 10). The enhanced metal–oxygen bond distances in **6** as compared to that in **4** clearly (see Table 6) indicate that the formation of the trimetallic core in the case of **6** is favored as the bulky 'Cp*$_2$Zr(μ-O)' core moves further away from the central metal. The other bond distances and angles involving the Zr center in **6** compare well with those observed in **4**. Compound **6** exhibits two different types of bent Zr–O–Hf cores. The Zr(1)–O(1)–Hf(1) bond angle in **6** is 169.38(10)º which is similar to the observed Zr(1)–O(1)–Ti(1) bond angle (169.73(6)º) in **4**. The other Zr(2)–O(2)–Hf(1) bond angle in compound **6** is 151.25(11)º which is considerably bent and probably this bending can be attributed to the internal requirement for the formation of a trimetallic core putting the three metal centers in an optimum steric environment.
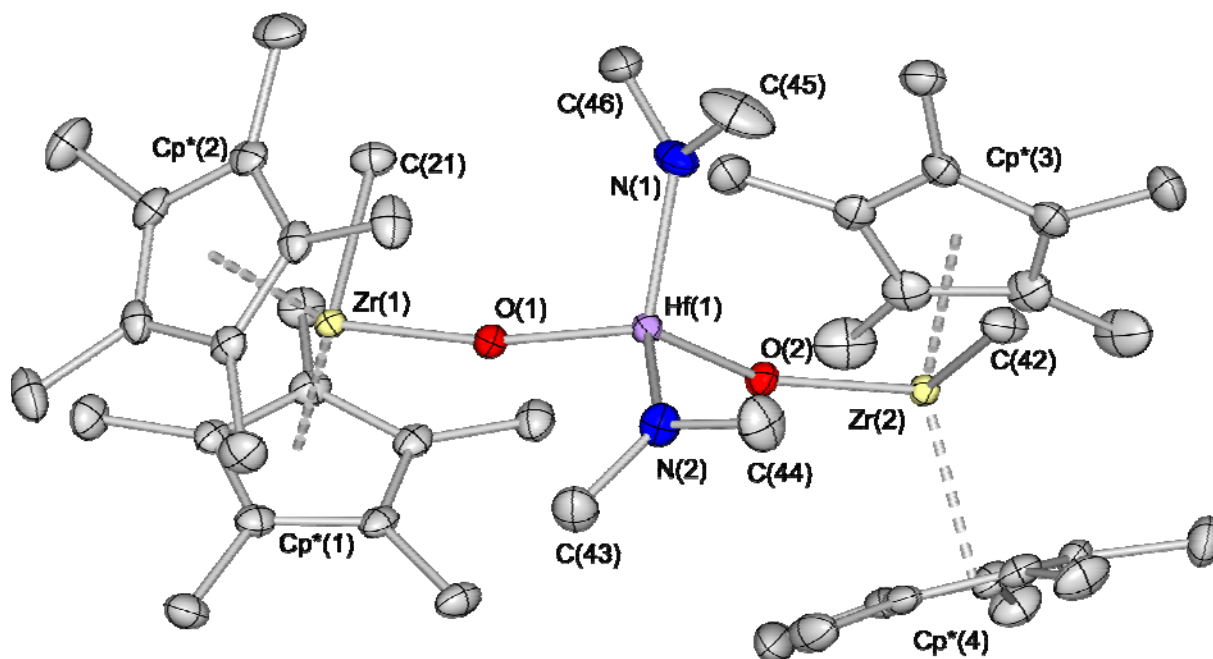
Figure 10. Molecular structure of Cp*$_2$MeZr(μ-O)Hf(NMe$_2$)$_2$(μ-O)ZrMeCp*$_2$ (**6**). Thermal ellipsoids are set at 50% probability level. H atoms are omitted for clarity.

Table 6. Selected Bond Distances (Å) and Angles (deg) for **6**

Hf(1)–O(1)	1.9265(18)	Hf(1)–O(2)	1.9660(18)
Hf(1)–N(1)	2.042(2)	Hf(1)–N(2)	2.040(2)
Zr(1)–O(1)	1.9992(18)	Zr(1)–C(21)	2.292(3)
Cp*(1)–Zr(1)	2.274(9)	Cp*(2)–Zr(1)	2.279(9)
Zr(2)–O(2)	1.9754(18)	Zr(2)–C(42)	2.302(3)
Cp*(3)–Zr(2)	2.287(9)	Cp*(4)–Zr(2)	2.282(9)
O(1)–Hf(1)–N(1)	108.42(9)	O(1)–Hf(1)–N(2)	108.81(9)
O(1)–Hf(1)–O(2)	111.39(8)	N(1)–Hf(1)–N(2)	107.94(10)
O(2)–Hf(1)–N(1)	109.64(9)	O(2)–Hf(1)–N(2)	110.55(9)
Hf(1)–O(1)–Zr(1)	169.38(10)	Hf(1)–O(2)–Zr(2)	151.25(11)
O(1)–Zr(1)–C(21)	95.28(9)	Cp*(1)–Zr(1)–Cp*(2)	134.9(3)
Cp*(1)–Zr(1)–C(21)	102.7(3)	Cp*(2)–Zr(1)–C(21)	102.9(3)
Cp*(1)–Zr(1)–O(1)	106.1(2)	Cp*(2)–Zr(1)–O(1)	107.8(2)
O(2)–Zr(2)–C(42)	94.08(10)	Cp*(3)–Zr(2)–Cp*(4)	134.7(3)
Cp*(3)–Zr(2)–C(42)	102.4(3)	Cp*(4)–Zr(2)–C(42)	102.5(3)
Cp*(3)–Zr(2)–O(2)	107.8(3)	Cp*(4)–Zr(2)–O(2)	107.4(2)

Cp* = Centroid of the Cp* ring

2.2.4. Polymerization of Ethylene

Compound **4** catalyzes the polymerization of ethylene in toluene when activated with MAO. All polymeric materials were isolated as white powders. Table 7 represents the results of ethylene polymerization data. Figure 11 exhibits a graph of activity against MAO to catalyst ratio of **4** revealing the highest activity is achieved at 400:1 MAO to catalyst ratio. The polymerization data exhibits that complex **4** is a quite active catalyst at moderately low MAO to catalyst ratio.

Table 7. Ethylene Polymerization Data for Compounds **4** and **6**[a]

Catalyst	MAO: catalyst	PE (g)	$A \times 10^5$	M_w	M_w/M_n	T_m[b] (°C)
4	200	0.23	0.46	$(-)$[c]	$(-)$[c]	125.9
4	300	0.25	0.50	$(-)$[c]	$(-)$[c]	126.1
4	400	0.91	1.82	170000	2.87	125.2
4	600	0.93	1.86	127000	2.74	127.1
6	400	0.470	0.94	205000	2.71	128.7

[a] Polymerization condition; **4** and **6** = 10 μmol, 100 mL of toluene at 25 °C, at 1 atm ethylene pressure for 0.5 h. Activity (A) = g PE/mol cat·h. [b]DSC. [c] Not measured.
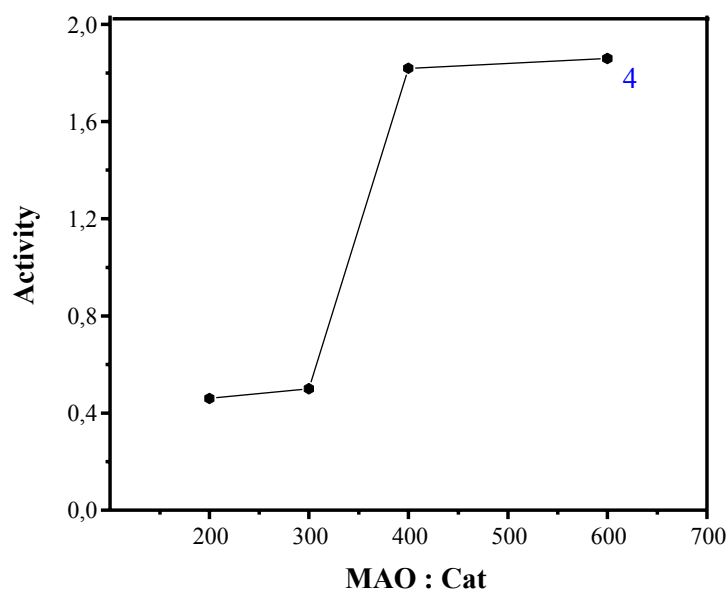
Figure 11. Plot of activity against MAO to catalyst ratios of **4** in ethylene polymerization.

2.2.5. Polymer Characteristics

DSC measurements show that the melting points (T_m) of the polyethylene produced by **4** are in the range of 125 to 129 ºC. The ^{13}C NMR data exhibits a singlet at 30.0 ppm corresponding to the backbone carbon of linear polyethylene chain.[95] In the present case, the polyethylene seems to be produced largely by the Zr center as revealed by the control experiments carried out with Cp*$_2$Zr(Me)$_2$ and Ti(NMe$_2$)$_4$ as catalysts. Cp*$_2$Zr(Me)$_2$ exhibits less but comparable activity in ethylene polymerization and Ti(NMe$_2$)$_4$ reveals almost two orders lower activity in magnitude for ethylene polymerization when compared to the activity observed for **4** under identical conditions (See Table S3 Supporting Material). This fact was further supported by the catalytic activity observed for complex **6** which shows activity higher of one order in magnitude than the Hf(NMe$_2$)$_4$ under identical polymerization condition indicating that the ethylene polymerization is controlled by the Zr center. Also the monomodal GPC traces, molecular weight, and product polydispersities (Table 7) are

consistent with single-site processes during the ethylene polymerization. However, a cooperative effect between the metal centers through oxygen bridging cannot be completely excluded as the bridging oxygen brings the metallic centers in close proximity.

2.2.6. Styrene Polymerization Studies

The catalytic property of complex **4** for the polymerization of styrene was preliminarily investigated. This complex shows moderate activity at ambient temperature in toluene when activated with MAO. All polymeric materials were isolated as white amorphous powders and Table 8 summarizes the activity values of catalyst **4** which increases gradually with MAO to catalyst ratio (Figure 12). The polystyrene is most likely to be produced by the Ti center as revealed by the control experiments carried out with $Ti(NMe_2)_4$ as catalysts exhibiting comparable activity in styrene polymerization when compared to the activity observed for **4** under identical conditions. The DSC measurements of the polystyrene obtained show that the characteristic glass-transition temperatures (T_g) are in the range from 72 to 76 °C. Melting points (T_m) for the polymers were not observed. This unusually low T_g might be attributed to the branching in the atactic polystyrene.

Table 8. Styrene Polymerization Data for Compound **4** as Catalyst[a]

catalyst	MAO:catalyst	PS(g)	$A \times 10^4$	$T_g^{[b]}$ (°C)
4	800	0.44	4.4	75.3
4	1000	0.55	5.5	70.2
4	1200	0.61	6.1	74.8
4	1600	0.84	8.4	72.0

[a] Polymerization condition; **4** =10 μmol, 100 mL of toluene with 10 mL of styrene at 25 °C, for 1 h. Activity (A) = g PS/mol cat·h. [b] DSC.
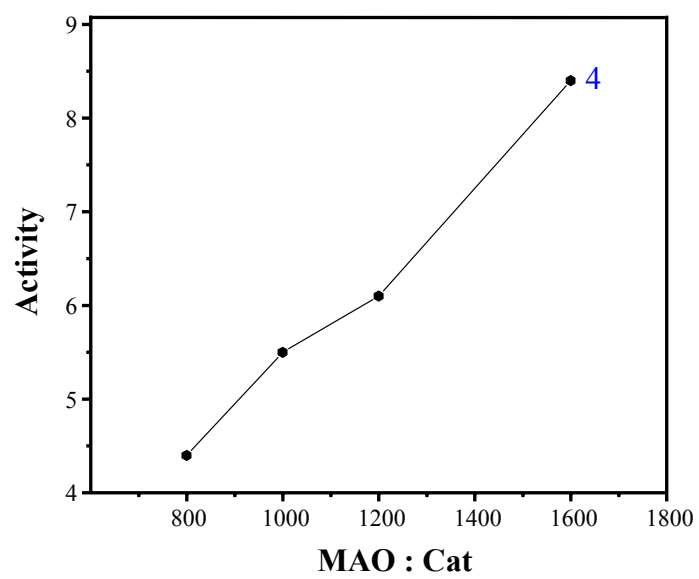
Figure 12. Plot of activity against MAO to catalyst ratios of **4** in styrene polymerization.

2.3. Synthesis, Structural Characterization, and Catalytic Studies of Compounds Containing Al(μ–O)M (M = Ti, Hf) Core

The development of metallocene catalysts[6] was closely linked to the discovery of MAO as a cocatalyst, which is thought to generate a cationic metal alkyl active site by alkylation of the catalyst precursor and abstraction of an anionic ligand.[72] Recently we isolated the unprecedented LMeAl(OH) (**7**) [L = CH(N(Ar)(CMe))$_2$, Ar = 2,6-iPr$_2$C$_6$H$_3$] which has only one –[Al(Me)–O–] unit.[45] We have demonstrated that the liquid ammonia/toluene two-phase system is highly effective for the hydrolysis of organoaluminum compounds. Instead of routine long-chain and three-dimensional cage compounds, our group was able to isolate aluminum dihydroxide with terminal OH groups, LAl(OH)$_2$ (Chart 1) [L = CH(N(Ar)(CMe))$_2$, Ar = 2,6-iPr$_2$C$_6$H$_3$],[60] and the first dinuclear alumoxane hydroxide, [LAl-(OH)]$_2$(μ-O), in a two-phase system.[61] The latter compound, when treated with Me$_2$AlH, affords a six-membered alumoxane with a three coordinate Al center and two coordinate O atoms, (LAl)$_2$(MeAl)(μ-O)$_3$.[61] Then we reported an improved route to LAl(OH)$_2$ by using a strong nucleophilic reagent N-heterocyclic carbene as a HCl acceptor for the reaction of LAlCl$_2$ and stoichiometric amounts of water.[122] In the course of the synthesis of LMeAl(OH) (**7**) from LMeAlCl a stepwise process was followed with one equivalent amount of water.

2.3.1. Synthesis of LMeAl(μ-O)MMeCp$_2$ (M = Ti (8), Hf (9))

Using the advantage of the oxophilicity of group 4 metals and the Brönsted acidic character of the proton of the Al(O−H) moiety, we isolated compounds **8** and **9** by treatment of equivalent amounts of LMeAl(OH) (**7**) [L = CH(N(Ar)(CMe))$_2$, Ar = 2,6-iPr$_2$C$_6$H$_3$] and Cp$_2$MMe$_2$ (M = Ti,[123] Hf [124]). Reaction of **7** with Cp$_2$TiMe$_2$ at 80 ºC led to intermolecular elimination of methane and the formation of the (μ-O) bridged heterobimetallic complex

LMeAl(μ-O)TiMeCp$_2$ (**8**; Scheme 7) in moderate yield (61%). Similarly treatment of **7** with a stoichiometric amount of Cp$_2$HfMe$_2$ in ether in the range from −30 ºC to ambient temperature results in the formation of the (μ-O) bridged heterobimetallic compound LMeAl(μ-O)HfMeCp$_2$ (**9**; Scheme 7) in good yield (67%).

Scheme 7
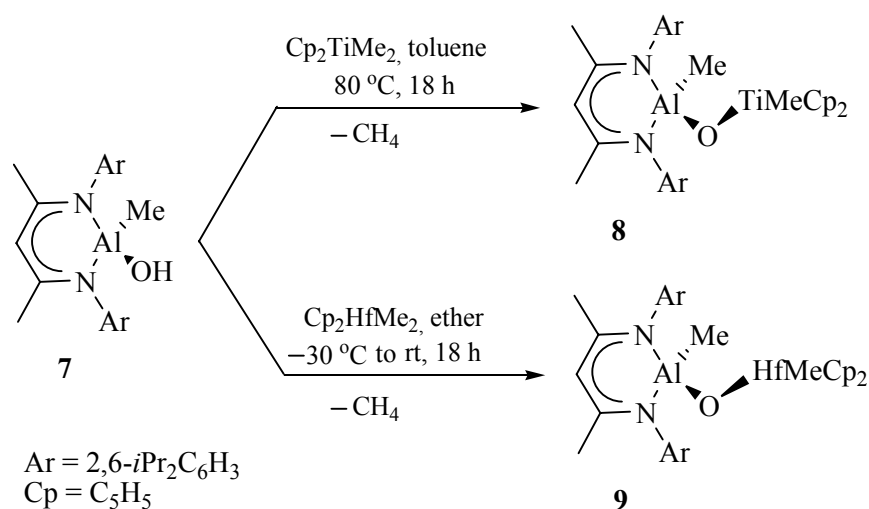
Compounds **8** and **9** are not soluble in toluene, hexane, and ether but soluble in hot toluene and are characterized by analytical, spectroscopic, and single-crystal X-ray diffraction studies. The IR spectra of **8** and **9** show no OH absorptions in the range from 3000 to 3600 cm^{-1} confirming the completion of the reaction by deprotonation. Compound **8** is a yellow crystalline solid that melts at 250 ºC while **9** is a colorless crystalline solid melting at 391 ºC. Decomposition was observed at the melting points of **8** and **9**. Unlike Cp$_2$TiMe$_2$ complex **8** is thermally stable and not photosensitive. Compound **8** is stable and can be stored for a period of time at room temperature in the absence of air and moisture. The mass spectral data for both **8** and **9** are in accord with the assigned structures. Neither of them exhibits a molecular ion. Compound **8** shows the base peak at *m/z* 638 corresponding to [*M*−2Me]$^+$. The next most intense peak for compound **8** is observed at *m/z* 653 which can be assigned to [*M*−Me]$^+$. The

base peak for compound **9** is observed at *m/z* 785 representing [*M*−Me]⁺. The next most

intense peak at *m/z* 770 shows the loss of another methyl group corresponding to [*M*−2Me]⁺.

Both compounds **8** and **9** exhibit ions at *m/z* 202 which can be assigned to [DippNCMe]⁺.[125]

The ¹H NMR spectrum of **8** exhibits two resonances (δ −0.91 and −0.18 ppm) which can be

attributed to the Me protons of AlMe and TiMe groups, respectively, whereas the respective

AlMe and HfMe groups in compound **9** resonate at δ −0.27 and 0.08 ppm. The characteristic

Cp protons for **8** and **9** appear as singlets (δ 5.3 and 5.4 ppm). In addition, a set of resonance

assignable to the isopropyl and methyl protons associated with the β-diketiminate ligand is

found in the range between δ 1.76 and 1.01 ppm, and the absence of the OH proton resonance

features both **8** and **9**. The ²⁷Al NMR is silent due to the quadruple moment of aluminum.

2.3.2. Molecular Structure Description of LMeAl(μ-O)MMeCp₂ (M = Ti (8), Hf (9))

The yellow crystals of **8** and the colorless single crystals of **9** were obtained from

cooling their hot toluene solutions and were unambiguously analyzed by X-ray diffraction

studies (Figures 13 and 14). The important bond parameters are listed in Tables 9 and 10.

Compounds **8** and **9** crystallize in the triclinic space group *P*1̄. Both compounds show

the aluminum atom bonded through an oxygen atom to titanium and hafnium respectively,

and contain a bent Al(μ-O)M (M = Ti, Hf) core. The aluminum atom exhibits a highly

distorted tetrahedral geometry with two nitrogen atoms of the β-diketiminato ligand, a methyl

group, and one (μ-O) unit. The titanium and hafnium exhibit tetrahedral geometry and their

coordination spheres are completed by two Cp ligands and one methyl group around each

metal atom. The Me groups on Al and Ti in **8** and **9** are bent out of the Al(μ-O)M (M = Ti,

Hf) plane in a *cis* configuration.

The Al(μ-O) bond length (1.715(3) Å) in **8** is in good agreement with LAl(μ-O)

ZrRCp₂ (L = CH(N(Ar)(CMe))₂, Ar = 2,6-*i*Pr₂C₆H₃, R = Me, Cl) (1.711(2) Å)[45] but longer

than those found in compounds $[((Me_3Si)_2HC)_2Al]_2(\mu\text{-O})$ (1.687(4) Å),[126] and

$[HC((CMe)(NMe))_2AlCl]_2(\mu\text{-O})$ (1.677(6) Å).[127] The Al(μ-O)Ti angle (151.7(2)°) in **8** is

smaller than the Al(μ-O)Hf (158.4(1)°) angle in **9**, and the corresponding Al(μ-O)Zr bond

angle in LAl(μ-O)ZrRCp$_2$ (L = CH(N(Ar)(CMe))$_2$, Ar = 2,6-iPr$_2$C$_6$H$_3$, R = Me, Cl)

(158.2(1)°).[45] This can probably be attributed to the increasing atomic radii from Ti to Zr

causing gradual opening of the Al(μ-O)M (M = Ti or Zr) bond angle and to the bulkiness of

the ligands surrounding the metal centers. However, the Al(μ-O)M (M = Ti, Hf) angles in **8**

and **9** are significantly less opened than those of homobimetallic M(μ-O)M (M = Zr, Hf) in

$(Cp_2ZrMe)_2(\mu\text{-O})$ (174.1(3)°)[119] and $(Cp_2HfMe)_2(\mu\text{-O})$ (173.9(3)°).[128] The Al−Me bond length

in compound **8** (1.958(4) Å) is similar to that of LMeAl(OH) and LAl(μ-O)ZrRCp2 (L =CH

(N(Ar)(CMe)), Ar = 2,6-iPr$_2$C$_6$H$_3$, R = Me, Cl) (1.961(3) Å).[45]
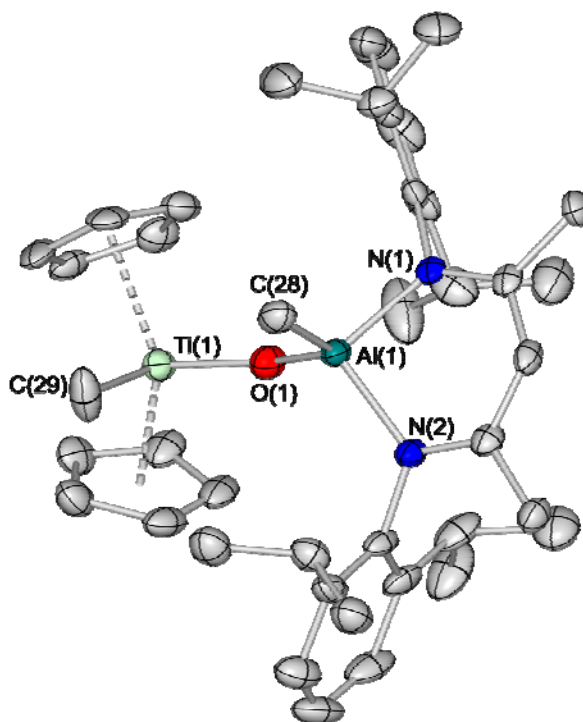
Figure 13. Molecular structure of LMeAl(μ-O)TiMeCp$_2$ (**8**). Thermal ellipsoids are set at 50% probability level. H atoms are omitted for clarity.

The Ti(1)–O(1) bond distance (1.808(3) Å) in compound **8** is significantly shorter

when compared to those in [Cp$_2$Ti(CF$_3$C=C(H)CF$_3$)]$_2$O (av Ti–O, 1.856(6)Å)[120] and the

alkoxide bridged cluster $(Ti_4Zr_2O_4(OBu)_n(OMc)_{10}$, (OMc = methacrylate), (n=2,4,6), Ti–O, av 2.041(5) Å).[121] The Ti(1)–C(29) bond length (2.239(9) Å) is slightly longer when compared to those (av 2.175(5)) in Cp_2TiMe_2.[129]
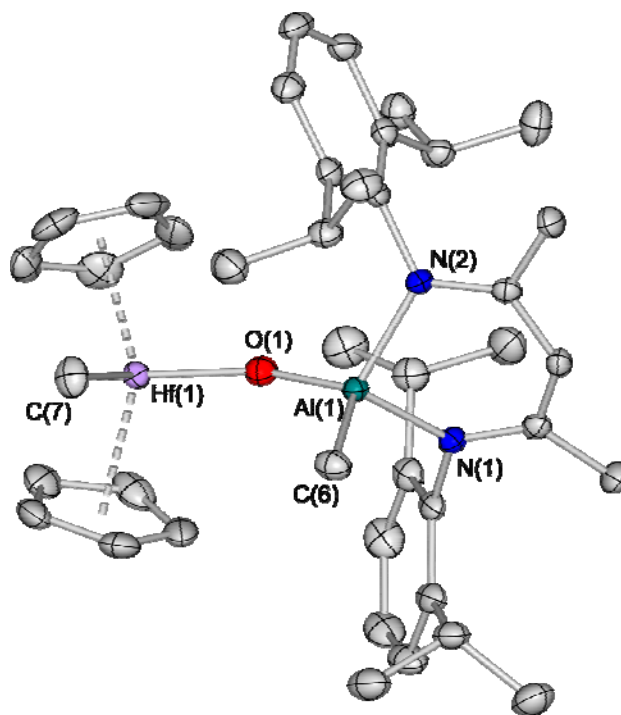
Figure 14. Molecular structure of $LMeAl(\mu\text{-O})HfMeCp_2$ (**9**). Thermal ellipsoids are set at 50% probability level. H atoms are omitted for clarity.

Table 9. Selected Bond Distances (Å) and Angles (deg) for Compound **8**

Ti(1)–O(1)	1.808(3)	Ti(1)–C(29)	2.239(9)
Al(1)–N(1)	1.926(3)	Al(1)–O(1)	1.715(3)
Al(1)–N(2)	1.919(3)	Al(1)–C(28)	1.958(4)
X_{cp1}–Ti(1)	2.134	X_{cp2}–Ti(1)	2.081
N(2)–Al(1)–N(1)	95.7(1)	O(1)–Al(1)–N(2)	113.9(2)
O(1)–Al(1)–N(1)	111.0(2)	O(1)–Al(1)–C(28)	115.2(2)
N(2)–Al(1)–C(28)	110.9(2)	N(1)–Al(1)–C(28)	108.2(2)
Al(1)–O(1)–Ti(1)	151.7(2)	X_{cp1}–Ti(1)–X_{cp2}	130.6
X_{cp1}–Ti(1)–C(29)	100.6	X_{cp2}–Ti(1)–C(29)	99.7
O(1)–Ti(1)–C(29)	95.6(5)	X_{cp2}–Ti(1)–O(1)	110.4

X_{Cp} = Centroid of the Cp ring

The Ti–X_{Cp} (X_{Cp} = centroid of the Cp ring) distances in **8** are almost identical (av 2.108 Å), and are similar to those in dimethyltitanocene (Ti-X_{Cp}, av 2.078 Å).[129] The X_{Cp1}–Ti–X_{Cp2} (X_{Cp} = centroid of the Cp ring) bond angle (130.6º) in compound **8** is comparable to that in Cp_2TiMe_2 (X_{Cp1}–Ti–$X_{Cp2,}$ 134.5º).[129]

The Al(μ-O) (1.71(2) Å) and Al−Me (1.965(2) Å) bond lengths in **9** are in the same range as those observed in **8**. The Hf(1)–O(1) (1.919(2) Å) and Hf(1)–C(7) bond lengths (2.281(2) Å) in **9** are shorter when compared to those of (Hf–O, av 1.943 Å), and (Hf–C av 2.350 Å) in the homobimetallic compound ($Cp_2RHf(\mu$-O)$HfRCp_2$) (R = Me,[128] Cl [117]). The Hf–X_{Cp} (X = centroid of the Cp ring) distance in **9** (av 2.237 Å), is comparable to those of the homobimetallic ($Cp_2HfMe)_2(\mu$-O) Hf–X_{Cp} (av 2.210 Å).[128] The X_{Cp1}–Hf–X_{Cp2} (X = centroid of the Cp ring) bond angle (129.8º) in compound **9** is close to that in [($Cp_2HfMe)_2(\mu$-O)] (128.5º).[128]

Table 10. Selected Bond Distances (Å) and Angles (deg) for Compound **9**

Hf(1)–O(1)	1.919(2)	Hf(1)–C(7)	2.281(2)
Al(1)–N(1)	1.932(2)	Al(1)–O(1)	1.71(2)
Al(1)–N(2)	1.913(2)	Al(1)–C(6)	1.965(2)
X_{cp1}–Hf	2.249	X_{cp2}–Hf	2.224
N(2)–Al(1)–N(1)	95.1(1)	O(1)–Al(1)–N(2)	114.0(1)
O(1)–Al(1)–N(1)	111.6(1)	O(1)–Al(1)–C(6)	113.3(1)
N(2)–Al(1)–C(6)	111.7(1)	N(1)–Al(1)–C(6)	109.8
Al(1)–O(1)–Hf(1)	158.4(1)	X_{cp1}–Hf–X_{cp2}	129.8
X_{cp1}–Hf–C(7)	102.3	X_{cp2}–Hf–C(7)	103.3
O(1)–Hf–C(7)	99.5(1)	X_{cp2}–Hf–O(1)	107.3
X_{cp1}–Hf–O(1)	110.0		

X_{Cp} = Centroid of the Cp ring

2.3.3. Ethylene Polymerization Studies of LMeAl(μ-O)MMeCp$_2$ (M = Ti (8), Hf (9))

The methylalumoxane (MAO)-activated compound of **8** exhibits high catalytic activity for the polymerization of ethylene, whereas the methylalumoxane (MAO)-activated compound of **9** shows low activity for the ethylene polymerization. All polymeric materials were isolated as white powders. Table 11 summarizes the polymerization results of catalysts **8** and **9**. Under comparable polymerization conditions, the MAO/**8** catalyst system shows almost similar activity to that of MAO/LAl(μ-O)ZrRCp$_2$ (L = CH(N(Ar)(CMe))$_2$, Ar = 2,6-iPr$_2$C$_6$H$_3$, R = Me, Cl) (1.711(2) Å).[45] Figure 15 exhibits the plot of activity for different ratios of MAO/**8** revealing a gradual increase in the activity with the MAO/**8** ratios. The data presented in Table 11 clearly demonstrate that compound **8** acts as moderately active catalyst even at low MAO/**8** ratios, a similar result was previously observed for the corresponding Zr-analogue of **8**.[45]

Table 11. Ethylene Polymerization Data for Compounds **8** and **9** as Catalysts[a]

Catalyst	MAO:catalyst	t (min)	PE(g)	A×10^6	Mw	Mw/Mn
8	50	45	1.16	0.08	152817	6.01
8	100	30	3.5	0.36		
8	200	30	5.0	0.51		
8	300	17	3.3	0.60	97909	4.74
8	400	15	4.2	0.86	121996	4.57
8	500	15	5.0	1.03	106020	2.86
9	300	30	0.17	0.02		
9	400	30	0.43	0.04		
9	500	30	0.61	0.06		

[a] Polymerization conditions; **8** and **9** =19.5 μmol, 100 mL of toluene at 25 ºC, and 1 atm of ethylene pressure. Activity (A) = g PE/mol cat·h.
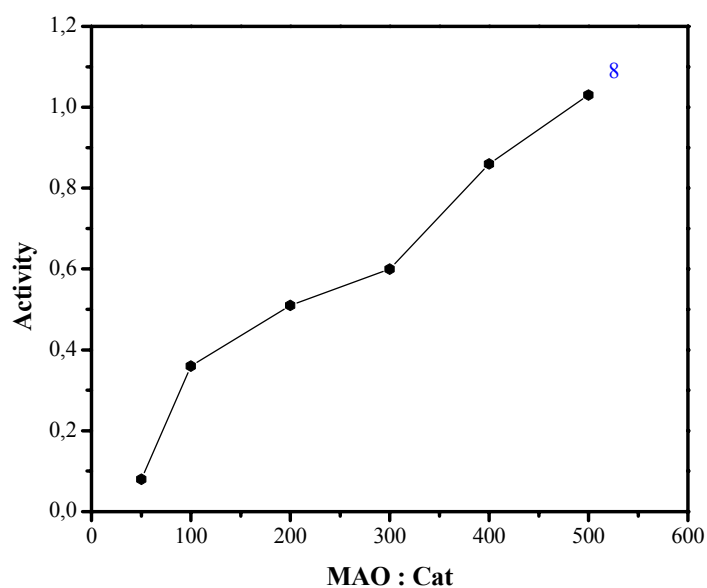
Figure 15. Plot of the activity against MAO ratios for **8** in ethylene polymerization.

2.3.4. Styrene Polymerization Studies of LMeAl(μ-O)TiMeCp₂ (8)

The catalytic property of complex **8** for the polymerization of styrene was preliminarily investigated. This complex shows living catalyst activity at ambient temperature in toluene when activated with MAO. All polymeric materials were isolated as white powders and Table 12 summarizes the activity values of catalyst **8**.

Table 12. Styrene Polymerization Data for Compound **8** as Catalyst[a]

Catalyst	MAO:catalyst	t(min)	PS(g)	$A \times 10^4$	Mw	Mw/Mn	$T_g^{[c]}$(ºC)
8	500	120	0.35	0.78			83.5
8	800	120	0.8	1.8	12989	7.46	76.5
8	1500	120	1.7	3.8			81.7

[a] Polymerization conditions; **8** = 22.5 μmol, 100 mL of toluene at 25 ºC, and 10 mL styrene. Activity (A) = g PE/mol cat.h. [c] DSC.

2.3.5. Properties of Polystyrene Produced by LMeAl(μ-O)TiMeCp₂ (8)

The DSC measurements of the polymers show that the characteristic glass transition temperatures (T_g) are in the range from 76 to 83 ºC which is within the typical T_g range for the atactic polymers.[95] Melting points (T_m) for the polymers were not observed. The GPC for polyethylene exhibits *monomodal* for measured polyethylene samples. The polydispersities show narrow distribution ranging from 2 to 6, which is typical for single site catalysts.

2.4. From Unstable to Stable and Highly Active–The Heterobimetallic Half-Metallocene Catalysts for Olefin Polymerization and Co-polymerization Reactions

Although considerable attention has been devoted to the synthesis, characterization, and catalytic studies of sandwich group 4 metallocene complexes,[130-152] homogeneous half-metallocene complexes of group 4 metals bearing terminal methyl groups (except for the Cp*TiMe$_3$) have received little attention due to the instability of these complexes at ambient temperature.[153-155] However, in recent years there is growing interest[156-168] in monocyclopentadienyl group 4 metal complexes due to the fact that the most active catalysts are those containing the lowest number of valence electrons.[169] The recent developments of mono-cyclopentadienyl based metallocene catalysts are heterogeneous oxide-supported complexes of the type Cp*MMe$_3$ (M = Ti, Zr) for olefin polymerization.[170] These systems exhibit moderate to good catalytic activity and were characterized by some advanced techniques (such as ^{13}C CPMAS, EXAFS).[171] There are some reports on Zr and Ti compounds bearing bulky ligands and terminal methyl groups.[172-175] However, preparing the complexes bearing one Cp′ (Cp′ = Cp/Cp*) and methyl groups still remains a synthetic challenge. Overall, well-characterized, catalytically well studied homogeneous compounds containing one Cp and methyl groups are still elusive.

2.4.1. Synthesis of LMeAl(μ-O)TiMe$_2$Cp (10)

The high oxophilicity of titanium and also the Brönsted acidic character of the proton of the (O−H) moiety on aluminum center allowed us to isolate compound **10** under methane elimination at low temperature in high yield. CpTiMe$_3$ was added slowly to the solution of LMeAl(OH) (**7**) [L = CH(N(Ar)(CMe))$_2$, Ar = 2,6-iPr$_2$C$_6$H$_3$] in hexane at −78 ℃ under

vigorous stirring. The mixture was allowed to stir for 10 min before slowly rising the temperature. At −30 ºC the transparent solution becomes turbid indicating the formation of compound **10**. The temperature of the reaction was raised to 0 ºC and stirred for additional two hours. The stirring is continued at room temperature for another two more hours before filtration (Scheme 8).

Efforts were made to isolate the corresponding chloro-analogues. The reaction of CpTiMeCl$_2$ with LMeAl(OH) (**7**) yielded the eight-membered Ti$_4$O$_4$ ring (by X-ray structural analysis), indicating that Al and Ti center exchange the chlorine and oxygen atoms (Scheme 9).[176(a)]

Scheme 8

Ar = 2,6-iPr$_2$C$_6$H$_3$

Scheme 9

Ar = 2,6-iPr$_2$C$_6$H$_3$
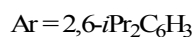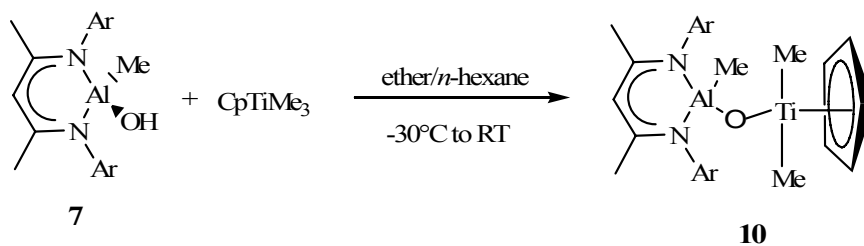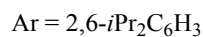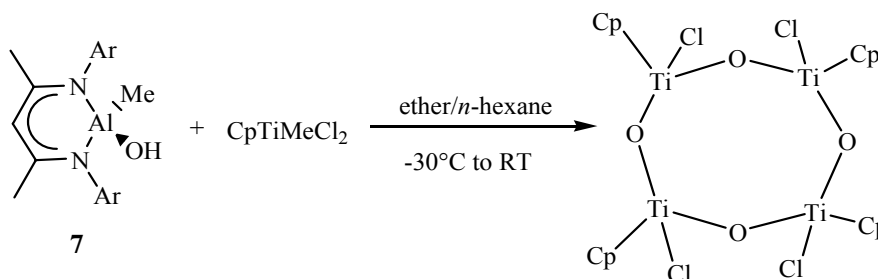
Compound **10** is insoluble in hexane, toluene, and pentane, but sparingly soluble in THF and ether whereas it is freely soluble in hot toluene. Complex **10** was characterized by ^{1}H NMR spectroscopy, EI mass spectrometry, elemental analysis, and by X-ray structural determination. Compound **10** is a yellow solid that melts at 225 ºC. Decomposition was observed at the melting point. Unlike CpTiMe$_3$, compound **10** is thermally stable and not photosensitive. Compound **10** is stable and can be stored for a period of time at room temperature in the absence of air and moisture. The mass spectral data for **10** is in accordance with the assigned structure. Complex **10** does not exhibit a molecular ion. The base peak at *m/z* 588 corresponding to [*M*−2Me]$^+$. The next most intense peak for compound **2** is observed at *m/z* 202 which can be assigned to [DippNCMe]$^+$.[125] The ^{1}H NMR spectrum of **10** exhibits two resonances (δ −0.84 and −0.32 ppm) of 1:2 relative intensities which can be attributed to the Me protons of AlMe and TiMe$_2$ groups, respectively. The characteristic Cp protons for **10** resonate as singlet (δ 5.5 ppm). In addition, a set of resonances assignable to the isopropyl and methyl protons associated with the β-diketiminate ligand is found in the range between δ 1.76 and 1.01 ppm, and the absence of the OH proton resonance features complex **10**. The ^{27}Al NMR is silent due to the quadruple moment of aluminum.
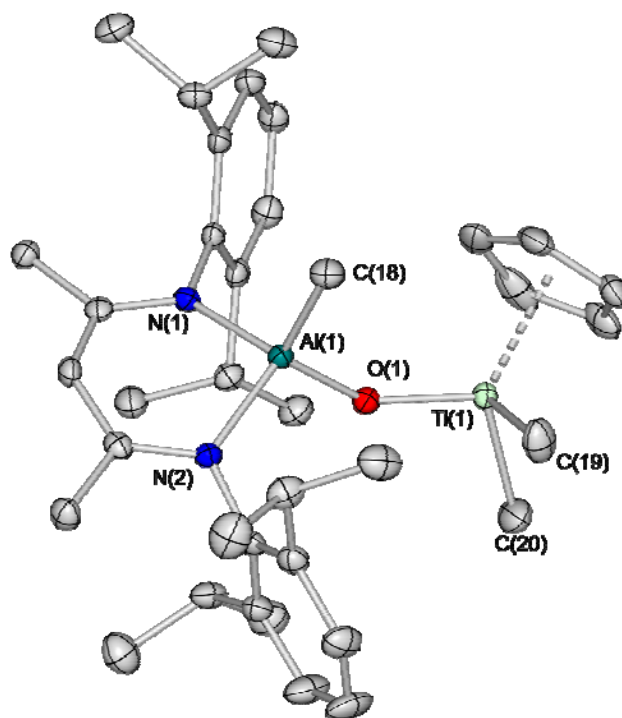
Figure 16. Molecular structure of LMeAl(μ-O)TiMe$_2$Cp (**10**). Thermal ellipsoids are set at 50% probability level. H atoms are omitted for clarity.

2.4.2. Molecular Structure Description of LMeAl(μ-O)TiMe₂Cp (10)

Compound **10** crystallizes in the triclinic space group $P\bar{1}$. Complex **10** shows the aluminum atom bonded through an oxygen atom to titanium and contains a bent Al(μ-O)Ti core. The aluminum atom exhibits a highly distorted tetrahedral geometry with two nitrogen atoms of the β-diketiminate ligand, a methyl group, and one (μ-O) unit. The titanium shows tetrahedral geometry and its coordination sphere is completed by one Cp ligand and two methyl groups around the metal atom. The Me groups on Al and Ti in **10** are bent out of the Al(μ-O)Ti plane in a *trans* configuration (Figure 16).

The Al(μ-O) bond length (1.743(1) Å) in **10** is slightly longer than those for bis(cyclopentadineyl) analogues LMeAl(μ-O)MMeCp$_2$ (L = CH(N(Ar)(CMe))$_2$, Ar = 2,6-iPr$_2$C$_6$H$_3$, M = Ti (**8**), Zr,[45] Hf (**9**)) (av 1.71 Å) but significantly longer than those found in compounds [((Me$_3$Si)$_2$HC)$_2$Al]$_2$(μ-O) (1.69(4) Å),[126] and [HC{(CMe)(NMe)}$_2$AlCl]$_2$(μ-O)

(1.68(6) Å).[127] The Al(μ-O)Ti angle (142.2(4)°) in **10** is significantly narrower than the corresponding Al(μ-O)M, (M = Ti, Zr) bond angles in **11** (154.1°), **8** (151.7(2)°), **12** (155.4(1)°), and LMeAl(μ-O)MMeCp$_2$ (M = Zr,[45] Hf (**9**)) (av 158.3°) complexes. Furthermore, the Al(μ-O)Ti angle in **10** is considerably less opened than those of homobimetallic M(μ-O)M (M = Zr, Hf) in (Cp$_2$ZrMe)$_2$(μ-O) (174.1(3)°),[119] Cp$_2$Ti(CF$_3$C=C(H)CF$_3$)}$_2$(μ-O) (170.0(2)°).[120] and (Cp$_2$HfMe)$_2$(μ-O) (173.9(3)°).[128] The Al$-$Me bond length in compound **10** (1.96(17) Å) is similar to that of LMeAl(OH) (**7**) and LMeAl(μ-O)MMeCp$_2$ (M = Zr,[45] Ti (**8**)) (av 1.96 Å). Selected bond parameters are listed in Table 13.

The Ti(1)–O(1) bond distance (1.764(1) Å) in compound **10** is slightly shorter than the Ti-O bond length (1.81(3) Å) in compound **8** but significantly shorter when compared to those in [Cp$_2$Ti(CF$_3$C=C(H)CF$_3$)]$_2$O (av Ti–O, 1.86(6)Å)[120] and the alkoxide bridged clusters (Ti$_4$Zr$_2$O$_4$(OBu)$_n$(OMc)$_{10}$, (OMc = methacrylate), (n = 2,4,6), Ti–O, av 2.04(5) Å)[121] and Ti$_2$(OiPr)$_2${[(O-2,4-Me$_2$C$_6$H$_2$-6-CH$_2$)$_2$(μ-OCH$_2$CH$_2$)N]}$_2$ Ti-O av 1.98 Å).[176(b)] The Ti–Me bond lengths in **10** (2.11 Å) are similar when compared to those (av 2.11) in Cp$_2$TiMe$_2$.[129] The Ti–X1A (X1A = centroid of the Cp ring) (2.08 Å), distance in **10** is identical and is similar to those in dimethyltitanocene (Ti-X1A, av 2.08 Å).[129]

Table 13. Selected Bond Distances (Å) and Angles (deg) for Compound **10**

Ti(1)-O(1)	1.764(1)	Al(1)-O(1)	1.743(1)
Ti(1)-C(19)	2.104(2)	Al(1)-N(1)	1.913(1)
Ti(1)-C(20)	2.112(2)	Al(1)-N(2)	1.894(1)
Ti(1)- X1A	2.084	Al(1)-C(18)	1.957(2)
Al(1)-O(1)-Ti(1)	142.2(4)	O(1)-Al(1)-C(18)	113.27(7)
O(1)-Ti(1)-C(19)	105.19(7)	O(1)-Al(1)-N(1)	110.51(6)
O(1)-Ti(1)-C(20)	102.50(7)	O(1)-Al(1)-N(2)	109.46(6)
C(19)-Ti(1)-C(20)	97.85(8)	N(1)-Al(1)-N(2)	96.65(6)
X1A- Ti(1)-O(1)	121.9	X1A –Ti(1)- C(19)	114.3
X1A -Ti(1)- C(20)	111.9		

X1A = Centroid of the Cp ring

2.4.3. Synthesis of LMeAl(μ-O)MMe₂Cp*(M = Ti (11), Zr (12))

The higher stability of Cp*MMe₃ (M = Ti, Zr) compared to CpTiMe₃ allowed its reaction with LMeAl(OH) (**7**) at room temperature to form oxygen-bridged heterobimetallic compound LMeAl(μ-O)MMe₂Cp* (M = Ti (**11**), Zr (**12**)) [L = CH(N(Ar)(CMe))₂, Ar = 2,6-iPr₂C₆H₃]. The solution of Cp*MMe₃ (M = Ti, Zr) in ether was added drop by drop to the stirred ethereal solution of **7** at −30 ºC using cannula. The solution was allowed to stir for 10 min and warmed to room temperature. After stirring for 4 hours the precipitate was filtered off and washed with n-hexane before drying under vacuum (Scheme 10).

Scheme 10
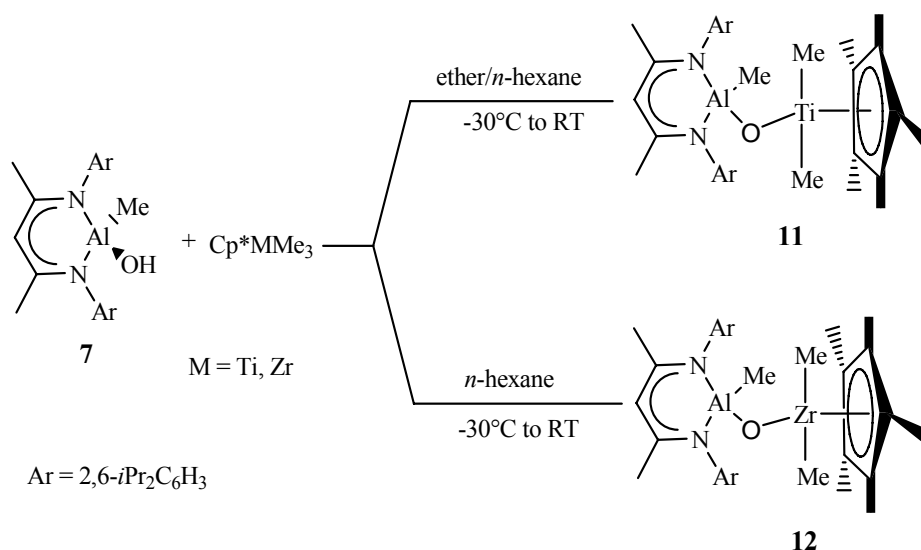
Compounds **11** and **12** are insoluble in hexane, toluene, and pentane, but sparingly soluble in THF and ether whereas freely soluble in hot toluene. Complex **11** was characterized by ^{1}H NMR spectroscopy, EI mass spectrometry, elemental analysis, and X-ray structural analysis while compound **12** was characterized by ^{1}H NMR spectroscopy, elemental analysis, and X-ray structural analysis. Compound **11** is a yellow crystalline solid that melts at 235 ºC while **12** is a colorless crystalline solid which melts at 181 ºC. Decomposition was observed at the melting points of **11** and **12**. Unlike Cp*MMe₃ (M = Ti, Zr) complexes **11** and **12** are

thermally stable for a long period of time. Compound **11** and **12** can be stored for a period of

time at room temperature in the absence of air and moisture. The mass spectral data for **11** is

in accord with the assigned structure. Compound **11** does not exhibit a molecular ion, but

shows the base peak at *m/z* 658 corresponding to $[M-2Me]^+$. The next most intense peak was

observed at *m/z* 202 which can be assigned to $[DippNCMe]^+$.[125] The ^1H NMR spectrum of **11**

exhibits two resonances (δ −0.22 and −0.11 ppm) of 1:2 intensities which can be attributed to

the Me protons of AlMe and TiMe$_2$ groups, respectively, whereas the respective AlMe and

ZrMe$_2$ groups in compound **12** resonate in 1:2 intensities at δ −0.23 and -0.32 ppm. The

characteristic Cp* protons for **11** and **12** appear as singlets (δ 1.67 and 1.85 ppm). In addition,

a set of resonance assignable to the isopropyl and methyl protons associated with the *β*-

diketiminate ligand is found in the range between δ 1.9 and 1.0 ppm, and the absence of the

OH proton resonance features both **11** and **12**. The ^{27}Al NMR is silent due to the quadruple

moment of aluminum.

2.4.4. Molecular Structure of LMeAl(μ-O)MMe₂Cp*(M = Ti (11), Zr (12))

The yellow single crystals of **11** and the colorless single crystals of **12** were obtained

from cooling their hot toluene solutions and were unambiguously analyzed by X-ray

diffraction studies (Figures 17 and 18). The important bond parameters for compounds **11** and

12 are listed in Tables 14 and 15 respectively.

Compounds **11** and **12** crystallize in the monoclinic space group *P*2(1)/*n*. Both

compounds show the aluminum atom bonded through an oxygen atom to titanium and

zirconium respectively, and contain a bent Al(μ-O)M (M = Ti, Zr) core. The aluminum atom

exhibits a highly distorted tetrahedral geometry with two nitrogen atoms of the *β*-diketiminate

ligand, a methyl group, and one (μ-O) unit. The titanium and zirconium exhibit tetrahedral

geometry and their coordination spheres are completed by one Cp* ligand and two methyl

groups around each metal atom. The Me groups on Al and Ti in **11** and Al and Zr in **12** are

bent out of the Al(μ-O)M (M = Ti, Zr) plane in a *trans* configuration.

The Al(μ-O) bond length (1.736(2) Å) in **11** is similar to that of **10** but slightly longer

than those for the bis(cyclopentadineyl) analogues LMeAl(μ-O)MMeCp$_2$ (M = Ti (**8**), Zr,[45]

Hf (**9**)) (av 1.71 Å) and significantly longer than those found in compounds

[{(Me$_3$Si)$_2$HC}$_2$Al]$_2$(μ-O) (1.69(4) Å),[126] and [HC{(CMe)(NMe)}$_2$AlCl]$_2$(μ-O) (1.68(6) Å).[127]

The Al(μ-O)Ti angle (154.04(1)°) in **11** is wider than the corresponding bond angle in **10**

(142.2(2)°), LMeAl(μ-O)TiMeCp$_2$ (**8**) (av 151.7(2)°) but slightly smaller than the Al(μ-O)Zr

bond angle (155.37(10)°) in compound **12** and significantly smaller than LMeAl(μ-

O)MMeCp$_2$ (M = Zr,[45] Hf (**9**)) (av 158.3°) complexes. Furthermore, the Al(μ-O)M (M = Ti,

Zr) angles in **11** and **12** are considerably less opened than those of the homobimetallic M(μ-

O)M (M = Zr, Hf) in (Cp$_2$ZrMe)$_2$(μ-O) (174.1(3)°)[119] and (Cp$_2$HfMe)$_2$(μ-O) (173.9(3)°).[128]

The Al−Me bond length in compound **11** (1.956(3) Å) is similar to thoseof LMeAl(OH) (**7**)

and LMeAl(μ-O)MMeCp$_2$ (M = Zr,[45] Ti (**8**)) (av 1.96 Å).
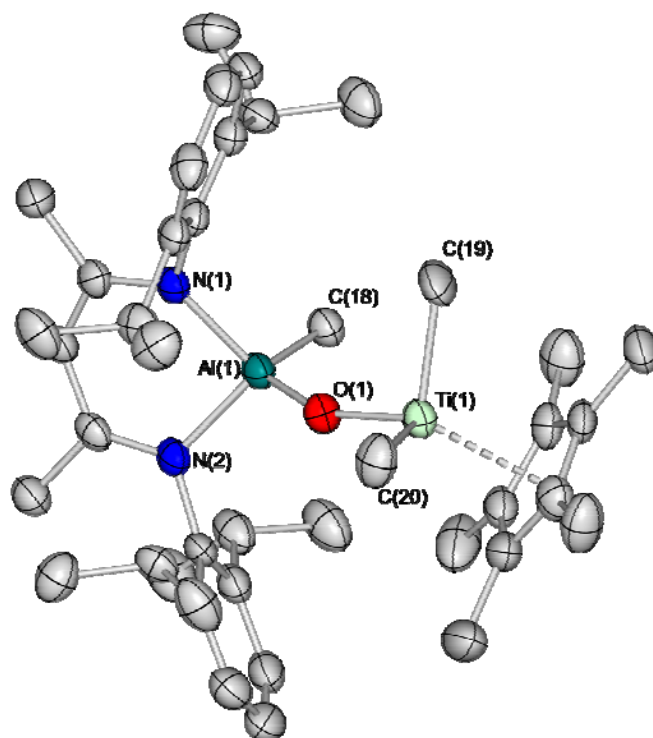
Figure 17. Molecular structure of LMeAl(μ-O)TiMe$_2$Cp* (**11**). Thermal ellipsoids are set at 50% probability level. H atoms are omitted for clarity.

Table 14. Selected Bond Distances (Å) and Angles (deg) for Compound **11**

Ti(1)-O(1)	1.778(2)	Al(1)-O(1)	1.736(2)
Ti(1)-C(19)	2.111(3)	Al(1)-N(1)	1.916(2)
Ti(1)-C(20)	2.116(3)	Al(1)-N(2)	1.921(2)
Ti(1)- X1A	2.082	Al(1)-C(18)	1.956(3)
Al(1)-O(1)-Ti(1)	154.04(1)	O(1)-Al(1)-C(18)	114.42(1)
O(1)-Ti(1)-C(19)	101.12(11)	O(1)-Al(1)-N(1)	112.57(10)
O(1)-Ti(1)-C(20)	106.42(12)	O(1)-Al(1)-N(2)	111.30(10)
C(19)-Ti(1)-C(20)	97.02(15)	N(1)-Al(1)-N(2)	96.32(11)
X1A- Ti(1)-O(1)	124.5	X1A –Ti(1)- C(19)	112.5
X1A -Ti(1)- C(20)	111.4		

X1A = Centroid of the Cp* ring
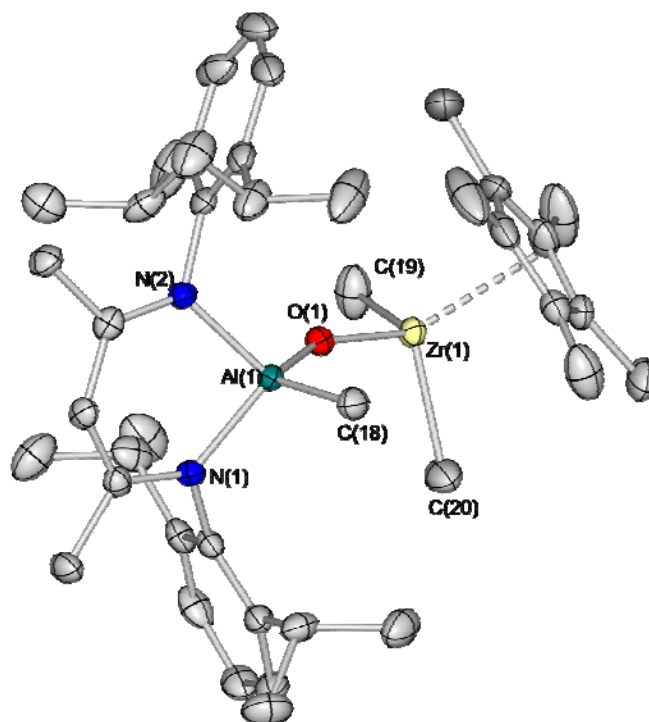
Figure 18. Molecular structure of LMeAl(μ-O)ZrMe$_2$Cp* (**12**). Thermal ellipsoids are set at 50% probability level. H atoms are omitted for clarity.

The Ti(1)–O(1) bond distance (1.778(2) Å) in compound **11** is slightly shorter than Ti–O bond length (1.81(3) Å) in compounds **10** (1.76(11) Å), and **8** (1.808(3) Å) but significantly shorter when compared to those in [Cp$_2$Ti(CF$_3$C=C(H)CF$_3$)]$_2$O (av Ti–O, 1.86(6)Å)[120] and the alkoxide bridged clusters (Ti$_4$Zr$_2$O$_4$(OBu)$_n$(OMc)$_{10}$, (OMc = methacrylate), (n=2,4,6), Ti–O, av 2.04(5) Å)[121] and Ti$_2$(OiPr)$_2$\{[(O-2,4-Me$_2$C$_6$H$_2$-6-CH$_2$)$_2$(μ-OCH$_2$CH$_2$)N]\}$_2$ Ti-O av 1.90 Å).[176(b)] The Ti–Me bond lengths in **11** (2.111(3) and 2.116(3) Å) are similar when compared to those (av 2.18(5) in Cp$_2$TiMe$_2$.[129] The Ti–X1A (X1A = centroid of the Cp ring) (2.082 Å), distance in **11** is identical and are similar to those in dimethyltitanocene (Ti-X1A, av 2.08 Å).[129]

The Al(μ-O) (1.732(2) Å) and Al−Me (1.958(2) Å) bond lengths in **12** are in the same range as those observed in **10** (Al(μ-O), 1.74(11) Å; Al−Me, 1.96 (17) Å) and **11** (Al(μ-O), 1.74(2) Å; Al−Me,1.97(3) Å). The Zr(1)–O(1) (1.920(2) Å) bond distance in **12** is shorter when

compared to the corresponding bond length in the oxygen-bridged (μ-O) compounds $(Cp_2ZrL)_2(\mu$-O) (L = Me, SC_6H_5)[119] (1.95(1) and 1.97(5) Å) and $Cp*_2MeZr(\mu$-O)TiMe_2Cp*$ (**3**) complex (Zr-O, 2.02(4) Å). The Zr–C bond lengths (2.271(3) and 2.249(2) Å) in **12** are comparable to that (2.30 Å) in the heterobimetallic compound $Cp*_2MeZr(\mu$-O)TiMe_2Cp*$ (**3**). The Zr–X1A (X1A = centroid of the Cp ring) distances (2.231 Å) in **12** are appreciably longer than to those in dimethyltitanocene (Ti-X1A av 2.08 Å).[129]

Table 15. Selected Bond Distances (Å) and Angles (deg) for Compound **12**

Zr(1)-O(1)	1.920(2)	Al(1)-O(1)	1.732(2)
Zr(1)-C(19)	2.271(3)	Al(1)-N(1)	1.910(2)
Zr(1)-C(20)	2.249(2)	Al(1)-N(2)	1.921(2)
Zr(1)- X1A	2.231	Al(1)-C(18)	1.958(2)
O(1)-Zr(1)-C(19)	109.08(9)	O(1)-Al(1)-N(1)	111.19(7)
O(1)-Zr(1)-C(20)	102.32(8)	O(1)-Al(1)-N(2)	111.23(7)
C(19)-Zr(1)-C(20)	100.07(11)	N(1)-Al(1)-N(2)	96.36(7)
Al(1)-O(1)-Zr(1)	155.37(10)	O(1)-Al(1)-C(18)	114.57(10)
X1A- Zr(1)-O(1)	122.2	X1A –Zr(1)- C(19)	109.7
X1A -Zr(1)- C(19)	111.0		

X1A = Centroid of the Cp* ring

2.4.5. Account for the Thermal Stability of Compounds 10, 11, and 12

The thermal stability of the metallocene catalysts is one of the most important factors for their application in the industry.[177] For efficient catalytic processes, the model situation is that the catalyst has to be both highly active and thermally stable. The instability of the $Cp'MMe_3$ (Cp′ = Cp or Cp*, M = Ti[153,154] or Zr[155]) complexes do not allow to use them in the polymerization reactions. The heterobimetallic complexes **10, 11,** and **12** exhibit good thermal stability and can be stored for a long period of time in the absence of air or moisture unlike their precursors which should be stored only at very low temperature (Table 16). The

heterobimetallic complexes are stable to air and moisture for a short period of time while their precursors are very sensitive to air and moisture.

Table 16. Comparison of Stabilities of Half-Metallocenes with Heterobimetallic Complexes

Precursor	Thermal Stability	Bimetallic Complexes	Thermal Stability
CpTiMe$_3$	Thermally unstable, decomposes at room temp. Stable only below -30 ºC	10	Thermally stable at room temp for long time. Stable upto 230 ºC
Cp*TiMe$_3$	Thermally stable at room temp for short period. Decomposes above 80 ºC	11	Thermally stable at room temp for long time. Decomposes above 235 ºC
Cp*ZrMe$_3$	Thermally unstable at room temp. Decomposes after 24h. Stable only at -20 ºC	12	Thermally stable for long time. Decomposes above 180 ºC

2.4.6. Ethylene Polymerization Studies of Compounds 10 and 11

In the presensce of methylaluminoxane (MAO), compounds **10** and **11** act as catalysts and exhibit high catalytic activity for the polymerization of ethylene. All polymeric materials were isolated as white powders. Table 17 summarizes the polymerization results of catalysts **10** and **11**. Under comparable polymerization conditions, both MAO/**10** and MAO/**11** catalyst systems show low activity compared to that of MAO/LMeAl(μ-O)M(Me)Cp$_2$ (M = Ti (**8**), Zr[45]). Figure 19 exhibits the plot of activities for different ratios of MAO/**10** and MAO/**11** revealing a gradual increase in the activity with the MAO to catalyst ratios. In general, the

activities of the bis Cp′ (Cp′ = Cp or Cp*) complexes were found to be the highest, about twice those of the monoCp′ analogues. The same trend was previously reported in the literature.[171] The data presented in Table 17 clearly demonstrate that both compounds **10** and **11** act as active catalysts even at low MAO to catalyst ratios, a similar result was previously observed for the corresponding LMeAl(μ-O)M(Me)Cp$_2$ (M = Ti (**8**), Zr[45]) complexes. The plot of activities for compounds **10** and **11** indicates that compound **11** is more active than compound **10** under comparable conditions. This may be due to the formation of a more stable cation in **11** which has a bulky and more electron donating Cp* ligand in its coordination sphere compared to **10** which has a less steric and less electron donating Cp ligand.

2.4.7. Properties of Polyethylene Produced by 10 and 11

Melting points (T$_m$) for the polymers are in the range of 121 to 129 ºC and ^{13}C NMR spectra exhibit single resonance around 30 ppm which can be attributed to the backbone carbon of linear polyethylene. The GPC for polyethylene exhibits *monomodal* for measured polyethylene samples. The polydispersities show narrow distribution ranging from 2 to 5, which corresponds to single site catalysts.[95]

Table 17. Ethylene Polymerization Data for Compounds **10** and **11**[a]

Catalyst	MAO:catalyst	t (min)	PE (g)	$A \times 10^5$	M_w	M_w/M_n	T_m (°C)
10	100	30	0.3	0.3			121
10	200	30	0.9	0.9	103263	2.84	127
10	300	30	1.7	1.6	225027	4.23	124
10	400	30	3.1	3.0			129
11	100	30	0.8	0.8			119
11	200	30	1.7	1.6	124265	4.02	127
11	300	30	3.6	3.4	470431	3.14	130
11	400	30	5.0	4.8			129

[a] polymerization conditions; **10** and **11** = 21 μmol, 100 mL of toluene at 25 °C, 1 atm ethylene pressure. Activity (A) = g PE/mol cat·h
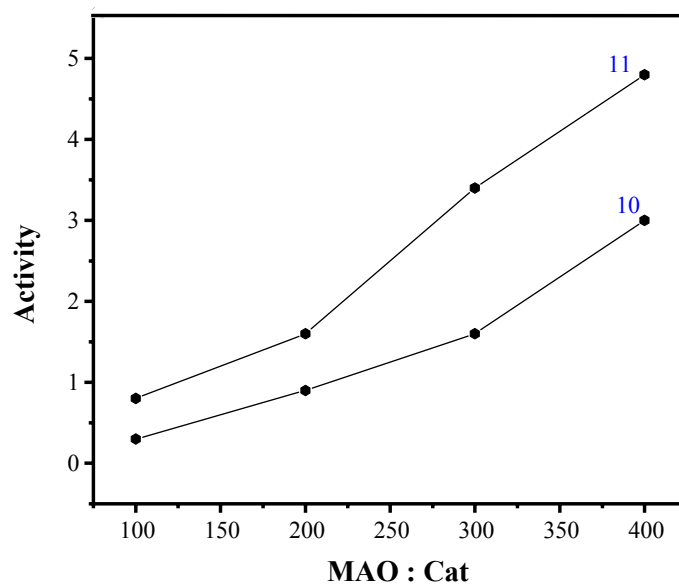
Figure 19. Comparative plot of the activity towards the MAO: cat. for compounds **10** and **11** in ethylene polymerization.

2.4.8. Styrene Polymerization Studies for Compounds 10 and 11

The catalytic property of complexes **10** and **11** for the polymerization of styrene were preliminarily investigated. These complexes show living catalyst activity at ambient temperature in toluene when activated with MAO. All polymeric materials were isolated as white powders and Table 18 summarizes the activity values of catalysts **10** and **11**. Figure 20 exhibits the plot for activity against to MAO to catalyst ratio.

Table 18. Styrene Polymerization Data for Compounds **10** and **11**[a]

Catalyst	MAO:catalyst	t (min)	PS (g)	$A \times 10^4$	T_g (°C)
10	400	60	0.3	1.4	87
10	800	60	0.8	3.8	93
10	1200	60	1.1	5.2	87
10	1600	60	1.7	8.1	81
11	400	60	0.4	1.9	91
11	800	60	1.0	4.8	89
11	1200	60	1.4	6.7	97
11	1600	60	2.5	12.0	88

[a] polymerization conditions; **10** and **11** = 21 μmol, 100 mL of toluene at 25 °C, 10 mL styrene under argon. Activity (A) = g PS/mol cat·h

2.4.9. Properties of Polystyrene Produced by 10 and 11

The DSC measurements of the polymers show that the characteristic glass transition temperatures (T_g) are in the range from 81 to 97 °C which is within the typical T_g range for the atactic polymers.[95] As expected, compound **11** shows more activity compared to compound **10**.
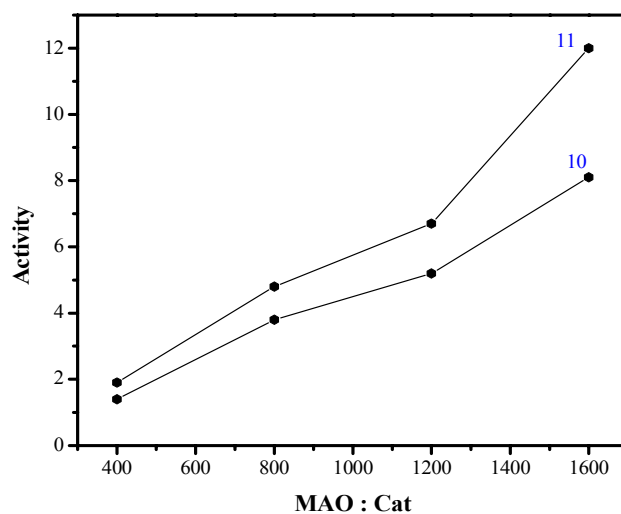
Figure 20. Comparative plot of the activity towards the MAO: cat for compounds **10** and **11** in styrene polymerization.

2.4.10. Ethylene and Styrene Copolymerization Studies for Compounds 10 and 11

Preliminary investigations of ethylene and styrene copolymerization reactions were carried out. The MAO activated complexes **10** and **11** exhibit moderate catalytic activity and produce polymer products. These polymer products were characterized to know the incorporation of styrene into ethylene which can produce polymer of interesting microstructure. The DSC measurements of the polymers show that the melting point temperatures (T_m) are in the range from 116 to 119 ºC. The ^{13}C NMR exhibits only one peak (~30.0 ppm) corresponding to the backbone carbon. These data indicate that the polymer produced by **10** and **11** is polyethylene. The styrene incorporation is negligible (even there is no styrene incorporation) as we did not observe any other resonances in the ^{13}C NMR measurements. The copolymerization results in the homopolymerization of ethylene.

Table 19. Ethylene+Styrene Copolymerization Data for Compounds **10** and **11**[a]

catalyst	MAO:catalyst	t (min)	PE (g)	$A\times 10^{-6}$	$M_w\times 10^{-3}$	M_w/M_n	T_m (°C)
10	400	60	1.7	0.081			116
11	400	60	2.0	0.095	422018	7.17	119

[a] polymerization conditions; **10** and **11** = 21 μmol, 100 mL of toluene at 25 °C, at 1 atm ethylene pressure. 10 mL of styrene. Activity (A)= g PE/mol cat·h

2.5. Synthesis and Reactivity of the Ethyl Substituted Aluminum Hydroxide and Catalytic Properties of its Derivative

2.5.1. Synthesis of LAlEt(Cl) (13) and LAlEt(OH) (14)

Following the protocol of preparing LMeAl(OH) (L = CH(N(Ar)(CMe))$_2$, Ar = 2,6-iPr$_2$C$_6$H$_3$),[45] our interest was intrigued by varying the group R on the aluminum site to extend the perspective of LRAl(OH). In this regard, ethyl substituted aluminum hydroxide LEtAl(OH) (**14**) was prepared by controlled hydrolysis of LEtAlCl (**13**). Then heterobimetallic oxide LEtAl(μ-O)ZrMeCp$_2$ (**15**) was prepared. Compound **13** was obtained in high yield by the similar reaction as reported earlier.[122] The reaction of LLi·OEt$_2$ with 1 equiv of EtAlCl$_2$ in toluene at room temperature afforded the colorless complex **13**. Subsequent hydrolysis of compound **13** was carried out with 1 equiv of H$_2$O in presence of 1,3-diisopropyl-4,5-dimethylimidazol-2-ylidene in toluene at 0 °C to afford compound **14** as a white solid.

The composition of both compounds was confirmed by analytical and spectroscopic methods. The ^{1}H NMR spectrum of **13** shows one quartet (δ –0.04 ppm) and one triplet (δ 0.80 ppm) corresponding to methylene and methyl proton resonances of the ethyl group on aluminum, while in the ^{13}C NMR spectrum the resonances of these groups are assigned to δ –1.00 and 8.54 ppm. In contrast, in the ^{1}H NMR spectrum of **14** the methylene and methyl proton resonances of the ethyl group on aluminum show upfield shifts (δ -0.22 and 0.72 ppm) relative to those of **13**, whereas the corresponding ^{13}C NMR resonances are downfield shifted (δ 1.36 and 9.23 ppm). The singlet (δ 0.64 ppm) in the ^{1}H NMR spectrum of **14** is assigned to the OH proton resonance, while for LMeAl(OH) this resonance was observed at δ 0.53 ppm.[45] This downfield shift is probably due to the electronic effect of the substituent changing from methyl to ethyl group on aluminum. In the IR spectrum of **14,** the OH stretching frequency is

found at 3729 cm^{-1}. The mass spectrum of **14** indicates the monomeric composition with m/z

473 (24) [M^+–OH] and 461 (100) [M^+–Et].

2.5.2. Synthesis of LEtAl(μ-O)ZrMeCp₂ (15)

Reaction of **14** with 1 equiv of Cp$_2$ZrMe$_2$ in toluene at 100 °C afforded the (μ-O)

bridged LEtAl(μ-O)ZrMeCp$_2$ (**15**) (Scheme 11) accompanied by methane evolution.

Scheme 11

Ar = 2,6-iPr$_2$C$_6$H$_3$
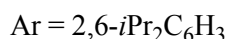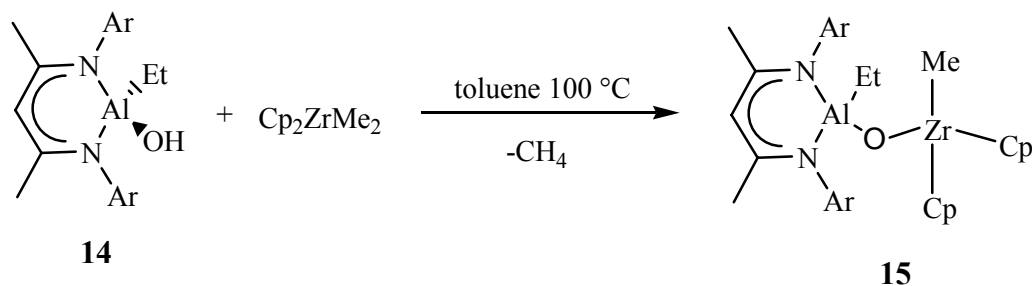
The mass spectrum of **15** exhibits a peak at m/z 709 (88) representing the fragment

[M^+–Me]. In the ^{13}C NMR spectrum of **15** the characteristic Cp resonances appear at δ 109.9

ppm. In the ^{1}H NMR spectrum the Cp resonances exist as singlet (δ 5.30 ppm). One singlet (δ

–0.32 ppm) is assigned to the Me protons of ZrMe, while one quartet (δ –0.14 ppm) and one

triplet (δ 1.14 ppm) are attributed to the methylene and methyl proton resonances of the AlEt

group. No hydroxyl proton resonance is shown in the range of δ 0.50 to 0.65 ppm, which is

consistent with the absence of any OH absorption in the range 3400-3800 cm^{-1} in the IR

spectrum.

2.5.3. Ethylene Polymerization Studies of LEtAl(μ-O)ZrMeCp₂ (15)

Table 20 summarizes the polymerization results of catalyst **15**. All polymeric materials were isolated as white powders. Under comparable polymerization conditions, the methylaluminoxane (MAO)/**15** catalyst system shows lower activity compared to that of MAO/LAlMe(μ-O)MMeCp$_2$ (M = Zr,[45] Ti (**8**)) However the MAO activated compound **15** still exhibits good catalytic activity for the polymerization of ethylene. Figure 21 visualizes the MAO/**15** ratios dependence activity, which reveals a gradual increase in the activity with the MAO/**15** till to 400, followed by a slow decrease as the MAO/**15** ratio is raised further.

Table 20. Ethylene Polymerization Data for Compound **15**

Catalyst	MAO	t (min)	PE (g)	$A \times 10^{-5}$	T_m (ºC)
15	200	30	0.31	0.50	123
15	300	30	0.75	1.20	127
15	400	30	1.21	1.95	121
15	600	30	1.01	1.61	119

[a] polymerization conditions; **15** = 12.4 μmol, 100 mL of toluene at 25 ºC, at 1 atm ethylene pressure. Activity (A) = g PE/mol cat·h

2.5.4. Polymer Properties

DSC measurements show that the melting points (T_m) of the polyethylene produced by MAO activated **15** are in the range of 119 to 127 ºC. The ^{13}C NMR data exhibits a resonance (δ 30.12 ppm) corresponding to the backbone carbon. On the basis of NMR and DSC measurements the polyethylene produced by **15** can be attributed to the linear polyethylene.[95]
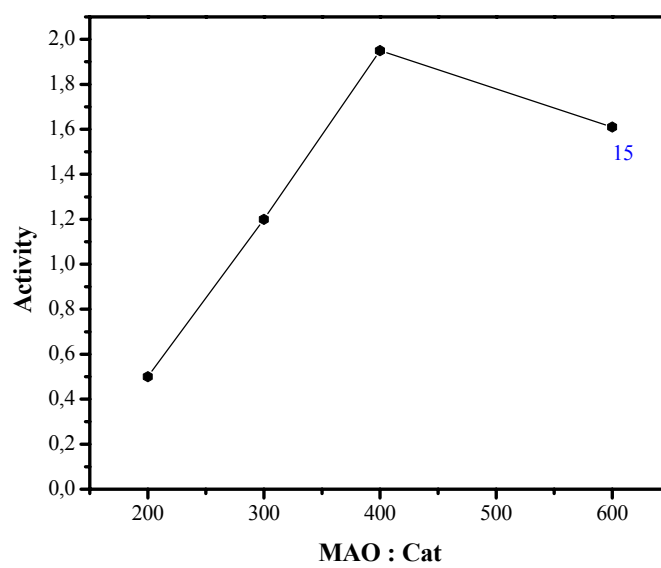
Figure 21. Plot of activity against MAO to catalyst ratio for compound **15**.

2.6. Synthesis and Structural Characterization of Compounds Containing an Al(μ–O)M(μ–O)Al (M = Ti, Zr) Core for Polymerization Reactions

2.6.1. Synthesis of LMeAl(μ–O)M(NMe$_2$)$_2$(μ–O)AlMeL (M = Ti (16), Zr (17))

For sometime, we have been actively involved in the synthesis of a compound bearing the Al(μ-O)M(μ-O)Al trimetallic core with a catalytically active transition metal center (M = Ti, Zr). It was initially anticipated that if instead of one (Me)Al–O unit two such units can be grafted around the active metallic center, the catalytic activity of these complexes might be enhanced many times at even lower cocatalyst to catalyst ratio. Unfortunately, all attempts by varying the starting metallocene based precursors and reaction condition to synthesize such a complex were unsuccessful by reacting LMeAl(μ-O)ZrMeCp$_2$,[45] LMeAl(μ-O)TiMe$_2$Cp (10) or LMeAl(μ-O)TiMe$_2$Cp* (11) with another equivalent of LMeAl(OH) (7). This might be attributed to the high steric crowding around the metal center (M) imposed by bulky C$_5$Me$_5$ or C$_5$H$_5$ ligand hindering the approach of another molecule of 7 to the M–Me unit. Also further reactivity of the M–Me unit in the heterobimetallic complexes might be responsible for this reluctance. However, synthesis of complexes bearing the oxygen bridged trimetallic Al(μ-O)M(μ-O)Al (M = Ti, Zr) core was accomplished by reacting the monometallic hydroxide precursor, LMeAl(OH) (7) with sterically less-crowded group 4 nonmetallocene precursor M(NMe$_2$)$_4$ under elimination of Me$_2$NH. Reaction of two equivalents of 7 with an equivalent of M(NMe$_2$)$_4$ (M = Zr, Ti) in toluene leads to the intermolecular elimination of Me$_2$NH and the formation of the (μ-O) bridged trimetallic complex, LMeAl(μ-O)M(NMe$_2$)$_2$(μ-O)AlMeL (M = Ti (16), Zr (17)) (Scheme 12). The absence of the characteristic OH resonance of LMeAl(OH) (7) in the ^{1}H NMR spectrum of the reaction mixture indicates the complete consumption of 7 into 16 and 17 respectively. These complexes (16, 17) were characterized

by ^{1}H and ^{13}C NMR spectroscopy, elemental analysis, EI mass spectrometry, and single crystal X-ray diffraction studies. Both of these complexes are soluble in *n*-hexane, pentane, toluene, and benzene at room temperature. The ^{1}H NMR spectra of **16** and **17** feature a characteristic singlet each at ~ 2.8 ppm attributed to the –NMe$_2$ protons, and the Al–(Me) protons resonate at ~ –0.6 ppm as another singlet.

Scheme 12

7   Ar = 2,6-*i*Pr$_2$C$_6$H$_3$ M = Ti (**16**), Zr (**17**)
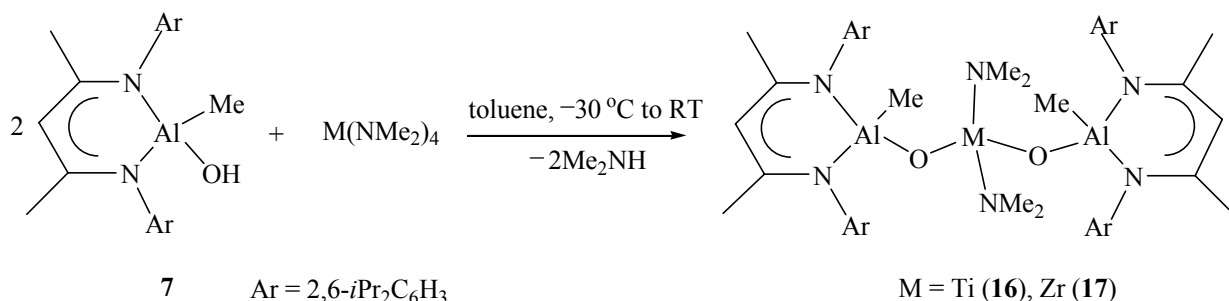
The singlet at ~ 2.8 ppm integrates twice against the singlet at ~ –0.6 ppm revealing the formation of trimetallic complexes as formulated in Scheme 12. In addition, a set of resonances assignable to the protons associated with the *β*-diketiminato ligand (L) are found in the ^{1}H NMR spectra of **16** and **17**. The ^{27}Al NMR is silent due to the quadrupolar nuclei of aluminum. The ^{13}C NMR spectra of **16** and **17** respectively reveal a singlet (~ –11.0 ppm) assigned to the aluminum bound methyl-carbon resonance and another singlet (~ 44.0 ppm) could be assigned to the four methyl carbon resonances arising from the two dimethylamino groups attached to the Ti or Zr center. The mass spectral data for **16** is in accord with the assigned structure. It exhibits the molecular ion peak at *m/z* 1086.8 and the next peak for compound **16** was observed at *m/z* 1071.8 corresponding to [*M*−Me]$^+$. However the mass spectrometry data of **17** is quite different from that of **16** revealing no characteristic fragment except the base peak at *m/e* 202, which can be assigned to [DippNCMe]$^+$.[125] Analytically pure

crystals of **16** and **17** were grown from pentane and *n*-hexane solution respectively and finally the structures of **16** and **17** were unambiguously determined by single crystal X-ray crystallography.

2.6.2. Crystal Structures of LMeAl(μ–O)M(NMe₂)₂(μ–O)AlMeL (M = Ti (16), Zr (17))

The yellow single crystals of **16** and colorless single crystals of **17** were analyzed by X-ray diffraction studies (Figures 22 and 23). Compound **16** was crystallized from pentane at –30 ℃ whereas complex **17** was crystallized from *n*-hexane at 0 ℃. The important bond parameters for compounds **16** and **17** are tabulated in Tables 21 and 22 respectively. Compounds **16** and **17** crystallize in the monoclinic space group $P2_1/c$. Both aluminum atoms are bonded through an oxygen atom to titanium (in **16**) and zirconium (in **17**) respectively, and contain a bent Al(μ-O)M (M = Ti, Zr) core as revealed by the corresponding bond angles (Tables 21 and 22). The aluminum atom exhibits a distorted tetrahedral geometry with two nitrogen atoms of the *β*-diketiminato ligand, a methyl group, and one (μ-O) unit. The titanium or zirconium center also adopts a distorted tetrahedral geometry and their coordination spheres are completed by two dimethylamino ligands and two (μ-O) units. The Al−C(Me) bond length (av 1.96 Å in both **16** and **17**) compares very well to the recently structurally characterized oxygen bridged heterobimetallic compounds of the general formula LMeAl(μ-O)MRCp₂ (R = Me or Cl; M = Ti (**8**) or Zr[45] or Hf (**9**)). The Al(μ-O) bond length (av 1.73 Å in **16** and 1.72 Å in **17**) is in good agreement with that observed for LMeAl(μ-O)TiMeCp₂ (**8**) (1.715(3) Å) and LMeAl(μ-O)ZrRCp₂ (av 1.72 Å, R = Me or Cl)[45] but longer than those found in compounds [{(Me₃Si)₂HC}₂Al]₂(μ-O) (1.687(4) Å),[126] and [HC{(CMe)(NMe)}₂AlCl]₂(μ-O) (1.677(6) Å).[127] The Ti–O bond distance in **16** (av 1.80 Å) and the Zr–O bond length in **17** (av 1.94 Å) are in good agreement with that observed for LMeAl(μ-O)TiMeCp₂ (**8**) (1.808(3) Å) and LMeAl(μ-O)ZrRCp₂ (av 1.92 Å) respectively.[45] Two types of Al(μ-O)M bond angles are noticed in both **16** and **17**. For example, one Al(μ-

O)M bond angle is almost linear (175.58(8)° in **16** and 173.21(10)° in **17**) while the other Al–(μ-O)M bond angle is slightly bent (166.18(9)° in **16** and 166.50(10)° in **17**). These bond angles sharply contrast to the Al(μ-O)M bond angle observed in the heterobimetallic complexes, LMeAl(μ-O)TiMeCp$_2$ (**8**) (151.7(2)°), and LMeAl(μ-O)ZrRCp$_2$ (av 156.8°)[45] or the recently characterized trimetallic complex LMeAl(μ-O)Mg(THF)$_2$(μ-O)AlMeL (av 154.9°)[178] though these values compare well with that observed for the homobimetallic angle, M(μ-O)M (M = Zr, Hf) observed in (Cp$_2$ZrMe)$_2$(μ-O) (174.1(3)°)[119] and (Cp$_2$HfMe)$_2$(μ-O) (173.9(3)°).[128]

2.6.3. Ethylene Polymerization Studies

Preliminary experiments were carried out for ethylene polymerization using compounds **16** and **17** respectively as precatalyst in the presence of methylalumoxane (MAO) as cocatalyst. The results reveal two orders lower activity in magnitude (in the order of 10^4 with MAO to catalyst ratio 800:1, activity = g PE/mol cat·h) even at relatively high MAO to catalyst ratio, when compared to the activity observed in ethylene polymerization with metallocene based heterobimetallic complexes [LMeAl(μ-O)MMeCp$_2$ (M = Ti (**8**), Zr[45]) bearing the Al(μ-O)M moiety] reported from our laboratory. This relatively lower activity in the present study might be attributed to the lower stability of the supposed coordinatively unsaturated cationic intermediate of **16** or **17**.
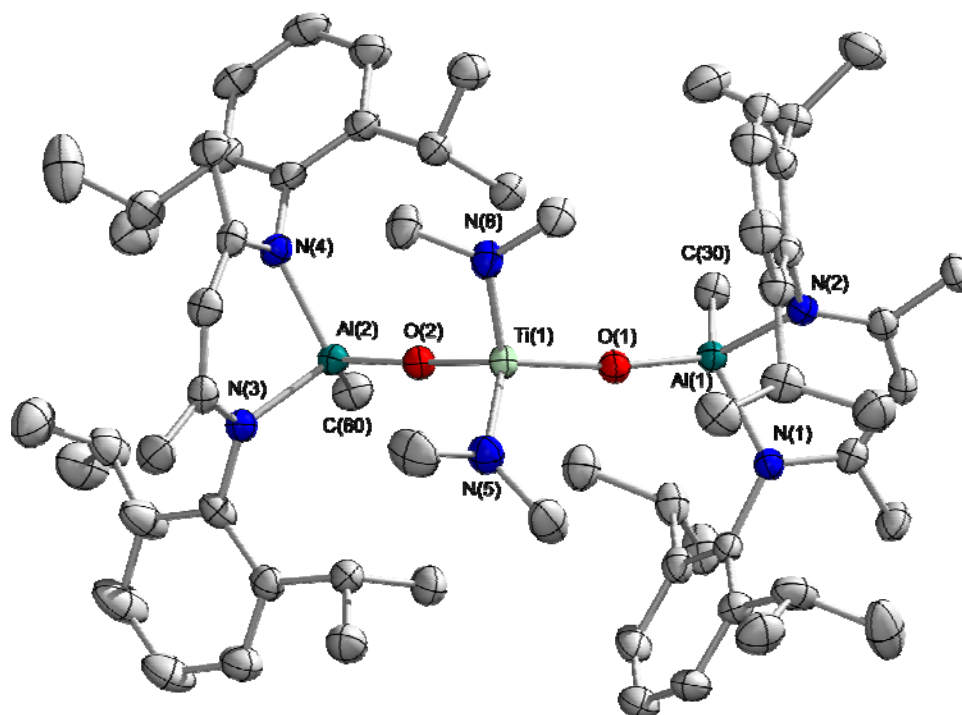
Figure 22. Molecular structure of.LMeAl(μ-O)Ti(NMe$_2$)$_2$(μ-O)AlMeL (**16**) Thermal ellipsoids are set at 50% probability level. H atoms are omitted for clarity.

Table 21. Selected Bond Distances (Å) and Angles (deg) for Compound **16**

Ti(1)–O(1)	1.798(1)	Ti(1)–O(2)	1.809(1)
Ti(1)–N(5)	1.923(2)	Ti(1)–N(6)	1.910(2)
Al(1)–O(1)	1.725(1)	Al(1)–N(1)	1.916(2)
Al(1)–N(2)	1.936(2)	Al(1)–C(30)	1.965(2)
Al(2)–O(2)	1.734(2)	Al(2)–N(3)	1.908(2)
Al(2)–N(4)	1.926(2)	Al(2)–C(60)	1.950(2)
O(1)–Ti(1)–O(2)	119.58(6)	O(1)–Ti(1)–N(6)	108.55(7)
O(2)–Ti(1)–N(6)	106.35(7)	O(1)–Ti(1)–N(5)	106.61(7)
O(2)–Ti(1)–N(5)	109.64(7)	N(6)–Ti(1)–N(5)	105.24(7)
Al(1)–O(1)–Ti(1)	166.18(9)	Al(2)–O(2)–Ti(1)	175.58(8)
O(1)–Al(1)–N(1)	113.34(7)	O(1)–Al(1)–N(2)	113.68(7)
N(1)–Al(1)–N(2)	94.97(7)	O(1)–Al(1)–C(30)	116.96(8)
N(1)–Al(1)–C(30)	108.46(8)	N(2)–Al(1)–C(30)	107.08(8)
O(2)–Al(2)–N(3)	108.22(7)	O(2)–Al(2)–N(4)	107.85(7)
N(3)–Al(2)–N(4)	95.32(7)	O(2)–Al(2)–C(60)	119.24(8)
N(3)–Al(2)–C(60)	110.00(9)	N(4)–Al(2)–C(60)	113.49(8)
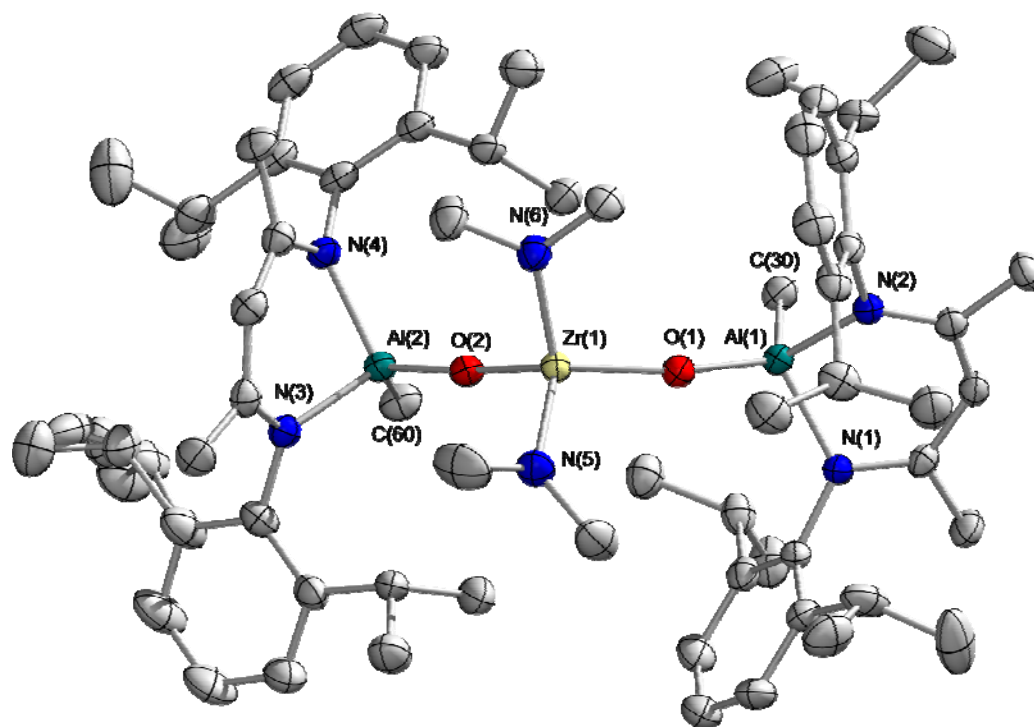
Figure 23. Molecular structure of LMeAl(μ-O)M(NMe$_2$)$_2$(μ-O)AlMeL (**17**) in the crystal (50% probability ellipsoids); hydrogen atoms are omitted for clarity.

Table 22. Selected Bond Distances (Å) and Angles (deg) for Compound and **17**

Zr(1)–O(1)	1.941(2)	Zr(1)–O(2)	1.944(2)
Zr(1)–N(5)	2.072(2)	Zr(1)–N(6)	2.057(2)
Al(1)–O(1)	1.716(2)	Al(1)–N(1)	1.913(2)
Al(1)–N(2)	1.926(2)	Al(1)–C(30)	1.974(2)
Al(2)–O(2)	1.723(2)	Al(2)–N(3)	1.907(2)
Al(2)–N(4)	1.926(2)	Al(2)–C(60)	1.955(3)
O(1)–Zr(1)–O(2)	117.05(7)	O(1)–Zr(1)–N(6)	109.09(7)
O(2)–Zr(1)–N(6)	107.07(7)	O(1)–Zr(1)–N(5)	107.87(7)
O(2)–Zr(1)–N(5)	110.21(8)	N(6)–Zr(1)–N(5)	104.88(8)
Al(1)–O(1)–Zr(1)	166.50(10)	Al(2)–O(2)–Zr(1)	173.21(10)
O(1)–Al(1)–N(1)	112.86(8)	O(1)–Al(1)–N(2)	112.98(8)
N(1)–Al(1)–N(2)	95.20(9)	O(1)–Al(1)–C(30)	117.65(10)
N(1)–Al(1)–C(30)	108.81(10)	N(2)–Al(1)–C(30)	106.92(10)
O(2)–Al(2)–N(3)	107.74(8)	O(2)–Al(2)–N(4)	107.56(9)
N(3)–Al(2)–N(4)	95.20(9)	O(2)–Al(2)–C(60)	119.15(10)
N(3)–Al(2)–C(60)	110.60(11)	N(4)–Al(2)–C(60)	113.83(10)

2.7. Synthesis of Lithiated Salt of Cp$_2$Ti(SH)$_2$

Organometallic hydrosulfido complexes are potentially valuable for study to develop an understanding of metal sulfide based catalysis, especially hydrogenation processes such as hydrodesulfurization. However, these species are still quite rare. One of the older examples, Cp$_2$Ti(SH)$_2$, was first synthesized by Köpf and Schmidt in 1965.[179] The preparation was improved in 1980 by McCall and Shaver,[180,181] but the reactivity studies of Cp$_2$Ti(SH)$_2$ (**18**) reported in literature are limited.[182-186] Important questions are whether deprotonated anionic forms of hydrosulfide complexes are stable and whether they show higher reactivity than neutral sulfides with electrophiles such as SO$_2$.[187-191] Previous work showed that SO$_2$ disproportionates to sulfur and SO$_3$ and also can undergo catalytic hydrogenation on certain sulfur bridged Cr and Mo complexes,[192-194] and earlier metal sulfides may give similar or increased reactivity. Anionic titanium sulfur containing complexes themselves are rare,[195,196] and to our knowledge, there are no reports of triple sulfur bridged titanium bimetallic complexes. The elimination of CpH from a bisCp complex to form a monoCp coordinated Ti is also noteworthy in that [Cp$_2$Ti(S)(SH)]- appears to be unstable, while the related Cp*$_2$Ti(O)L and Cp*$_2$Zr(S)L systems are isolable.[197-200]

2.7.1. Synthesis of Li$_6$[CpTi(μ-S)$_3$]$_2$·6THF (19)

Titanocene bis(hydrosulfide) (**18**) reacts with 1 equiv of LiNMe$_2$ or methyl lithium to produce the anionic titanium sulfido species Li$_6$[CpTi(μ-S)$_3$]$_2$·6THF (**19**), according to Scheme 13. This reaction occurs at room temperature with the solution changing color from red to green in 5 min. The color change is accompanied by the evolution of a gas. This reaction proceeds very slowly at low temperature. The complex can be best stored under cooling in the presence of THF vapor. Compound **19** is also extremely air and moisture sensitive, and elemental analysis was not possible.

Scheme 13

$Cp_2Ti(SH)_2$ ——⟨ MeLi, RT / THF —— LiNMe$_2$, RT / THF ⟩—— $Li_6[CpTi(\mu\text{-}S)_3]_2$ 6THF

18

19
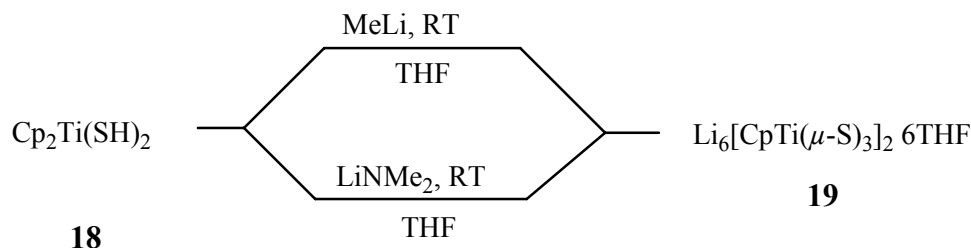
When the reaction is performed on an NMR-tube scale in THF-d_8, a color change occurs within 2 min. During this time, the evolution of a gas is evident. A ^{1}H NMR spectrum of the resulting solution indicates the formation of H$_2$ (δ 4.54 ppm), CpH (δ 6.50 (m), 6.41 (m), 2.94 (s) ppm), and the product complex (δ 6.10 ppm). After some time a signal (δ 5.73 ppm) attributed to a decomposition product, appears in the NMR spectra as reported earlier.[186]
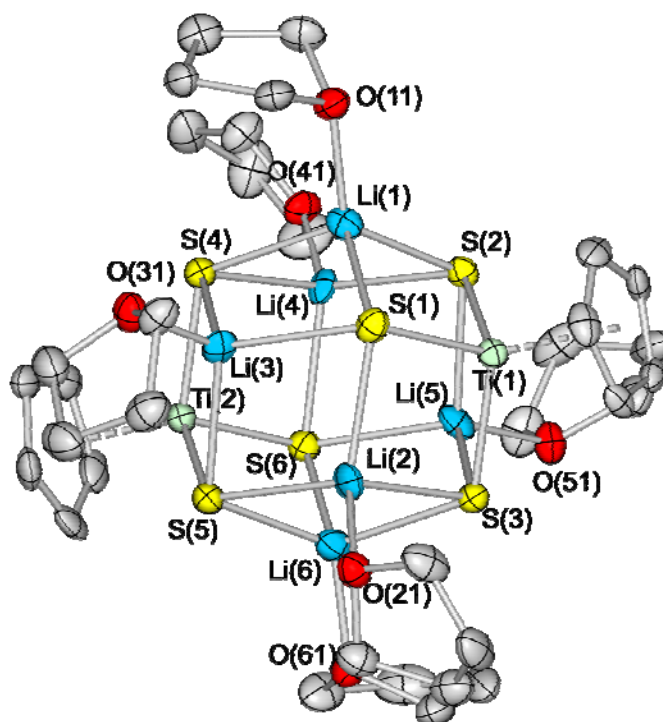
Figure 24. **Molecular structure of [CpTiS$_3$Li$_3$]$_2$·6THF (19), hydrogen atoms are ommited for clarity.**
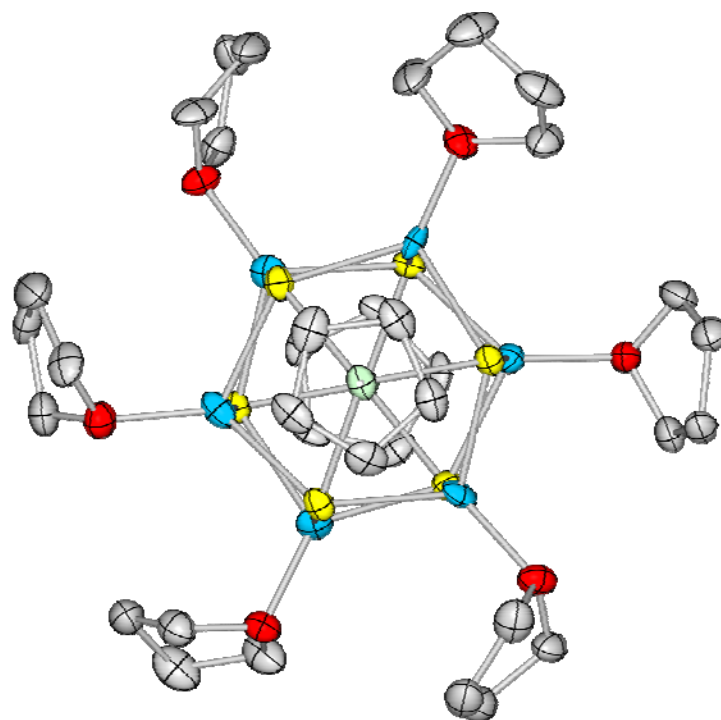
Figure 25. Another view of molecular structure of [CpTiS₃Li₃]₂·6THF (19), hydrogen atoms are ommited for clarity.
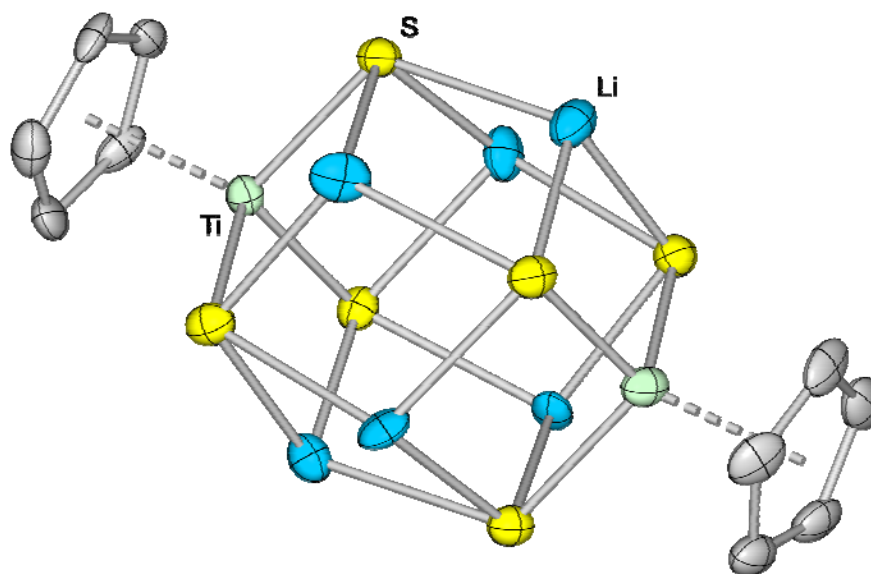
Figure 26. Molecular structure of [CpTiS₃Li₃]₂ (19), without solvent molecules, hydrogen atoms are ommited for clarity.

2.7.2. Molecular Structure of [CpTiS₃Li₃]₂·6THF (19)

The green complex is crystallized by THF at -30 ºC. The THF molecules in the crystal lattice are extremely labile and can be removed in vacuo. The compound crystallizes in triclinic $P\bar{1}$. X-ray structural analysis of **19** shows that the species exists as dimer in the solid state. The dinuclear units stitched together by weak interactions of bridging sulfide ligands with THF-solvated lithium cations (Figure 22). All Li-S distances range from 2.367(11) Å in Li(1)-S(2) to 2.478(12) Å in Li(2)-S(5). Each dimer contains three bridging sulfur atoms, and the dimensions of the nearly planar Ti₃(μ-S)₃ unit (Figure 22) are typical of those found in other μ-S titanium complexes. The Ti(μ-S) bond lengths range from 2.283 to 2.305 Å, and the Ti-Ti distances range from 3.120 to 3.597 Å which are in good agreement with there in earlier reports.[186] Table 24 exhibits the selected bond parameters for compound **19**.

Table 24. Selected Bond Distances (Å) and Angles (deg) for Compound **19**

Ti(1)-S(1)	2.299(2)	Ti(2)-S(4)	2.290(2)
Ti(1)-S(2)	2.290(2)	Ti(2)-S(5)	2.294(2)
Ti(1)-S(3)	2.283(2)	Ti(2)-S(6)	2.305(2)
Ti(1)-X1A	2.409	Ti(2)-X1A	2.410
Li(1)-S(1)	2.444(12)	Li(2)-S(1)	2.412(12)
Li(1)-S(2)	2.367(11)	Li(2)-S(3)	2.437(12)
Li(1)-S(4)	2.551(11)	Li(2)-S(5)	2.478(12)

X1A = Centroid of the Cp ring

3. Summary and Outlook

3.1. Summary

New methods for the preparations of oxygen-bridged heterobi and heterotrimetallic complexes of early transition metals and main group metals which are difficult to achieve by other methods, have been developed during the present work.

The hydrolysis of bis(pentamethylcyclopendienyl) complexes of Zr and Hf resulted in the formation of monohydroxo and dihydroxo complexes. The zirconium monohydroxide (**1**) complex acts as a building block for the preparation of heterobi- and heterotrimetallic complexes which act as catalysts in polymerization reactions. X-ray structural data for complex (**1**) shows the presence of a methyl and an OH group at the same zirconium metal center and reveals the interesting fact that these groups are not involved in any kind of hydrogen bonding.
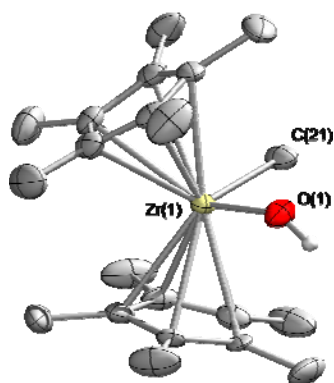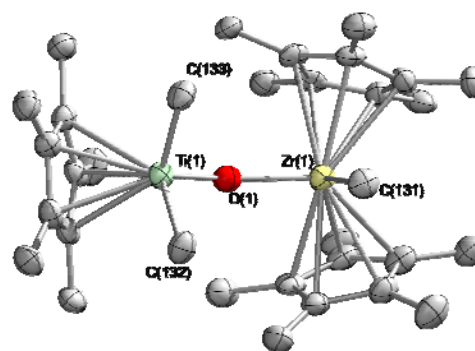
Molecular structure of 1   *Molecular structure of 3*

The unusual kinetic stability of complex **1** allows its reaction with Cp*TiMe$_3$ to yield the first structurally characterized oxygen bridged heterobimetallic complex of group 4 metals. The presence of the Zr(μ-O)Ti core in the compound Cp*$_2$MeZr(μ-O)TiMe$_2$Cp* (**3**) is

confirmed by X-ray structural analysis. Complex **3** exhibits high activity in the ethylene polymerization and produces linear low density polyethylene (LLDPE).

Furthermore, complex **1** helps to achieve a new route to synthesize the hybrid metallocene-nonmetallocene catalysts bearing more than one active catalytic center through oxygen bridging. Heterobi- and heterotrimetallic compounds were isolated by reacting complex **1** with $Ti(NMe_2)_4$ and $Hf(NMe_2)_4$. Reaction of **1** with $Ti(NMe_2)_3$ resulted in the formation of the heterobimetallic complex $Cp*_2MeZr(\mu\text{-}O)Ti(NMe_2)_3$ (**4**) which is further confirmed by X-ray structural study. Compound **4** exhibits moderately high activity in the polymerization reaction of ethylene and styrene and produces linear polyethylene and atactic polystyrene respectively. It produces polyethylene largely controlled by the Zr center and polystyrene seems to be formed predominantly by the Ti center and thus demonstrating that two different catalytic centers can be used for bimodal activity in olefin polymerization.
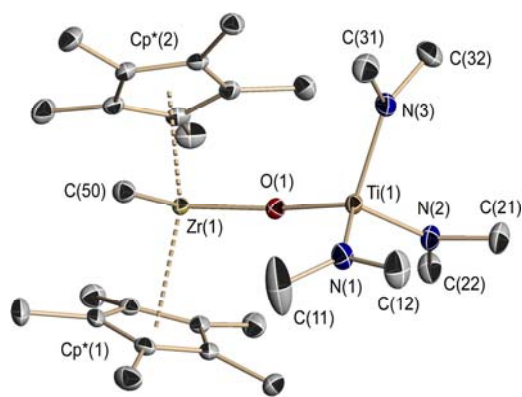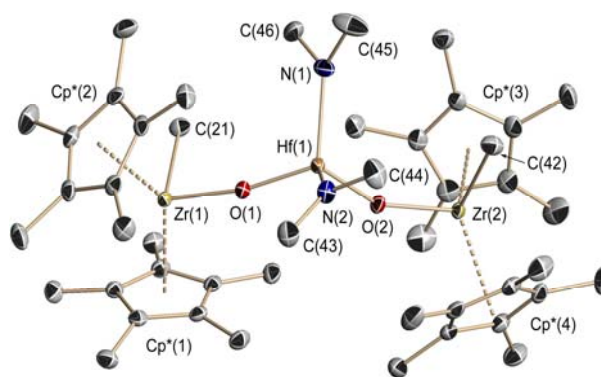
Molecular Structure of 4   *Molecular Structure of 6*

The hafnium amide reacts with **1** in 1:1 and 2:1 stoichiometry to yield heterobi- and heterotrimetallic complexes $Cp*_2MeZr(\mu\text{-}O)Hf(NMe_2)_3$ (**5**) and $Cp*_2MeZr(\mu\text{-}O)Hf(NMe_2)_2(\mu\text{-}O)ZrMeCp*_2$ (**6**) respectively. Characterization of **6** by X-ray diffraction method shows the bent $Zr(\mu\text{-}O)Hf(\mu\text{-}O)Zr$ core. Compound **6** exhibits low activity in the ethylene polymerization reaction.

Taking the advantage of the Brönsted acidic character of the (Al-OH) moiety in the previously reported LMeAl(OH) (**7**) [L = CH(N(Ar)(CMe))$_2$, Ar = 2,6-iPr$_2$C$_6$H$_3$] two kinetically stable heterobimetallic complexes of Al(III) with titanocene and hafnocenes binding through an oxygen bridge were synthesized. Compounds LMeAl(μ-O)TiMeCp$_2$ (**8**) and LMeAl(μ-O)HfMeCp$_2$ (**9**) were characterized by X-ray structural analysis. Unlike Cp$_2$TiMe$_2$ which is highly photosensitive and cannot be used for polymerization, compound **8** was found to be stable, non-photosensitive, and can be used for polymerization reactions. Complex **8** exhibits high catalytic activity in ethylene and styrene homopolymerization while compound **9** shows low activity in ethylene homopolymerization reactions.
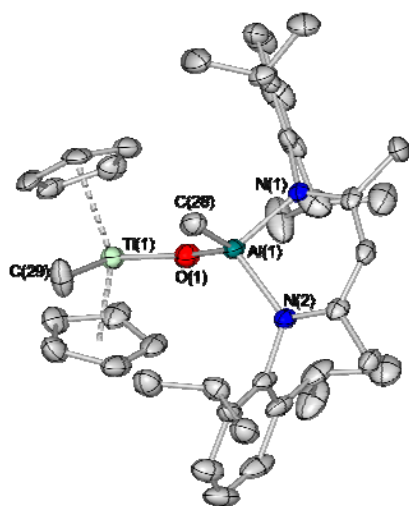
Molecular Structure of 8   *Molecular structure of 9*
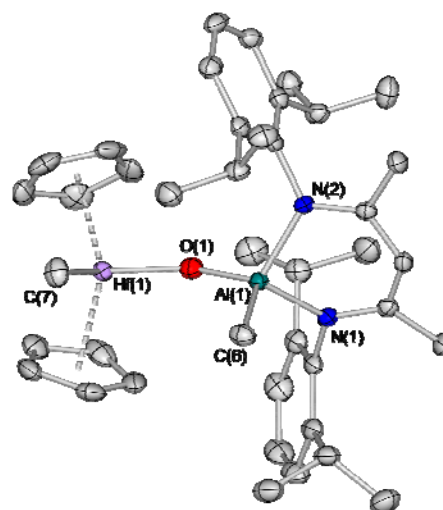
The study of the half-metallocenes of titanium and zirconium bearing terminal methyl groups is limited because of their thermal and kinetic instability. A series of heterobimetallic complexes of half-metallocenes bearing terminal methyl groups have been prepared. The high Brönsted acidic character of LMeAl(OH) **7** allows the preparation of heterobimetallic complexes with Cp′MMe$_3$ (M = Ti, Zr; Cp′ = Cp or Cp*) even at low temperature. Compounds LMeAlOTiMe$_2$Cp (**10**), LMeAlOMMe$_2$Cp* (M = Ti (**11**), Zr (**12**)) were isolated,

characterized by X-ray methods and were used for polymerization reactions. These complexes exhibit both kinetic and thermal stability and are stable for a long period of time. X-ray structural analysis reveals the presence of a bent Al(μ-O)Zr core. Compounds **10** and **11** show high activity in ethylene and styrene polymerization reactions and produce linear polyethylene and atactic polystyrene respectively. Ethylene and styrene copolymerization reactions by using **10** and **11** as catalysts resulted in polyethylene without the incorporation of styrene.
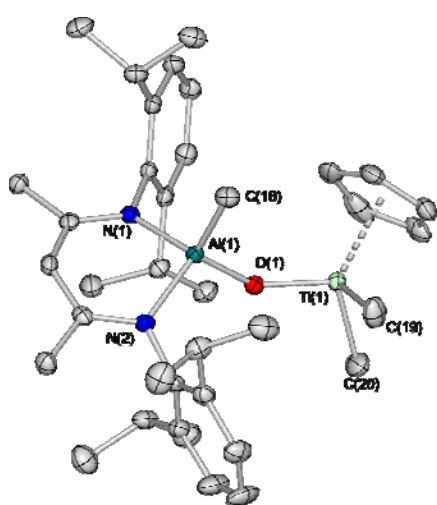
Molecular Structure of 10   *Molecular Structure of 11*
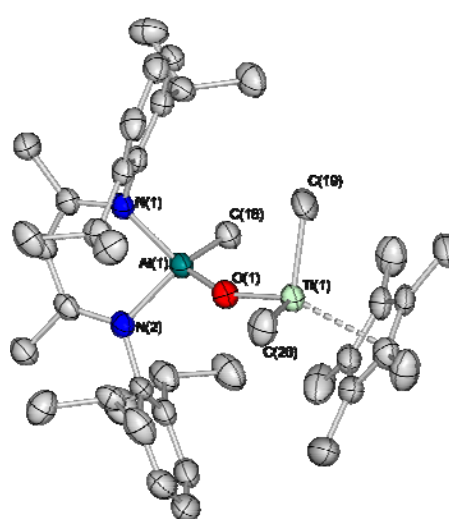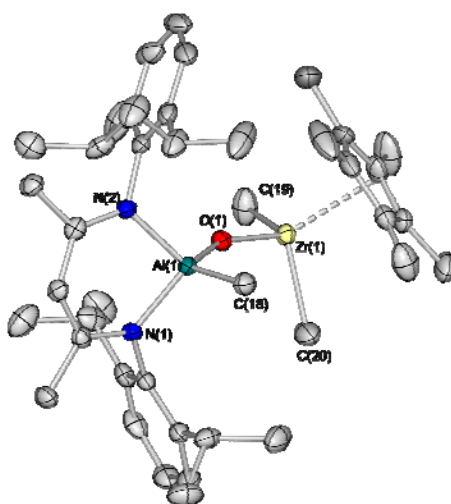
Molecular Structure of 12

Furthermore, the synthetic strategy takes advantage of the kinetically stable precursor LMeAl(OH) (**7**) as a building block. The Brönsted acidic character of the proton in the Al(O−H) moiety allows almost clean reaction with less sterically hindered group 4 metal precursor M(NMe$_2$)$_4$ (M = Ti, Zr) forming compounds with the trimetallic core. X-ray structural study confirms the formation of the trimetallic Al(μ-O)M(μ-O)Al (M= Ti, Zr) core. Preliminary investigation on the catalytic activity of complexes LMeAl(μ-O)Ti(NMe$_2$)$_2$(μ-O)AlMeL (**16**) and LMeAl(μ-O)Zr (NMe$_2$)$_2$(μ-O)AlMeL (**17**) reveal that these complexes exhibit low activity in ethylene polymerization as compared to the oxygen bridged metallocene based heterobimetallic complexes L(Me)Al(μ-O)M(Me)Cp$_2$ (M = Ti, Zr), which could be attributed to the relatively lower stability of the supposed cationic intermediate.
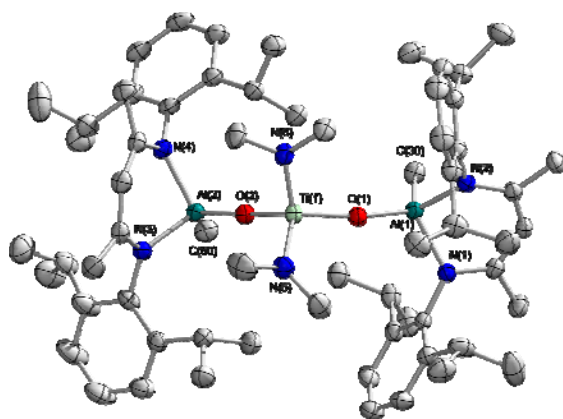
Molecular structure of 16   *Molecular Structure of 17*
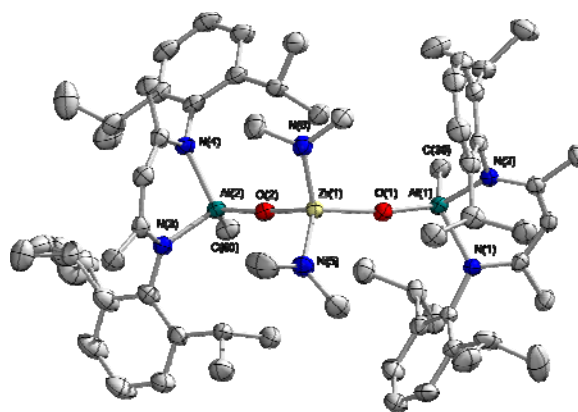
A novel ethyl substituted aluminum hydroxide LAlEt(OH) (**14**) was synthesized by controlled hydrolysis of LAlEtCl (**14**) and characterized analytically and spectroscopically. In subsequent reactions, the proton of the OH group exhibited an expected reactivity by intermolecular elimination of CH$_4$ to afford (μ-O) bridged heterobimetallic compound LEtAl(μ-O)ZrMeCp$_2$ (**15**). Compound **15** was used as catalyst for ethylene polymerization. It exhibits good catalytic activity in ethylene polymerization and produces linear polyethylene.

Lithiation of $Cp_2Ti(SH)_2$ (**18**) was carried out in attempt to prepare sulfur bridged heterobimetallic complexes. The lithiation of **18** by using $LiNMe_2$ or methyl lithium resulted in the formation of an interesting dimeric product of composition $(CpTiS_3Li_3)_2·6THF$ (**19**). The mechanism for this reaction is not clear yet but NMR study reveals the elimination of CpH during the reaction.
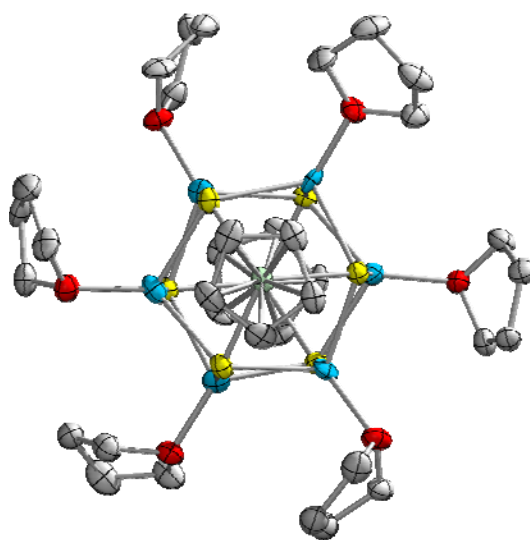
Molecular Structure of 19

The new complexes have been fully characterized analytically and spectroscopically. The solid state structural data for the complexes has been presented. Complexes **3**, **4**, **6**, **8**, **9**, **10**, **11**, **15**, **16**, and **17** were tested as catalysts for the polymerization reactions. The polymer products were characterized analytically and spectroscopically.

3.2. Outlook

The thesis presented here has focused on generating OH functionalities on zirconium and hafnium and studying their reactivity. This resulted in the development of new synthetic strategies for generating heterobi and heterotrimetallic complexes for polymerization reactions. Heterogeneous metal oxides have long been used extensively as very useful catalysts for a variety of inorganic and organic reactions and used directly in the chemical industry, but studies on homogeneous metal oxides are limited because of difficulties in synthesizing molecular species. A new method has been developed in this work for the preparation of metal oxides which are difficult or very expensive to be synthesized by other methods. A great variety of metal and nonmetal oxides could be easily prepared by these methods. Extension of this work in the polymerization reactions resulted in obtaining the polymers in high yield and with interesting microstructure. The bi- and trimetallic catalysts required lower amount of cocatalysts to activate and exhibit high activity in the polymerization reactions.

Furthermore these stable hydroxides of aluminum and zirconium allowed the preparation of very stable complexes from the unstable complexes (such as CpMMe$_3$, M = Ti, Zr) and make them useful to study their catalytic activity in polymerization reactions. In summary, this thesis represents the preparation, structural characterization, and catalytic property of kinetically stable heterobimetallic complexes. Computational study on complex **3** reveals the "Oxygen effect". Moreover, complexes **1**, **2,** and **18** can act as building blocks for the preparation and catalytic studies of the heterobi- and trimetallic complexes bearing later transition and f- block elements.

4. Experimental Section

4.1. General Procedures

All reactions and handling of reagents were performed under an atmosphere of dry nitrogen or argon using Schlenk techniques[201] or a glovebox where the O_2 and H_2O levels were usually kept bellow 1 ppm. All glassware was oven-dried at 140 °C for at least 24 h, assembled hot and cooled under high vacuum prior to use. Toluene (Na/benzophenone ketyl and diphenylether), benzene (K/benzophenone ketyl and diphenylether), hexane (Na/K/benzophenone ketyl and diphenylether), pentane (Na/K/benzophenone ketyl and diphenylether), tetrahydrofuran (K/benzophenone ketyl), diethylether (Na/benzophenone ketyl), dichloromethane (CaH_2) were dried and distilled prior to use. Methanol for termination of polymerization was used of bottle grade (98%).

4.2. Physical Measurements

Melting points were measured in sealed glass tubes on a Büchi B-540 melting point apparatus. NMR spectra were recorded on Bruker Avance 200, Bruker Avance 300, and Bruker Avance 500 NMR spectrometers. Chemical shifts are reported in ppm with reference to $SiMe_4$ (external) for ^1H, ^{13}C and ^{29}Si isotopes, and $[Al(H_2O)_6]^{3+}$ (external) for ^{27}Al nuclei, Downfield shifts from the reference are quoted positive; upfield shifts are assigned negative values. The NMR grade deuterated solvents were dried and in following manners: C_6D_6 − overnight stirring with Na/K alloy followed by vacuum distillation, $CDCl_3$ − 3 min. stirring with P_4O_{10} followed by filtration, THF − storing over freshly activated molecular sieves for one week. Heteroatom NMR spectra were recorded ^1H decoupled. IR spectra were recorded on a Bio-Rad Digilab FTS7 spectrometer in the range of 4000−350 cm^{-1} as KBr pellets. Only the absorption of significant moieties (OH) are listed except for compounds **2−17**, where all

the absorptions (weak to very strong) are reported as the only method for their identification. Mass spectra were obtained with a Finnigan MAT 8230 or a Varian MAT CH5 instrument (70 eV) by EI-MS methods. Elemental analyses were performed at the Analytical Laboratory of the Institute of Inorganic Chemistry at Göttingen, Germany. Crystal structure determination: Intensity data for compounds **1, 9, 16** and **17** were collected on an IPDS II Stoe image-plate diffractometer and compounds **4** and **6** were measured on Bruker SMART-APEX II diffractometer with a D8 goniometer (graphite-monochromated Mo Kα radiation, $\lambda = 0.71073$ Å) equipped with a low-temperature device. The diffraction data for the compounds **2**, **3**, **8, 9**, **10-12**, and **19** were measured on a Bruker three-circle diffractometer equipped with a SMART 6000 CCD detector using mirror monochromated Cu-Kα radiation ($\lambda = 1.54178$ Å). The data for all compounds were collected at low temperature (for exact values see Tables in Section 6). The structures were solved by direct methods (SHELXS-97)[202] and refined with all data by full-matrix least squares methods on F^2 using SHELXL-97.[203] The restraints and constraints as AFIX, DELU, EADP, FLAT, SAME, SADI, SIMU were used to treat disordered groups, lattice solvents such as THF, toluene and trichloromethane and the hydrogen atoms. The non-hydrogen atoms were refined anisotropically; the hydrogen atoms of C−H bonds except the ones on γ-C of the ligand were placed in idealized positions, and refined with a riding model, whereas the hydrogen atoms from the OH, and γ-CH moieties were localized from the difference electron density map and refined isotropically. The crystal data for all compounds along with the final residuals and other pertaining details are tabulated in Section 6.

4.3. Polymerization Reactions

4.3.1. Polymerization of Ethylene and Styrene

On a high vacuum line (10^{-5} Torr), polymerizations were carried out in a 200 mL autoclave (Büchi). In a typical experiment, 100 mL of dry toluene (from Na/K) was vacuum-transferred into the polymerization flask and saturated with 1.0 atm of rigorously purified ethylene (for ethylene homopolymerization) or with argon in the presence of 10 mL of dry styrene (from CaH_2) (for styrene homopolymerization). The catalyst (see corresponding tables) was placed in the Schlenk flask and appropriate MAO (1.6 M in toluene) was added. The mixture was stirred for 20 minutes at room temperature to activate the catalyst. The catalyst solution was then quickly injected into the rapidly stirred flask using a gas-tight syringe. After a measured time interval, the polymerization was quenched by the addition of 5 mL methanol and the reaction mixture was then poured into 800 mL of methanol. The polymer was allowed to fully precipitate overnight and then collected by filtration, washed with fresh methanol, and dried.

4.3.2. Ethylene + Styrene Copolymerization Experiments

On a high vacuum line (10^{-5} Torr), polymerizations were carried out in a 200 mL autoclave (Büchi). In a typical experiment, 100 mL of dry toluene (from Na/K) was vacuum-transferred into the polymerization flask which was previously saturated with 1.0 atm of rigorously purified ethylene in the presence of 10 mL of dry styrene (from CaH_2) The catalyst (see corresponding tables) was placed in the Schlenk flask and appropriate MAO (1.6 M in toluene) was added. The mixture was stirred for 20 minutes at room temperature to activate the catalyst. The catalyst solution was then quickly injected into the rapidly stirred flask using a gas-tight syringe. After a measured time interval, the polymerization was quenched by the addition of 5 mL methanol and the reaction mixture was then poured into 800 mL of

methanol. The polymer was allowed to fully precipitate overnight and then collected by filtration, washed with fresh methanol, and dried.

4.3.3. Polymer Characterization

^{13}C NMR assays of polymer microstructure were conducted in 1,1,2,2-tetrachloroethane-d$_2$ at 110 $^{\circ}$C. Resonances were assigned according to the literature for polyethylene and ethylene + α-olefin copolymers.

Differential Scanning Calorimetric measurements of the polymer melting curves were measured on a TA instrument 2920 (Modulated Differential Scanning Calorimeter) which was calibrated against indium metal. Typically ca. 4 mg samples were used (10 $^{\circ}$C/min).

Gel Permeation Chromatography (GPC) was carried out at Basell R & D Polymer Physics and Characterization, Industriepark, Hoechst, Frankfurt (Germany). 1,2,4-Trichlorobenzene was used as solvent. The columns were calibrated with narrow molar mass distribution standards of polystyrene.

The polymer melting range was measured on a TA instrument 2920 (Modulated Differential Scanning Calorimeter) which was calibrated against indium metal. Typically ca. 4 mg samples were used (10 $^{\circ}$C/min).

4.4. Computational Details

The calculations were performed at the well established DFT level of theory making use of the B3LYP-functional[204,205] as implemented in the Gaussian program package[206] making use of basis-sets termed LANL2DZ[207] for Ti and 6-31G.[208,209] with additional double-diffuse functions for the remaining atoms. In the first step the compound was fully optimized to its equilibrium structure. The analysis of the resulting electronic wavefunction for this

structure was then used to obtain the shape of the molecular orbitals and to analyze the bonding situation by means of a NBO-analysis.[169, 211]

4.5. Starting Materials

Cp$'_2$MCl$_2$ (Cp$'$ = Cp/Cp*; M = Ti, Zr, Hf) (Aldrich), Cp$'$MCl$_3$ (Cp$'$ = Cp/Cp*; M = Ti, Zr, Hf)(Aldrich), Cp*MMe$_2$ (M = Zr, Hf) (Aldrich), Methlyaluminoxane (MAO) (Aldrich), M(NMe$_2$)$_4$ (M = Ti, Zr, Hf) (Aldrich), LiNMe$_2$ (Aldrich), were used as received. Cp$'$MMe$_3$ (Cp$'$ = Cp/Cp*; M = Ti[153,154], Zr[155]) Cp$_2$MMe$_2$ (M = Ti,[123] Zr, Hf[124]) Cp$_2$Ti(SH)$_2$,[180] LMeAl(OH) (**7**)[122] were prepared according to the literature.

4.6. Synthesis of Compounds from 1-19

4.6.1. Synthesis of Cp*$_2$ZrMe(OH) (1)

Cp*$_2$ZrMe$_2$ (0.5 g, 1.28 mmol) was dissolved in n-hexane (30 mL). The resulting solution was cooled to –30 ºC and 1 equivalent of H$_2$O (23 μL) was added rapidly under vigorous stirring. The temperature of the solution was maintained at –30 ºC for 10 min, then was slowly warmed to ambient temperature and stirred for another 30 min till methane evolution has ceased. The solvent was removed in vacuum to obtain colorless crystalline material. Yield 0.36 g (72%). Mp 202 ºC (decomp). IR (KBr): $\tilde{v}$ = 3680, 2965, 2908, 1492, 1440, 1380, 1262, 1099, 1022, 941, 865, 801 cm^{-1}; ^{1}H NMR (500 MHz, C$_6$D$_6$, 25 ºC, TMS): δ: –0.2 (s, 3H, Zr–CH_3), 1.8 (s, 30H, C$_5$(CH_3)$_5$), 4.2 (s, 1H, OH); ^{13}C NMR (500 MHz, C$_7$D$_8$, 25 ºC, TMS): δ: 118.7 (s, Cp*$_2$, C_{10}), 27.0 (s, CH$_3$); MS (EI) m/z (%): 377 (100) [M–Me]$^+$. Anal. Calcd for C$_{21}$H$_{34}$OZr (393.72): C 64.06, H 8.70. Found: C 63.86, H 8.62.

4.6.2. Synthesis of Cp*$_2$Hf(OH)$_2$ (2)

Cp*$_2$HfMe$_2$ (0.52 g, 1.5 mmol) was dissolved in *n*-hexane (30 mL). The resulting solution was cooled to −30 ºC and 1 equivalent of H$_2$O (27 μL) was added rapidly under vigorous stirring. The temperature of the solution was maintained at −30 ºC for 10 min, then was slowly warmed to ambient temperature and stirred for another 30 min till methane evolution has ceased. The solvent was removed in vacuum to obtain colorless crystalline material. Yield 0.36 g (72%). ^{1}H NMR is according the earlier report.[115]

4.6.3. Synthesis of Cp*$_2$MeZr(μ-O)TiMe$_2$Cp*(3)

A solution of Cp*TiMe$_3$ (0.228 g, 1.00 mmol) in diethyl ether (30 mL) was added dropwise to a solution of **1** (0.394 g, 1.00 mmol) in diethyl ether (30 mL) at   −30 ºC. The resulting solution was stirred at −30 ºC for 5 min and was slowly warmed to ambient temperature. Vigorous methane elimination was noticed with concomitant formation of a precipitate. After stirring for additional 12 h the solvent was removed in vacuum and the crude product was washed with *n*-hexane, to give a yellow powder. Yield 0.5 g (64%). Mp 224 ºC (decomp). ^{1}H NMR (500 MHz, C$_6$D$_6$, 25 ºC, TMS): δ: 0.22 (s, 6H, Ti–(CH_3)$_2$), 0.4 (s, 3H, Zr–CH_3), 1.8 (s, 30H, C$_5$(CH_3)$_5$), 2.2 (s, 15H, C$_5$(CH_3)$_5$); ^{13}C NMR (500 MHz, C$_7$D$_8$, 25 ºC, TMS): δ: 118.2 (s, Cp*$_2$Zr, C_{10}), 121.4 (s, Cp*Ti, C_5), 52.3 (s, Ti–(CH$_3$)$_2$), 34.8 (s, Zr–CH_3); MS (EI) *m/z* (%): 574.2 (100) [*M*–2Me]$^+$, 589.2 (6%) [*M*–Me]$^+$. Anal. Calcd for C$_{33}$H$_{54}$OTiZr (605.88): C 65.42, H 8.98. Found: C 64.72, H 8.92.

4.6.4. Synthesis of Cp*$_2$(Me)Zr(μ-O)Ti(NMe$_2$)$_3$ (4)

A solution of Cp*$_2$MeZr(OH) (**1**) (0.394 g, 1.00 mmol) in toluene (20 mL) was added dropwise over a period of 15 min to a solution of Ti(NMe$_2$)$_4$ (0.224 g, 1.00 mmol) in toluene

(30 mL) at 25 ºC. The solution was then stirred at 25 ºC for 24 h. The resulting light yellow solution was then passed through an activated celite pad, concentrated to approximately 15 mL under reduced pressure and kept at –20 ºC for a day yielding yellow micro-crystals of analytical purity. Yield 0.520 g (91 %). Mp 171-172 ºC. ^{1}H NMR (500 MHz, C_6D_6, 25 ºC, TMS): δ: 0.01 (s, 3H, Zr–CH_3); 1.89 (s, 30H, Zr–C$_5$(CH_3)$_5$); 3.14 (s, 18H, Ti–N(CH_3)$_2$). ^{13}C NMR (125.75 MHz, C_6D_6, 25 ºC, TMS): δ: 11.3 (s, Zr–C$_5$(CH$_3$)$_5$); 29.1 (s, Zr–CH$_3$); 45.4 (s, Ti–N(CH$_3$)$_2$); 117.7 (s, Zr–C$_5$(CH$_3$)$_5$). MS (EI) m/z (%) : 556.2 (14) [M – Me]$^+$; 526.2 (56) [M – NMe$_2$]$^+$; 511.1 (100) [M – Me and NMe$_2$]$^+$. Anal. Calcd for $C_{27}H_{51}N_3OTiZr$ (572.83): C 56.61, H, 8.97, N 7.33. Found: C 56.46, H 8.65, N 7.17.

4.6.5. Synthesis of Cp*$_2$(Me)Zr(μ-O)Hf(NMe$_2$)$_3$ (5)

A solution of Cp*$_2$MeZr(OH) (**1**) (0.394 g, 1.00 mmol) in toluene (20 mL) was added dropwise over a period of 15 min to a solution of Hf(NMe$_2$)$_4$ (0.354 g, 1.00 mmol) in toluene (30 mL) at –30 ºC. The resulting solution was slowly warmed to ambient temperature. This solution was then stirred at 25 ºC for 24 h. The title compound could not be isolated in a pure form. ^{1}H NMR spectroscopy of the reaction mixture showed formation of the title compound as the major product along with the trimetallic compound **6** as the minor product.
^{1}H NMR (200 MHz, C_6D_6, 25 ºC, TMS): δ: –0.07 (s, 3H, Zr–CH_3); 1.88 (s, 30H, Z– C$_5$(CH_3)$_5$); 3.00 (s, 18H, Hf–N(CH_3)$_2$).

4.6.6. Synthesis of Cp*$_2$(Me)Zr(μ-O)Hf(NMe$_2$)$_2$(μ-O)Zr(Me)Cp*$_2$ (6)

A solution of Cp*$_2$MeZr(OH) (**1**) (0.433 g, 1.1 mmol) in toluene (20 mL) was added dropwise over a period of 15 min to a solution of Hf(NMe$_2$)$_4$ (0.177 g, 0.50 mmol) in toluene

(20 mL) at −30 ºC. This solution was slowly warmed to ambient temperature and was stirred at 25 ºC for 24 h. The resulting solution was filtered, concentrated to approximately 15 mL under reduced pressure and kept at −20 ºC for several days yielding colorless crystals of analytical purity. Yield 0.420 g (80 %). Mp 312-313 ºC. ^{1}H NMR (500 MHz, C_6D_6, 25 ºC, TMS): δ: −0.05 (s, 6H, Zr–CH_3); 1.92 (s, 60H, Zr–$C_5(CH_3)_5$); 2.99 (s, 12H, Hf–N(CH_3)$_2$). ^{13}C NMR (125.75 MHz, C_6D_6, 25 ºC, TMS): δ: 11.6 (s, Zr–$C_5(CH_3)_5$); 27.9 (s, Zr–CH_3); 43.5 (s, Hf–N(CH_3)$_2$); 117.7 (s, Zr–$C_5(CH_3)_5$). MS (EI) m/z (%) : 1037.4 (24) $[M – Me]^+$, 1007.4 (32) $[M – NMe_2]^+$, 992.3 (100) $[M – Me$ and $NMe_2]^+$. Anal. Calcd for $C_{46}H_{78}Hf$ $N_2O_2Zr_2$ (1052.03): C 52.51, H 7.47, N 2.66. Found: C 51.95, H 7.29, N 2.53.

4.6.7. Synthesis of LA(Me(µ-O)TiMeCp$_2$ (8)

A solution of freshly prepared Cp$_2$TiMe$_2$ (0.21g, 1.01mmol) in toluene (20 mL) was added via cannula to a solution of LMeAl(OH) (7) [L = CH(N(Ar)(CMe))$_2$, Ar = 2,6-iPr$_2$C$_6$H$_3$] (0.48g, 1.01 mmol) in toluene (20 mL) at ambient temperature. (NOTE: Care must be taken because Cp$_2$TiMe$_2$ is photosensitive). The reaction mixture was heated to 80 ºC for 18 h under stirring. The yellow precipitate formed was filtered off, washed with n-hexane, and dried in vacuum. Yield 0.41g (61%); decomp at 250 ºC ; ^{1}H NMR (500.13 MHz, C_6D_6, 25 ºC, TMS) δ 7.13-7.24 (m, 6H; m-, p-Ar-H), 5.30 (s, 10H; C$_5H_5$), 4.90 (s, 1H; γ-CH), 3.10 (sept, 4H; $^3J_{H-H}$ = 6.8 Hz; CH(CH$_3$)$_2$), 1.68 (s, 6H; CHB_3), 1.40 (d, 12H; $^3J_{H-H}$ = 6.8 Hz; CH(CH_3)$_2$), 1.31 (d, 12H; $^3J_{H-H}$ = 6.8 Hz; CH(CH_3)$_2$), −0.18 (s, 3H; Ti-CH_3), −0.91 (s, 3H; Al-CH_3) ppm; ^{13}C NMR (125.75 MHz, C_6D_6, 25 ºC, TMS) δ 165.4(CN), 145.3, 144.8, 142.8, 128.6, 125.9, 125.2 (i-, o-, m-, p-Ar), 111.3 (C$_5$H$_5$), 97.0 (γ-CH), 27.9 (Ti-CH$_3$), 26.5 (Al-CH$_3$) ppm; MS (EI) m/z (%): 653 (100) $[M^+ −Me]$, 638 (48) $[M^+ −2Me]$, 202 (26) [DippNCMe]$^+$. Anal. Calcd for $C_{41}H_{57}AlN_2OTi$ (668.75): C 73.64, H 8.59, N 4.19. Found: C 72.28, H 8.47, N 4.17.

4.6.8. Synthesis of LMeAl(μ-O)HfMeCp₂ (9)

Freshly sublimed Cp_2HfMe_2 (0.34g, 1 mmol) dissolved in ether (20 mL) was transferred using a cannula to a flask charged with LMeAl(OH) **7** (0.48g, 1 mmol) in diethyl ether (30 mL) at −30 ºC. The reaction mixture was slowly warmed to ambient temperature and stirred for 18 h. The precipitate was filtered, washed with *n*-hexane, and dried in vacuum. Yield 0.54 g (67.4%); decomp at 391 ºC; ^{1}H NMR (500.13 MHz, C_6D_6, 25 ºC, TMS) δ 7.13-7.24 (m, 6H; *m*-, *p*-Ar-*H*), 5.40 (s, 10H; C_5H_5), 4.80 (s, 1H; *γ*-C*H*), 3.30 (sept, 4H; $^3J_{H-H} = 6.8$ Hz; C*H*(CH₃)₂), 1.76 (s, 6H; C*H₃*), 1.61 (d, 12H; $^3J_{H-H} = 6.8$ Hz; CH(C*H₃*)₂), 1.42 (d, 12H; $^3J_{H-H} = 6.8$ Hz; CH(C*H₃*)₂), 0.08 (s, 3H; Hf-C*H₃*), −0.27 (s, 3H; Al-C*H₃*) ppm; ^{13}C NMR (125.75 MHz, C_6D_6, 25 ºC, TMS) δ 168.3(*C*N), 149.5, 146.6, 144.7, 132.4, 135.5, 137.9 (*i*-, *o*-, *m*-, *p*-Ar), 116.3 (C_5H_5), 102.0 (*γ*-CH), 52.9 (Hf-CH₃), 32.5 (Al-CH₃) ppm; MS (EI) *m/z* (%): 785 (100) [M^+ −Me], 770 (8) [M^+ −2Me], 202 (26) [DippNCMe]⁺. Anal. Calcd for $C_{41}H_{57}AlHfN_2O$ (799.36): C 61.60, H 7.19, N 3.50. Found: C 59.08, H 6.85, N 3.32.

4.6.9. Synthesis of LMeAl(μ-O)TiMe₂Cp (10)

A solution of freshly prepared $CpTiMe_3$ (0.21g, 1.01mmol) in toluene (20 mL) was added via cannula to a solution of LMeAl(OH) (**7**) (0.48g, 1.01 mmol) in toluene (20 mL) at −30 ºC. The mixture was stirred at −30 ºC for one hour and then slowly raised the temperature to 0 ºC and the stirring was continued. After 3 h the solution was allowed to attain room temperature and stirred for 12 h. (NOTE: Care must be taken because methyl derivatives of Ti are photosensitive). The yellow precipitate formed was filtered off, washed with *n*-hexane, and dried in vacuum. Yield 0.41g (61%); decomp at 135 ºC ; ^{1}H NMR (500.13 MHz, C_6D_6, 25 ºC, TMS) δ 7.1-7.2 (m, 6H; *m*-, *p*-Ar-*H*), 5.50 (s, 5H; C_5H_5), 5.14 (s, 1H; *γ*-C*H*), 3.38 (sept, 2H, $^3J_{H-H} = 6.8$ Hz; C*H*(CH₃)₂), 3.11 (sept, 2H, $^3J_{H-H} = 6.8$ Hz; C*H*(CH₃)₂),1.73 (s, 6H; C*H₃*), 1.25 (d, 12H, $^3J_{H-H} = 6.8$ Hz; CH(C*H₃*)₂), 1.15 (d, 12H, $^3J_{H-H} = 6.80$ Hz; CH(C*H₃*)₂), −0.32 (s,

3H; Ti-CH_3)), −0.84 (s, 3H; Al-CH_3)) ppm; MS (EI) m/z (%): 588 (100) [M^+ −2Me], 202 (26) [DippNCMe]$^+$. Anal. Calcd for $C_{37}H_{55}AlN_2OTi$ (618.69): C 71.83, H 8.96, N 4.53. Found: C 70.01, H 8.93, N 5.37.

4.6.10. Synthesis of LMeAl(µ-O)TiMe₂Cp* (11)

Freshly sublimed Cp*TiMe$_3$ (0.34g, 1 mmol) dissolved in ether (20 mL) was transferred using a cannula to a flask charged with LMeAl(OH) (**7**) (0.48g, 1 mmol) in diethyl ether (30 mL) at −30 ºC. The reaction mixture was slowly warmed to ambient temperature and stirred for 12 h. The yellow precipitate was filtered, washed with *n*-hexane, and dried in vacuum. Yield 0.54 g (67.4%); decomp at 391 ºC; ^{1}H NMR (500.13 MHz, C_6D_6, 25 ºC, TMS) δ 7.13-7.24 (m, 6H; *m*-, *p*-Ar-*H*), 4.90 (s, 1H; *γ*-C*H*), 3.69 (sept, 4H, $^3J_{H-H}$ = 6.8 Hz; C*H*(CH$_3$)$_2$), 3.34 (sept, 4H, $^3J_{H-H}$ = 6.8 Hz; C*H*(CH$_3$)$_2$) 1.67 (s, 15H; C$_5$(C*H*$_3$)$_5$), 1.64 (s, 6H; C*H*$_3$), 1.50 (d, 6H, $^3J_{H-H}$ = 6.8 Hz; CH(C*H*$_3$)$_2$), 1.44 (d, 6H, $^3J_{H-H}$ = 6.8 Hz; CH(C*H*$_3$)$_2$), 1.23 (d, 6H, $^3J_{H-H}$ = 6.8 Hz; CH(C*H*$_3$)$_2$), 1.22 (d, 6H, $^3J_{H-H}$ = 6.8 Hz; CH(C*H*$_3$)$_2$), -0.11 (s, 6H; Ti-C*H*$_3$)$_2$), −0.22 (s, 6H; Al-C*H*$_3$) ppm. MS (EI) m/z (%): 658 (100) [M^+ −2Me], 770 (8) [M^+ −2Me], 202 (26) [DippNCMe]$^+$. Anal. Calcd for $C_{42}H_{65}AlN_2OTi$ (688.83): C 73.23, H 9.51, N 4.07. Found: C 70.88, H 9.43, N 3.98.

4.6.11. Synthesis of LAlMe(µ-O)ZrMe₂Cp* (12)

A solution of freshly prepared Cp*ZrMe$_3$ (0.21g, 1.01mmol) in toluene (20 mL) was added via cannula to a solution of LMeAl(OH) (**7**) (0.48g, 1.01 mmol) in toluene (20 mL) at −30 ºC. The mixture was stirred at −30 ºC for 3 h and then slowly brought to 0 ºC and the stirring was continued for 12 h. The white precipitate formed was filtered off, washed with *n*-hexane, and dried in vacuum. Yield, 73%. Mp 181 ºC. ^{1}H NMR (500.13 MHz, C_6D_6, 25 ºC, TMS) δ 7.13-7.24 (m, 6H; *m*-, *p*-Ar-*H*), 4.92 (s, 1H; *γ*-C*H*), 3.65 (sept, 4H, $^3J_{H-H}$ = 6.8 Hz;

C*H*(CH$_3$)$_2$), 3.36 (sept, 4H, $^3J_{\text{H-H}}$ = 6.8 Hz; C*H*(CH$_3$)$_2$) 1.85 (s, 15H; C$_5$(C*H$_3$*)$_5$), 1.78 (s, 6H; C*H$_3$*), 1.63 (d, 6H, $^3J_{\text{H-H}}$ = 6.8 Hz; CH(C*H$_3$*)$_2$), 1.60 (d, 6H, $^3J_{\text{H-H}}$ = 6.8 Hz; CH(C*H$_3$*)$_2$), 1.30 (d, 6H, $^3J_{\text{H-H}}$ = 6.8 Hz; CH(C*H$_3$*)$_2$), 1.22 (d, 6H, $^3J_{\text{H-H}}$ = 6.8 Hz; CH(C*H$_3$*)$_2$), –0.23 (s, 3H; Al-C*H$_3$*), -0.32 (s, 6H; Zr-C*H$_3$*)$_2$) ppm. Anal. Calcd for C$_{42}$H$_{65}$AlN$_2$OZr (732.18): C 68.90, H 8.95, N 3.83. Found: C 68.28, H 8.93, N 3.58.

4.6.12 Synthesis of LEtAlCl (13)

EtAlCl$_2$ (11.2 mL, 1.8 molar in *n*-hexane, 20 mmol) was added drop by drop at –78 °C to LLi·OEt$_2$ (9.97 g, 20 mmol) in toluene (100 mL). The mixture was allowed to warm to room temperature and stirred for 12 h. After filtration the filtrate was concentrated (20 mL) and kept at 4 °C to afford colorless crystals. X-ray quality crystals were grown from toluene. Yield (8.05 g, 79 %). Mp 153-155 °C. ^{1}H NMR (200.13 MHz, C$_6$D$_6$): δ –0.04 (q, J = 8.0 Hz, 2 H, AlC*H$_2$*CH$_3$), 0.80 (t, J = 8.0 Hz, 3 H, AlCH$_2$C*H$_3$*), 1.00 (d, J = 6.8 Hz, 6 H, CH(C*H$_3$*)$_2$), 1.19 (d, J = 6.8 Hz, 6 H, CH(C*H$_3$*)$_2$), 1.30 (d, J = 6.8 Hz, 6 H, CH(C*H$_3$*)$_2$), 1.48 (d, J = 6.6 Hz, 6 H, CH(C*H$_3$*)$_2$), 1.55 (s, 6 H, C*Me*), 3.21 (sept, J = 6.8 Hz, 2 H, C*H*(CH$_3$)$_2$), 3.76 (sept, J = 6.8 Hz, 2 H, C*H*(CH$_3$)$_2$), 4.96 (s, 1 H, γ-C*H*), 7.05-7.15 (m, *Ar*) ppm. ^{13}C NMR (75.48 MHz, C$_6$D$_6$, 25 °C, TMS): δ 170.7 (*C*N), 146.0, 143.3, 139.7, 125.4, 123.9 (*i*-, *o*-, *m*-, *p*-, *Ar*), 98.7 (γ-*C*H), 29.2, 28.1 (*C*H(CH$_3$)$_2$), 26.9, 24.9, 24.5, 23.8 (CH(*C*H$_3$)$_2$), 23.2 (β-*C*H$_3$), 8.54 (AlCH$_2$*C*H$_3$), –1.00 (Al*C*H$_2$CH$_3$) ppm. IR (Nujol mull, cm^{-1}): $\tilde{\nu}$ = 3062 (s), 1587 (m), 1558 (s), 1534 (s), 1517 (s), 1442 (s), 1344 (s), 1319 (s), 1259 (s), 1177 (m), 1101 (m), 1021 (s), 938 (m), 878 (w), 834 (w), 801 (m), 777 (w), 759 (w), 718 (w), 648 (w), 618 (m), 533 (m). MS (EI) *m/z* (%): 479 (100) [*M*$^+$–Et]. Anal. Calcd for C$_{31}$H$_{46}$AlClN$_2$ (508.30): C, 73.13; H, 9.11; N, 5.50%. Found: C, 72.45; H, 8.86; N, 5.43%.

4.6.13. Synthesis of LAlEt(OH) (14)

To a mixture of **13** (2.04 g, 4 mmol) and [CN(iPr)C$_2$Me$_2$N(iPr)] (:C, 0.72 g, 4 mmol) in toluene (60 mL) at 0 ºC distilled H$_2$O (18 μL, 4 mmol) was added. The suspension was allowed to warm to room temperature and stirred for 12 h. The insoluble solid was removed by filtration and from the filtrate all volatiles were removed *in vacuo* and the resulting residue was washed with *n*-pentane (5 mL) to afford a white solid. X-ray quality crystals of **14** were grown from THF at 4 ºC. Yield (1.43 g, 73 %). Mp 163 °C. ^{1}H NMR (200.13 MHz, C$_6$D$_6$): δ –0.22 (q, J = 8.2 Hz, 2 H, AlCH_2CH$_3$), 0.64 (s, 1 H, OH), 0.72 (t, J = 8.2 Hz, 3 H, AlCH$_2$CH_3), 1.06 (d, J = 6.8 Hz, 6 H, CH(CH_3)$_2$), 1.21 (d, J = 7.0 Hz, 6 H, CH(CH_3)$_2$), 1.30 (d, J = 7.0 Hz, 6 H, CH(CH_3)$_2$), 1.35 (d, J = 6.6 Hz, 6 H, CH(CH_3)$_2$), 1.58 (s, 6 H, CMe), 3.23 (sept, J = 6.8 Hz, 2 H, CH(CH$_3$)$_2$), 3.68 (sept, J = 6.8 Hz, 2 H, CH(CH$_3$)$_2$), 4.93 (s, 1 H, γ-CH), 7.05-7.20 (m, Ar) ppm. ^{13}C NMR (125.8 MHz, C$_6$D$_6$, 25 °C, TMS): δ 169.3 (CN), 145.4, 143.4, 140.8, 127.3, 124.9, 123,9 (*i*-, *o*-, *m*-, *p*-, Ar), 97.3 (γ-CH), 28.9, 27.8 (CH(CH$_3$)$_2$), 26.1, 24.9, 24.4, 24.0 (CH(CH$_3$)$_2$), 23.1 (β-CH$_3$) , 9.23 (AlCH$_2$$CH_3$), 1.36 (Al$CH_2CH_3$) ppm. IR (Nujol mull, cm^{-1}): $\widetilde{\nu}$ = 3729 (m, -OH), 1654 (w), 1552 (w), 1529 (w), 1319 (m), 1261 (w), 1179 (w), 1101 (w), 1059 (w), 1021 (w), 938 (w), 875 (w), 834 (w), 802 (w), 761 (w), 723 (w), 657 (w). MS (EI) *m/z* (%): 473.3 (24) [M^+–OH], 461.3 (100) [M^+–Et]. Anal. Calcd for C$_{31}$H$_{47}$AlN$_2$O (490.70): C 75.88, H 9.65, N 5.11. Found: C 75.24, H 9.44, N 5.62.

4.6.14. Synthesis of LEtAl(µ-O)ZrMeCp$_2$ (15)

Toluene (40 mL) was added to the mixture of **14** (0.49 g, 1.00 mmol) and Cp$_2$ZrMe$_2$ (0.26 g, 1.00 mmol). The resulting solution was stirred for 2 h at room temperature, and then continuously for 24 h at 100 °C. After concentration and keeping the solution at room temperature for one day, colorless crystals of **15** (0.51 g) were isolated. Yield 0.48 g (67 %).

Mp 368-369 °C. ^{1}H NMR (500.13 MHz, CDCl$_3$): δ −0.32 (s, 3 H, ZrMe), −0.14 (q, J = 7.9 Hz,

2 H, AlCH_2CH$_3$), 1.04 (d, J = 6.8 Hz, 6 H, CH(CH_3)$_2$), 1.14 (t, J = 7.9 Hz, 3 H, AlCH$_2$CH_3),

1.25 (d, J = 6.8 Hz, 6 H, CH(CH_3)$_2$), 1.37 (d, J = 6.8 Hz, 6 H, CH(CH_3)$_2$), 1.41 (d, J = 6.8 Hz,

6 H, CH(CH_3)$_2$), 1.77 (s, 6 H, CMe) , 3.15 (sept, J = 6.8 Hz, 2 H, CH(CH$_3$)$_2$), 3.29 (sept, J =

6.8 Hz, 2 H, CH(CH$_3$)$_2$), 5.02 (s, 1 H, γ-CH), 5.30 (s, 10 H, C$_5H_5$), 7.24-7.27 (m, Ar) ppm. ^{13}C

NMR (125.8 MHz, C$_6$D$_6$, 25 °C, TMS): δ 170.5 (CN), 144.7, 143.9, 141.2, 127.0, 124.7,

124,2 (i-, o-, m-, p-, Ar), 109.9 (C_5H$_5$), 97.3 (γ-CH), 28.7, 27.1 (CH(CH$_3$)$_2$), 25.3, 25.2, 24.6

(CH(CH$_3$)$_2$), 23.8 (β-CH$_3$), 17.6 (ZrMe), 9.4 (AlCH$_2$$CH_3$), 3.4 (b, Al$CH_2CH_3$) ppm. IR (Nujol

mull, cm^{-1}): $\tilde{v}$ = 1734 (m), 1653 (w), 1624 (w), 1591 (w), 1530 (m), 1396 (s), 1317 (m),

1259 (m), 1177 (m), 1099 (m), 1059 (w), 1019 (m), 940 (w), 872 (w), 839 (m), 795 (s), 759

(w), 724 (w), 643 (w), 599 (w), 587 (w), 568 (w), 530 (w), 442 (w). MS (EI) m/z (%): 709.3

(88) [M^+−Me], 695.3 (100) [M^+−2Me]. Anal. Calcd for C$_{42}$H$_{59}$AlN$_2$OZr (726.10): C 69.47, H

8.19, N 3.86. Found: C 69.40, H 8.32, N 3.52.

4.6.15. Synthesis of LMeAl(μ-O)Ti(NMe$_2$)$_2$(μ-O)AlMeL (16)

A solution of LMeAl(OH) (**7**) (0.477 g, 1.0 mmol) in toluene (20 mL) was added

dropwise by a syringe over a period of 15 min to a solution of Ti(NMe$_2$)$_4$ (0.112 g, 0.50

mmol) in toluene (20 mL) at −30 ºC. The reaction mixture was slowly warmed to ambient

temperature and was stirred at 25 ºC for 14 h. The solvent was evaporated to dryness yielding

a pasty yellow solid and then it was dissolved in pentane (30 mL) and passed through an

activated celite pad. The yellow crystals of the title compound were grown from concentrated

pentane solution at −30 ºC. Nucleation of crystal growth sometimes starts on warming the

pentane solution from −30 ºC to room temperature. Yield 0.32 g (60%). Mp 170-171 ºC. ^{1}H

NMR (500 MHz, C$_6$D$_6$, 25 ºC, TMS) δ −0.53 (s, 6H, Al−CH_3); 1.17 (d, 12H, $^3J_{H-H}$ = 6.8 Hz,

CH(CH_3)$_2$); 1.19 (d, 12H, $^3J_{H-H}$ = 6.8 Hz, CH(CH_3)$_2$);1.29 (d, 12H, $^3J_{H-H}$ = 6.8 Hz,

CH(C*H*₃)₂); 1.31 (d, 12H, ³*J*ₕ₋ₕ = 6.8 Hz, CH(C*H*₃)₂); 1.52 (s, 12H, C*H*₃); 2.84 (s, 12H, Ti–

N(C*H*₃)₂); 3.26 (sept., 4H, ³*J*ₕ₋ₕ = 6.8 Hz, C*H*(CH₃)₂); 3.63 (sept., 4H, ³*J*ₕ₋ₕ = 6.8 Hz,

C*H*(CH₃)₂); 7.06-7.22 (m, 12H, aryl protons). ¹³C NMR (125.75 MHz, C₆D₆, 25 °C, TMS) *δ* –

10.9 (br.s, Al–C*H*₃); 23.9 (s, *C*H₃); 24.7 (s, CH(*C*H₃)₂); 26.5 (s, CH(*C*H₃)₂); 28.1 (s,

*C*H(CH₃)₂); 28.6 (s, *C*H(CH₃)₂); 46.1 (s, Ti–N(*C*H₃)₂); 98.5 (*γ*-*C*H);124.4, 127.0, 141.9,

144.3, 144.7, (s, aryl carbon, *p*-, *m*-, *o*-, and *i*- respectively); 170.2 (s, (*C*N)). MS (EI) *m/z*

(%): 1086.8 (4) [*M*]⁺, 1071.8 (64) [*M*–Me]⁺, 202 (100) [DippNCCH₃]⁺. Anal. Calcd for

C₆₄H₁₀₀Al₂N₆O₂Ti (1087.36): C 70.69, H 9.26, N 7.73. Found: C 70.24, H 9.25, N 7.61.

4.6.16. Synthesis of LMeAl(μ-O)Zr(NMe₂)₂(μ-O)AlMeL (17)

A solution of LMeAl(OH) (**7**) (0.477 g, 1.0 mmol) in toluene (20 mL) was added

dropwise by a syringe over a period of 15 min to a solution of Zr(NMe₂)₄ (0.133 g, 0.50

mmol) in toluene (20 mL) at –30 °C. The reaction mixture was slowly warmed to ambient

temperature and was stirred at 25 °C for 14 h. The solvent was evaporated to dryness yielding

a colorless solid and then it was dissolved in *n*-hexane (40 mL) and passed through an

activated celite pad. The resulting solution was concentrated to approximately 15 mL under

reduced pressure and kept at 0 °C for several days yielding colorless crystals of analytical

purity. Yield 0.42 g (75%). Mp 246-247 °C. ¹H NMR (500 MHz, C₆D₆, 25 °C, TMS) *δ* –0.58

(s, 6H, Al–C*H*₃); 1.12 (d, 12H, ³*J*ₕ₋ₕ = 6.8 Hz, CH(C*H*₃)₂); 1.18 (d, 12H, ³*J*ₕ₋ₕ = 6.8 Hz,

CH(C*H*₃)₂); 1.29 (d, 12H, ³*J*ₕ₋ₕ = 6.8 Hz, CH(C*H*₃)₂); 1.33 (d, 12H, ³*J*ₕ₋ₕ = 6.8 Hz,

CH(C*H*₃)₂); 1.52 (s, 12H, C*H*₃); 2.81 (s, 12H, Zr–N(C*H*₃)₂); 3.26 (sept., 4H, ³*J*ₕ₋ₕ = 6.8 Hz,

C*H*(CH₃)₂); 3.56 (sept., 4H, ³*J*ₕ₋ₕ = 6.8 Hz, C*H*(CH₃)₂); 7.06-7.24 (m, 12H, aryl protons). ¹³C

NMR (125.75 MHz, C₆D₆, 25 °C, TMS) *δ* –11.1 (s, Al–C*H*₃); 23.7 (s, *C*H₃); 24.5 (s,

CH(*C*H₃)₂); 26.1 (s, CH(*C*H₃)₂); 28.2 (s, *C*H(CH₃)₂); 28.6 (s, *C*H(CH₃)₂); 43.3 (s, Zr–

N(CH_3)$_2$);   98.1 (γ-CH);124.5, 127.0, 141.6, 144.1, 144.8, (s, aryl carbon, *p*-, *m*-, *o*-, and *i*-respectively); 169.8 (s, (CN)). MS (EI): *m/z* (%): 202 (100) [DippNCCH$_3$]$^+$. Anal. Calcd for C$_{64}$H$_{100}$Al$_2$N$_6$O$_2$Zr (1130.68): C 67.98, H 8.91, N 7.43. Found: C 67.66, H 9.00, N 7.34.

4.6.17. Synthesis of [CpTiS$_3$Li$_3$]$_2$·6THF (19)

The compounds Cp$_2$Ti(SH)$_2$ (0.496 g, 2 mmol) and LiNMe$_2$ (0.101g, 2 mmol) were mixed as solids. Dried THF (3mL) was added to the resulting solids. The resultant red-orange solution was stirred and periodically evacuated for 30 min since a small amount of gas, presumably H$_2$, was slowly evolved. The solution was then stirred at room temperature overnight, and the green solution was reduced in vacuo to a volume of ca. 1 mL. The solvent was evaporated, then fresh THF was added and the solution was kept at -30 ºC to obtain dark green crystals (345 mg) of **19** from a green-brown supernatant. ^{1}H NMR (THF-d_8) δ 6.10 (C$_5$*H*$_5$), 3.56, 1.76, 1.75, 1.74, 1.71 (C$_4$*H*$_8$O) ppm. The coordinated THF resonances are broad and overlap with the THF-d_8 resonances (δ 3.58, 1.73 ppm).

5. Handling and Disposal of Solvents and Residual Waste

1. The recovered solvents were distilled or condensed into a cold-trap under vacuum and collected in halogen-free or halogen-containing solvent containers, and stored for disposal.

2. Used NMR solvents were classified into halogen-free and halogen-containing solvents and were disposed as halogen containing wastes, respectively.

3. Drying agents such as KOH, $CaCl_2$ and P_4O_{10} were hydrolyzed and disposed as acid or base wastes.

4. Whenever possible, sodium metal used for drying solvents was collected for recycling.[212] The non-reusable sodium metal was carefully hydrolyzed in cold ethanol and poured into the base-bath used for cleaning glassware.

5. Ethanol and acetone used for cold-baths (with solid CO_2 or liquid N_2) were subsequently used for cleaning glassware.

6. The acid-bath used for cleaning glassware was neutralized with Na_2CO_3 and the resulting NaCl solution was washed-off in the communal water drainage.

7. The residue of the base-bath used for glassware cleaning was poured into container for base wastes.

Amounts of various types of disposable wastes generated during the work:

Heavy elements containing wastes 2 L

Halogen-containing solvent wastes 7 L

Halogen-free solvent wastes 40 L

Acid wastes 10 L

Base wastes 20 L

6. Crystal Data and Structure Refinement Details

Table CD1. Crystal Data and Structure Refinement Details for Compound Cp*$_2$MeZr(OH) (1).

Empirical formula	$C_{21}H_{34}OZr$
Formula weight	393.7
Temperature	100(2) K
Color	Colorless
Wavelength	0.71073 Å
Crystal system	Orthorhombic
Space group	$P2_12_12_1$
Unit cell dimensions	$a = 8.035(2)$ Å
	$b = 10.948(3)$ Å
	$c = 22.256(3)$ Å
Volume	1958(1) Å^3
Z	4
Density (calculated)	1.336 Mg/m^3
Absorption coefficient	0.565 mm^{-1}
F (000)	832
θ range for data collection	1.83 to 26.39º.
Index ranges	$-10 \leq h \leq 10, 0 \leq k \leq 13, 0 \leq l \leq 27$
Reflections collected	36648
Independent reflections	4003 ($R_{int} = 0.0297$)
Refinement method	Full-matrix least-squares on F^2
Goodness-of-fit on F^2	1.193
Final R indices ($I > 2\sigma(I)$)	$R1 = 0.0250$, w$R2 = 0.0621$
R indices (all data)	$R1 = 0.0252$, $wR2 = 0.0625$
Largest diff peak and hole	$-0.433/+0.782\ e$ Å^{-3}

Table CD2. Crystal Data and Structure Refinement Details for Compound Cp*₂Hf(OH)₂ (2).

Empirical formula	$C_{20}H_{32}HfO_2$
Formula weight	482.96
Temperature	100(2) K
Color	Colorless
Wavelength	1.54178 Å
Crystal system	Orthorhombic
Space group	$P2_12_12_1$
Unit cell dimensions	$a = 8.2204(16)$ Å
	$b = 10.844(2)$ Å
	$c = 22.102(5)$ Å
Volume	1970.3(7) Å^3
Z	4
Density (calculated)	1.621 Mg m^{-3}
Absorption coefficient	9.788 mm^{-1}
F (000)	960
θ range for data collection	4.0 to 59.14°
Index ranges	-9<=h<=9, -11<=k<=12, -24<=l<=24
Reflections collected	17228
Independent reflections	2829 ($R_{int} = 0.0369$)
Refinement method	Full-matrix least-squares on F^2
Goodness-of-fit on F^2	1.149
Final R indices ($I > 2\sigma(I)$)	$R1 = 0.0152$, w$R2 = 0.0388$
R indices (all data)	$R1 = 0.0155$, w$R2 = 0.0388$
Largest diff peak and hole	-0.439/ +0.419 e Å^{-3}

Table CD3. Crystal Data and Structure Refinement Details for Cp*₂MeZr(μ-O)TiMe₂Cp* (3).

Empirical formula	$C_{33}H_{54}OTiZr$
Formula weight	605.88
Temperature	100(2) K
Color	Yellow
Wavelength	1.54178 Å
Crystal system	Monoclinic
Space group	Pc
Unit cell dimensions	$a = 8.601(2)$ Å
	$b = 15.399(2)$ Å $\beta = 94.41(2)°$
	$c = 23.084(3)$ Å
Volume	3048.3(9) Å³
Z	4
Density (calculated)	1.320 Mg m⁻³
Absorption coefficient	5.184 mm⁻¹
F (000)	1288
θ range for data collection	2.87 to 59.42°
Index ranges	$-9 \le h \le 9, -16 \le k \le 17, -25 \le l \le 25$
Reflections collected	52720
Independent reflections	11233 ($R_{int} = 0.072$)
Refinement method	Full-matrix least-squares on F^2
Goodness-of-fit on F^2	1.017
Final R indices ($I > 2\sigma(I)$)	$R1 = 0.0496$, w$R2 = 0.1325$
R indices (all data)	$R1 = 0.0580$, w$R2 = 0.1377$
Largest diff peak and hole	$-0.799/+0.551$ e Å⁻³

Table CD4. Crystal Data and Structure Refinement Details for Cp*$_2$MeZr(μ-O)Ti(NMe$_2$)$_3$ (4).

Empirical formula	C$_{27}$H$_{51}$N$_3$OTiZr
Formula weight	572.83
Temperature	100(2) K
Color	Yellow
Wavelength	0.71073 Å
Crystal system	Triclinic
Space group	$P\bar{1}$
Unit cell dimensions	a = 10.6644 Å α = 89.4060(10)º
	b = 11.6310 Å β = 89.3900(10)º
	c = 12.9048 Å γ = 66.0210(10)º
Volume	1.46242(12) Å^3
Z	2
Density (calculated)	1.301 Mg m^{-3}
Absorption coefficient	0.651 mm^{-1}
F (000)	608
θ range for data collection	4.18 to 52.78 º
Index ranges	-13 $\leq h \leq$ 13,-14 $\leq k \leq$ 14,0 $\leq l \leq$ 16
Reflections collected	26990
Independent reflections	5981 (R_{int} = 0.0421)
Refinement method	Full-matrix least-squares on F^2
Goodness-of-fit on F^2	1.088
Final R indices ($I > 2\sigma(I)$)	R1 = 0.0226, wR2 = 0.0630
R indices (all data)	R1 = 0.0241, wR2 = 0.0637
Largest diff peak and hole	-0.503/+0.609 e Å^{-3}

Table CD5. Crystal Data and Structure Refinement Details for Cp*₂MeZr(μ-O)Hf(NMe₂)₂(μ-O)ZrMeCp*₂ (6).

Empirical formula	$C_{46}H_{78}Hf\,N_2O_2Zr_2$
Formula weight	1052.03
Temperature	100(2) K
Color	Colorless
Wavelength	0.71073 Å
Crystal system	Monoclinic
Space group	$P2_1/n$
Unit cell dimensions	$a = 14.8318(8)$ Å
	$b = 18.7743(10)$ Å $\beta = 111.0510(10)°$
	$c = 17.7562(9)$ Å
Volume	4.6144(4) Å³
Z	4
Density (calculated)	1.514 Mg m⁻³
Absorption coefficient	2.724 mm⁻¹
F (000)	2144
θ range for data collection	3.08 to 52.74 °
Index ranges	$-18 \le h \le 17, 0 \le k \le 23, 0 \le l \le 22$
Reflections collected	76389
Independent reflections	9408 ($R_{int} = 0.0216$)
Refinement method	Full-matrix least-squares on F^2
Goodness-of-fit on F^2	1.037
Final R indices ($I > 2\sigma(I)$)	$R1 = 0.0220$, w$R2 = 0.0606$
R indices (all data)	$R1 = 0.0234$, w$R2 = 0.0613$
Largest diff peak and hole	-0.705/+0.821 e Å⁻³

Table CD6. Crystal Data and Structure Refinement Details for LMeAl(μ-O)TiMeCp$_2$ (8).

Empirical formula	$C_{41}H_{57}AlN_2OTi$
Formula weight	668.77
Temperature	100(2) K
Color	Yellow
Wavelength	1.54178 Å
Crystal system	Triclinic
Space group	$P\bar{1}$
Unit cell dimensions	a = 9.572(2) Å α = 90.13(2) °
	b =10.422(2) Å β = 90.55(2)°
	c = 20.060(3) Å γ = 114.14(2)°
Volume	1886.0(6) Å^3
Z	2
Density (calculated)	1.216 Mg m^{-3}
Absorption coefficient	2.464 mm^{-1}
F (000)	720
θ range for data collection	4.41 to 58.99°
Index ranges	$-10 \le h \le 10, -11 \le k \le 11, -22 \le l \le 20$
Reflections collected	15952
Independent reflections	5056 (R_{int} = 0.0432)
Refinement method	Full-matrix least-squares on F^2
Goodness-of-fit on F^2	1.195
Final R indices ($I > 2\sigma(I)$)	R1 = 0.0603, wR2 = 0.1205
R indices (all data)	R1 = 0.0760, wR2 = 0.1265
Largest diff peak and hole	-0.368/+0.301 e Å^{-3}

Table CD7. Crystal Data and Structure Refinement Details for LMeAl(μ-O)HfMeCp$_2$ (9).

Empirical formula	$C_{41}H_{57}AlHfN_2O$
Formula weight	799.36
Temperature	133(2) K
Color	Colorless
Wavelength	0.71073 Å
Crystal system	Triclinic
Space group	$P\bar{1}$
Unit cell dimensions	a = 9.921(2) Å α = 88.28(2) º
	b = 10.276(2) Å β = 87.17(2)º
	c = 19.616(3) Å γ = 68.47(2)º
Volume	1857.9(6)Å^3
Z	2
Density (calculated)	1.429 Mg m^{-3}
Absorption coefficient	2.864 mm^{-1}
F (000)	820
θ range for data collection	2.08 to 24.81º
Index ranges	$-11 \le h \le 11, -12 \le k \le 12, -23 \le l \le 23$
Reflections collected	31559
Independent reflections	6373 (R_{int} = 0.0385)
Refinement method	Full-matrix least-squares on F^2
Goodness-of-fit on F^2	1.028
Final R indices ($I > 2\sigma(I)$)	$R1$ = 0.0178, w$R2$ = 0.0369
R indices (all data)	$R1$ = 0.0221, w$R2$ = 0.0375
Largest diff peak and hole	-0.412/0.370 e Å^{-3}

Table CD8. Crystal Data and Structure Refinement for Compound LMeAl(μ-O)TiMe$_2$Cp (10).

Empirical formula	$C_{37}H_{55}AlN_2OTi$
Formula weight	618.71
Temperature	100(2) K
Color	Yellow
Wavelength	1.54178 Å
Crystal system	Triclinic
Space group	$P\bar{1}$
Unit cell dimensions	$a = 09.24(10)$ Å $\quad \alpha = 91.54(10)$ º
	$b = 10.499(10)$ Å $\quad \beta = 90.02(10)$º
	$c = 19.982(10)$ Å $\quad \gamma = 115.26(10)$º
Volume	1752.3(3) Å^3
Z	2
Density (calculated)	1.173 Mg m^{-3}
Absorption coefficient	2.526 mm^{-1}
F (000)	668
θ range for data collection	4.43 to 59.06º
Index ranges	$-10 \leq h \leq 10, -11 \leq k \leq 11, -22 \leq l \leq 22$
Reflections collected	18081
Independent reflections	4915 (R_{int} = 0.0313)
Refinement method	Full-matrix least-squares on F^2
Goodness-of-fit on F^2	1.072
Final R indices ($I > 2\sigma(I)$)	$R1 = 0.0296$, w$R2 = 0.0810$
R indices (all data)	$R1 = 0.0305$, w$R2 = 0.0817$
Largest diff peak and hole	$-0.285/+0.249$ e Å^{-3}

Table CD9. Crystal Data and Structure Refinement for Compound LMeAl(μ-O)TiMe$_2$Cp*(11).

Empirical formula	C$_{42}$H$_{65}$AlN$_2$OTi
Formula weight	688.84
Temperature	100(2) K
Color	Yellow
Wavelength	1.54178 Å
Crystal system	Monoclinic
Space group	$P2_1/n$
Unit cell dimensions	$a = 12.033(10)$ Å
	$b = 19.076(2)$ Å $\beta = 96.79(10)°$
	$c = 17.519(10)$ Å
Volume	3993.1(6) Å^3
Z	4
Density (calculated)	1.146 Mg m^{-3}
Absorption coefficient	2.263 mm^{-1}
F (000)	1496
θ range for data collection	3.34 to 59.00°
Index ranges	$-13 \leq h \leq 13$, $-20 \leq k \leq 21$, $-19 \leq l \leq 19$
Reflections collected	30327
Independent reflections	5577 ($R_{int} = 0.0711$)
Refinement method	Full-matrix least-squares on F^2
Goodness-of-fit on F^2	1.050
Final R indices ($I > 2\sigma(I)$)	$R1 = 0.0509$, w$R2 = 0.1304$
R indices (all data)	$R1 = 0.0731$, w$R2 = 0.1449$
Largest diff peak and hole	$-0.521/+0.327$ e Å^{-3}

Table CD10. Crystal Data and Structure Refinement for Compound LMeAl(μ-O)ZrMe$_2$Cp*(12).

Empirical formula	C$_{42}$H$_{65}$AlN$_2$OZr
Formula weight	732.16
Temperature	100(2) K
Color	Colorless
Wavelength	1.54178 Å
Crystal system	Monoclinic
Space group	$P2_1/n$
Unit cell dimensions	a = 12.232(2) Å
	b = 19.009(2) Å β = 97.360(10)°
	c = 17.498(2) Å
Volume	4035.1(9) Å^3
Z	4
Density (calculated)	1.205 Mg m^{-3}
Absorption coefficient	2.675 mm^{-1}
F (000)	1568
θ range for data collection	3.45 to 59.39°
Index ranges	-13 $\leq h \leq$ 13,-21 $\leq k \leq$ 21,-19 $\leq l \leq$19
Reflections collected	35035
Independent reflections	5796 (R_{int} = 0.0532)
Refinement method	Full-matrix least-squares on F^2
Goodness-of-fit on F^2	1.045
Final R indices (I > 2σ(I))	R1 = 0.0291, wR2 = 0.732
R indices (all data)	R1 = 0.0339, wR2 = 0.0766
Largest diff peak and hole	-0.403/+0.389 e Å^{-3}

Table CD11. Crystal Data and Structure Refinement for Compound LMeAl(μ-O)Ti(NMe$_2$)$_2$(μ-O)AlMeL (16).

Empirical formula	$C_{64}H_{100}Al_2N_6O_2Ti$
Formula weight	1087.36
Temperature	133(2) K
Color	Yellow
Wavelength	0.71073 Å
Crystal system	Monoclinic
Space group	$P2_1/c$
Unit cell dimensions	$a = 22.6235(9)$ Å
	$b = 17.1285(4)$ Å $\beta = 103.433º$
	$c = 17.1933(5)$ Å
Volume	6480.2(4) Å^3
Z	4
Density (calculated)	1.115 Mg m^{-3}
Absorption coefficient	0.204 mm^{-1}
F (000)	2360
θ range for data collection	1.51 to 24.84º
Index ranges	$-26 \leq h \leq 26, -20 \leq k \leq 20, -20 \leq l \leq 20$
Reflections collected	98282
Independent reflections	11152 ($R_{int} = 0.0826$)
Refinement method	Full-matrix least-squares on F^2
Goodness-of-fit on F^2	0.966
Final R indices ($I > 2\sigma(I)$)	$R1 = 0.0395$, w$R2 = 0.0910$
R indices (all data)	$R1 = 0.0620$, w$R2 = 0.0977$
Largest diff peak and hole	$-0.353/+0.342$ e Å^{-3}

Table CD12. Crystal Data and Structure Refinement for Compound LMeAl(μ-O)Zr(NMe₂)₂(μ-O)AlMeL (17).

Empirical formula	$C_{64}H_{100}Al_2N_6O_2Zr$
Formula weight	1130.68
Temperature	133(2) K
Color	Colorless
Wavelength	0.71073 Å
Crystal system	Monoclinic
Space group	$P2_1/c$
Unit cell dimensions	$a = 22.6139(9)$ Å
	$b = 17.1826(8)$ Å $\beta = 102.419(3)°$
	$c = 17.2375(6)$ Å
Volume	6541.2(5) Å³
Z	4
Density (calculated)	1.148 Mg m⁻³
Absorption coefficient	0.239 mm⁻¹
F (000)	2432
θ range for data collection	1.50 to 24.90°
Index ranges	$-26 \leq h \leq 26, -20 \leq k \leq 19, -20 \leq l \leq 20$
Reflections collected	66342
Independent reflections	11255 ($R_{int} = 0.1005$)
Refinement method	Full-matrix least-squares on F^2
Goodness-of-fit on F^2	0.967
Final R indices ($I > 2\sigma(I)$)	$R1 = 0.0373$, w$R2 = 0.0744$
R indices (all data)	$R1 = 0.0647$, w$R2 = 0.0810$
Largest diff peak and hole	-0.321/+0.243 e Å⁻³

Table CD13. Crystal Data and Structure Refinement for Compound $Li_6[CpTi(\mu$-$S)_3]_2 \cdot 6THF$ (19).

Empirical formula	$C_{34}H_{58}O_6Li_6Ti_2S_6$
Formula weight	892.60
Temperature	100(2) K
Color	Green
Wavelength	1.54178 Å
Crystal system	Monoclinic
Space group	$P2_1/n$
Unit cell dimensions	$a = 19.4757(10)$ Å
	$b = 10.6671(5)$ Å $\beta = 96.975(2)°$
	$c = 32.4375(15)$ Å
Volume	6689.0(6) Å^3
Z	15
Density (calculated)	1.385 Mg m^{-3}
Absorption coefficient	4.635 mm^{-1}
F (000)	2906
θ range for data collection	2.52 to 58.79°
Index ranges	$-21 \leq h \leq 21, -11 \leq k \leq 11, -35 \leq l \leq 35$
Reflections collected	58391
Independent reflections	9514 ($R_{int} = 0.1783$)
Refinement method	Full-matrix least-squares on F^2
Goodness-of-fit on F^2	1.067
Final R indices ($I > 2\sigma(I)$)	$R1 = 0.0699$, w$R2 = 0.1188$
R indices (all data)	$R1 = 0.1379$, w$R2 = 0.1392$
Largest diff peak and hole	$-0.381/ +0.636$ e Å^{-3}

7. Supporting Materials

7.1 Computational Results.

Theoretical study results on complex Cp*$_2$ZrMe(OH) (**1**)

Table S1. Important Geometry Parameters for Complex **1** (Cp*$_2$ZrMe(OH))

	[Å]
Zr-CH3	2.29859
Zr-OH	2.02099
O-H	0.96156
angle C-Zr-O	93.92
angle H-O-Zr	123.98
angle cp*-Zr-cp*	136.96
dihedral angle C-Zr-O-H	80.47409

Table S2. Important Geometry Parameters for the Hydride Analogue of Complex (Cp*$_2$ZrH(OH))

	[Å]
Zr-H	1.84655
Zr-OH	2.01837
O-H	0.96122
angle H-Zr-O	97.87
angle H-O-Zr	125.58
angle cp*-Zr-cp*	134.32
dihedral angle H-Zr-O-H	83.57
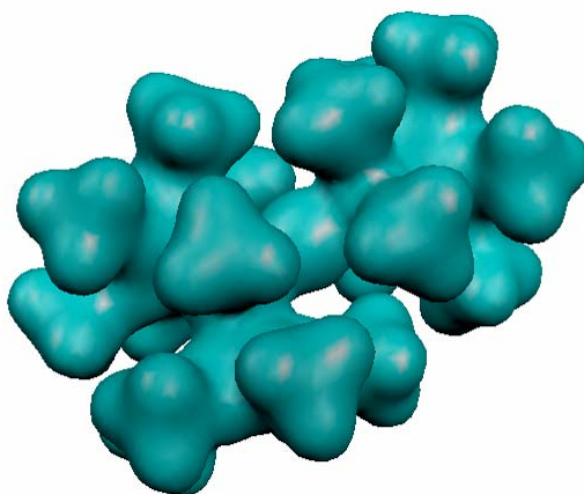
Figure S1. Space filling model of complex Cp*$_2$MeZr(μ-O)TiMe$_2$Cp* (**3**) obtained from ab initio calculation.

Table S3. Results of Control Experiment on Polymerization Using Starting Precursors[a]

catalyst	Monomer	MAO:catalyst	Polymer (g)	A $\times 10^5$
Cp*$_2$ZrMe$_2$	ethylene	400	0.680	1.36
Ti(NMe$_2$)$_4$	ethylene	400	0.12	0.24
Hf(NMe$_2$)$_4$	ethylene	400	0.06	0.12
Ti(NMe$_2$)$_4$	styrene	800	0.39	0.39

[a] Polymerization condition; 10 μmol catalyst, 100 mL of toluene at 1 atm ethylene for 0.5 h or with 10 mL of styrene for 1 h at 25 ºC. Activity (A) = g Polymer/mol cat·h.

8. References

[1]   Copéret, C.; Chabanas, M.; Saint-Arroman, R. P.; Basset, J. -M. *Angew. Chem.* **2003**, *115,* 164-191; *Angew. Chem. Int. Ed*. **2003**, *42*, 156-181.

[2]   Cornils, B.; Herrmann, W. A. *Applied Homogeneous Catalysis with Organometallic Compounds*; Wiley-VCH, Weinheim, Germany, **1996**.

[3]   Basset, J.-M.; Gates, B. C.; Candy, J. P.; Choplin, A.; Leconte, M.; Quignard, F.; Santini, C. *Surface Organometallic Chemistry: Molecular Approaches to Surface Catalysis*; Kluwer, Dordrecht, The Netherlands, **1988**, and references therein.

[4]   Basset, J.-M.; Candy, J. P.; Choplin, A.; Didillon, B.; Quignard, F.; Theólier, A. In *Perspectives in Catalysis*; Thomas, J. P.; Zamaraev, K. (Eds) Blackwell, Oxford, **1991**, pp 125.

[5]   Roesky, H. W.; Haiduc, I.; Hosmane, N. S. *Chem. Rev*. **2003**, *103*, 2579-2595.

[6]   Kaminsky, W. *Catalysis Today* **1994**, *20*, 257-271.

[7]   Sinn, H.; Kaminski, W. *Adv. Organomet. Chem.* **1980**, *18*, 99-149.

[8]   Brintzinger, H. H.; Fischer, D.; Mülhaupt, R.; Rieger, B.; Waymouth, R. M. *Angew Chem.* **1995**, *107*, 1255-1283; *Angew. Chem. Int. Ed. Engl.* **1995**, *34*, 1143-1170.

[9]   Andresen, A.; Cordes, H. -G.; Herwig, J.; Kaminsky, W.; Merck, A.; Mottweiler, R.; Pein, J.; Sinn, H.; Vollmer, H. -J. *Angew. Chem.* **1976**, *88*, 689-690; *Angew. Chem. Int. Ed. Engl.* **1976**, *15*, 630-632.

[10]   Gibson, V. C.; Spitzmesser, S. K. *Chem. Rev*. **2003**, *103*, 283-315.

[11]   Makio, H.; Kashiwa, N.; Fujita, T. *Adv. Synth. Catal.* **2002**, *344*, 477-493.

[12]   Janiak, C. *Metallocenes*; Togni, A.; Haltermann, R. L. (Eds.) Wiley-VCH, Weinheim, Germany, **1998**, Vols. 1 and 2.

[13]   Ittel, S. D.; Johnson, L. K.; Brookhart, M. *Chem. Rev.* **2000**, *100*, 1169-1203.

[14]   Bollmann, A.; Blann, K.; Dixon, J. T.; Hess, F. M.; Killian, E.; Maumela, H.; McGuinness, D. S.; Morgan, D. H.; Neveling, A.; Otto, S.; Overett, M.; Slawin, A. M. Z.; Wasserscheid, P.; Kuhlmann, S. *J. Am. Chem. Soc.* **2004**, *126*, 14712-14713.

[15]   Tian, J.; Hustad, P. D.; Coates, G. W. *J. Am. Chem. Soc.* **2001**, *123*, 5134-5135.

[16]   Arriola, D. J.; Carnahan, E. M.; Hustad, P. D.; Kuhlman, R. L.; Wenzel, T. T. *Science* **2006**, *312*, 714-719.

[17]   Vogt, D. *Applied Homogeneous Catalysis with Organometallic Compounds*; Cornils, B.; Herrmann, W. A. (Eds.) Wiley-VCH, Weinheim, Germany, **2002**, Vol. 1, pp 245-258.

[18]   Parshall, G. W.; Ittel, S. D. *Homogeneous Catalysis: The Applications and Chemistry of Catalysis by Soluble Transition Metal Complexes*; Wiley, New York, **1992**, pp 68-72.

[19]   Skupinska, J. *Chem. Rev.* **1991**, *91*, 613-648.

[20]   Rieger, B.; Baugh, L. S.; Kacker, S.; Striegler, S. *Late Transition Metal Polymerization Catalysis*; John Wiley & Sons: New York, **2003**, and references therein.

[21]   Blom, R.; Follestad, A.; Rytter, E.; Tilset, M.; Ystenes, M. *Organometallic Catalysts and Olefin Polymerization: Catalysts for a New Millennium*; Springer-Verlag, Berlin, Germany, **2001**, and references therein.

[22]   Galli, P.; Vecellio, G. *J. Polym. Sci. Part A: Polym. Chem.* **2004**, 42, 396-415.

[23]   Bonnet, M. C.; Dahan, F.; Ecke, A.; Keim, W.; Schulz, R. P.; Tkatchenko, I. *J. Chem. Soc., Chem Commun.*, **1994**, 615-616.

[24]   Yanjarappa, M. J.; Sivaram, S. *Prog. Polym. Sci.* **2002**, *27*, 1347-1398.

[25]   Mecking, S.; Held, A.; Bauers, F. M. *Angew. Chem.* **2002**, *114*, 564-582; *Angew. Chem. Int. Ed.* **2002***, 41,* 544-561.

[26] Abramo, G. P.; Li, L.; Marks, T. J. *J. Am. Chem. Soc.* **2002**, *124*, 13966-13967.

[27] Bazan, G. C.; Rodriguez, G.; Ashe, A. J., III.; Al-Ahmad, S.; Müller, C. *J. Am. Chem. Soc.* **1996**, *118*, 2291-2292.

[28] Barnhart, R. W.; Bazan, G. C.; Mourey, T. *J. Am. Chem. Soc.* **1998**, *120*, 1082-1083.

[29] Komon, Z. J. A.; Bazan, G. C. *Macromol. Rapid Commun.* **2001**, *22*, 467-478.

[30] Drouin, S. D.; Zamanian, F.; Fogg, D. E. *Organometallics* **2001**, *20*, 5495-5497.

[31] Quijada, R.; Rojas, R.; Bazan, G. C.; Komon, Z. J. A.; Mauler, R. S.; Galland, G. B. *Macromolecules* **2001**, *34*, 2411-2417.

[32] Denger, C.; Haase, U.; Fink, G. *Makromol. Chem., Rapid Commun*. **1991**, *12*, 697-701.

[33] Beach, D. L.; Kissin, Y. V. *J. Polym. Sci., Polym. Chem. Ed.* **1984**, *22*, 3027-3042.

[34] Kunrath, F. A.; de Souza, R. F.; Casagrande, O. L., Jr. *Macromol Rapid Commun.* **2000**, *21*, 277-280.

[35] Frediani, M.; Bianchini, C.; Kaminsky, W. *Kinetics and catalysis*, **2006**, *47*, 207-212.

[36] Wang, W-J.; Kolodka, E.; Zhu, S.; Hamielec, A. E. *J. Polym. Sci., Part A: Polym. Chem*. **1999**, *37*, 2949-2957.

[37] Rogers, J. S.; Bazan, G. C.; Sperry, C. K. *J. Am. Chem. Soc*. **1997**, *119*, 9305-9306.

[38] Wasilke, J.-C.; Obrey, S. J.; Baker, R. T.; Bazan, G. C. *Chem. Rev.* **2005**, *105,* 1001-1020.

[39] McKnight, A. L.; Waymouth, R. M. *Chem. Rev.* **1998**, *98*, 2587-2598.

[40] Komon, Z. J. A.; Diamond, G. M.; Leclerc, M. K.; Murphy, V.; Okazaki, M.; Bazan, G. C. *J. Am. Chem. Soc.* **2002**, *124*, 15280-15285.

[41] Green, M. L. H.; Popham, N. H. *J. Chem. Soc., Dalton Trans*. **1999**, 1049-1059.

[42] Lindenberg, F.; Shribman, T.; Sieler, J.; Hey-Hawkins, E.; Eisen, M. S. *J. Organomet. Chem.* **1996**, *515*, 19-25.

[43] Ishino, H.; Takemoto, S.; Hirata, K.; Kanaizuka, Y.; Hidai, M.; Nabika, M.; Seki, Y.; Miyatake, T.; Suzuki, N. *Organometallics* **2004**, *23*, 4544-4546.

[44] Britovsek, G. J. P.; Gibson, V. C.; Wass, D. F. *Angew. Chem., Int. Ed.* **1999**, *38*, 428-447.

[45] Bai, G.; Singh, S.; Roesky, H. W.; Noltemeyer, M.; Schmidt, H.-G. *J. Am. Chem. Soc.* **2005,** *127*, 3449-3455.

[46] Singh, S.; Jancik, V.; Roesky, H. W.; Herbst-Irmer, R. *Inorg. Chem.* **2006**, *45*, 949-951.

[47] Pineda, L. W.; Jancik, V.; Roesky, H. W.: Herbst-Irmer, R. *Inorg. Chem.* **2005**, *44*, 3537-3540.

[48] Burn, M. J.; Fickes, M. G.; Hartwig, J. F.; Hollander, F. J.; Bergman, R. G. *J. Am. Chem. Soc.* **1993**, *115*, 5875-5876.

[49] Arnold, D. P.; Bennet, M. A. *J. Organomet. Chem.* **1980**, *199*, 119-135.

[50] Bennet, M. A.; Yoshida, T. *J. Am. Chem. Soc.* **1978**, *100*, 1750-1759.

[51] Bennet, M. A.; Yoshida, T. *J. Am. Chem. Soc.* **1973**, *95*, 3030-3031.

[52] Jensen, C. M.; Trogler, W. C. *J. Am. Chem. Soc.* **1986**, *108*, 723-729.

[53] Jensen, C. M.; Trogler, W. C. *Science* **1986**, *233*, 1069-1071.

[54] Masters, C. *Homogeneous Transition Metal Catalysis: A Gentle Art*; Chapman & Hall: New York, **1981**.

[55] Yoshida, T.; Matsuda, T.; Okano, T.; Kitani, T.; Otsuka, S. *J. Am. Chem. Soc.* **1979**, *101*, 2027-2038.

[56] Carofiglio, T.; Floriani, C.; Rosi, M.; Chiesi-Villa, A.; Rizzoli, C. *Inorg. Chem.* **1991**, *30*, 3245-3246.

[57] Rau, M. S.; Kretz, C. M.; Geoffroy, G. L.; Rheingold, A. L.; Haggerty, B. S. *Organometallics* **1994**, *13*, 1624-1634.

[58] Erker, G.; Albrecht, M.; Werner, S. ; Krüger, C.; *Z. Naturforsch.* **1990**, *45b*, 1205-1209.

[59] Bansal, S.; Singh, Y.; Singh, A. *Heteroatom Chem*. **2004**, *15*, 21-25.

[60] Bai, G.; Peng, Y.; Roesky, H. W.; Li, J.; Schmidt, H.-G.; Noltemeyer, M. *Angew. Chem.* **2003**, *115*, 1164-1167; *Angew. Chem. Int. Ed.* **2003**, *42*, 1132-1135.

[61] Bai, G.; Roesky, H. W.; Li, J.; Noltemeyer, M; Schmidt, H.-G. *Angew. Chem.* **2003**, *115*, 5660-5664; *Angew. Chem. Int. Ed.* **2003**, *42*, 5502-5506.

[62] Jancik, V.; Pineda, L. W.; Stückl, A. C.; Roesky, H. W.; Herbst-Irmer, R. *Organometallics*, **2005**, *24*, 1511-1515.

[63] Pineda, L. W.; Jancik, V.; Roesky, H. W.; Neculai, D.; Neculai, A. M. *Angew. Chem.* **2004**, *116*, 1443-1445; *Angew. Chem. Int. Ed.* **2004**, *43*, 1419-1421.

[64] Boor, J., *Ziegler-Natta Catalysts and Polymerizations*; Academic Press, New York, **1979**.

[65] Chien, J. C. W. (Ed.) *Coordination Polymerization*; Academic Press, New York, **1975**.

[66] Natta, G.; Pasquon, I.; Zambelli, A. *J. Am. Chem. Soc.* **1962**, *84*, 1488-1490.

[67] Doi, Y.; Ueki, S.; Keii, T. *Macromolecules* **1979**, *12*, 814-819.

[68] Pillai, S. M.; Ravindranathan, M.; Sivaram, S. *Chem. Rev.* **1986**, *86*, 353-399.

[69] Keim, W.; Kowaldt, F. H.; Goddard, R.; Krüger, C. *Angew. Chem.* **1978**, *90*, 493; *Angew. Chem., Int. Ed. Engl.* **1978**, *17*, 466-467.

[70] Boor, J. Jr.; Youngman, E. A.; Dimbat, M. *Makromolekulare Chemie,* **1966**, *90*, 26-37.

[71] Reichert, K. H. *Transition Metal Catalyzed Polymerizations*; Quirk, R. P. (Ed.) Academic Press: New York, **1981**; p 465.

[72] Chen, E. Y-X.; Marks, T. J. *Chem. Rev.* **2000**, *100*, 1391-1434. and references therein.

[73] Sinn, H.; Kaminsky, W.; Vollmer, H.-J.; Woldt, R. *Angew. Chem.* **1980**, *92*, 396-402; *Angew. Chem., Int. Ed. Engl.* **1980**, *19*, 390-392.

[74]   Corradini, P: Guerra, G.; Cavallo, L. *Acc. Chem. Res.,* **2004**, *37,* 231-241.

[75]   Kaminsky, W.; Külper, K.; Brintzinger, H. H.; Wild, F. R. W. P. *Angew. Chem.* **1985**, *97*, 507-508; *Angew. Chem. Int. Ed. Engl.* **1985**, *24*, 507-508.

[76]   Coates, G. W.; Waymouth, R. M. *Science* **1995**, *267*, 217-219.

[77]   Gauthier, W. J.; Corrigan, J. F.; Taylor, N. J.; Collins, S. *Macromolecules* **1995**, *28*, 3771-3778.

[78]   Mallin, D. T.; Rausch, M. D.; Lin, Y-G.; Dong, S.; Chien, J. C. W. *J. Am. Chem. Soc.* **1990**, *112*, 2030-2031.

[79]   Ewen, J. A.; Jones, R. L.; Razavi, A.; Ferrara, J. D. *J. Am. Chem. Soc.* **1988**, *110*, 6255-6256.

[80]   Stehling, U.; Diebold, J.; Kirsten, R.; Röll, W.; Brintzinger, H.-H.; Jüngling, S.; Mülhaupt, R.; Langhauser, F. *Organometallics* **1994**, *13*, 964-970.

[81]   Vandenberg, E. J. *J. Polym. Sci.* **1960**, *47*, 486-489.

[82]   Barron, A. R. *Alumoxanes*; Macromolecular Symposia, Kaminsky, W., Hoker, H., (Eds.) Huthig & Wepf: Heidelberg, Germany, **1995**, *97*, 15-26.

[83]   Reddy, S. S.; Sivaram, S. *Prog. Polym. Sci*. **1995**, *20*, 309-367.

[84]   Sinn, H. *Alumoxanes*; Macromolecular Symposia, Kaminsky, W., Hoker, H. (Eds.) Huthig & Wepf: Heidelberg, Germany, **1995**, *97*, 27-52.

[85]   Mason, M. R.; Smith, J. M.; Bott, S. G.; Barron, A. R. *J. Am. Chem. Soc.* **1993**, *115*, 4971-4984.

[86]   Imhoff, D. W.; Simeral, L. S.; Sangokoya, S. A.; Peel, J. H. *Organometallics* **1998**, *17*, 1941-1945.

[87]   Sinn, H.; Schimmel, I.; Ott, M.; von Thienen, N.; Harder, A.; Hagendorf, W.; Heitmann, B.; Haupt, E. *Metalorganic Catalysts for Synthesis and Polymerization: Recent Results by Ziegler-Natta and Metallocene Investigations*; Kaminsky, W. (Ed.) Springer-Verlag: Berlin, **1999**. pp 105-122.

[88] Babushkin, D. E.; Semikolenova, N. V.; Panchenko, V. N.; Sobolev, A. P.; Zakharov, V. A.; Talsi, E. P. *Macromol. Chem. Phys.* **1997**, *198*, 3845-3854.

[89] Sugano, T.; Matsubara, K.; Fujita, T.; Takahashi, T. *J. Mol. Catal.* **1993**, *82*, 93-101.

[90] Siedle, A. R.; Lamanna, W. M.; Newmark, R. A.; Stevens, J.; Richardson, D. E.; Ryan, M. *Macromol. Symp.* **1993**, *66*, 215-224.

[91] Siedle, A. R.; Newmark, R. A.; Lamanna, W. M.; Schroepfer, J. N. *Polyhedron* **1990**, *9*, 301-308.

[92] Resconi, L.; Bossi, S.; Abis, L. *Macromolecules* **1990**, *23*, 4489-4491.

[93] Pasynkiewicz, S. *Polyhedron* **1990**, *9*, 429-453.

[94] Giannetti, E.; Nicoletti, G. M.; Mazzochi, R. *J. Polym. Sci., Polym. Chem. Ed.* **1985**, *23*, 2117-2134.

[95] Kulshrestha, A. K.; Talapatra, S. *Handbook of Polyolefins*; Vasile, C. (Ed.), Marcel Dekker, New York, **2000**, pp 1-70.

[96] Ewen, J. A. *J. Am. Chem. Soc.* **1984**, *106*, 6355-6364.

[97] Alt, H. G.; Samuel, E. *Chem. Soc. Rev.* **1998**, *27*, 323-329.

[98] Enders, M.; Fernandez, P.; Ludwig, G.; Pritzkow, H. *Organometallics* **2001**, *20*, 5005-5007.

[99] Piel, C.; Stadler, F. J.; Kaschta, J.; Rulhoff, S.; Münstedt, H.; Kaminsky, W. *Macromol. Chem. Phys.* **2006**, *207*, 26-38.

[100] Bae, C.; Hartwig, J. F.; Chung, H.; Harris, N. K.; Switek, K. A.; Hillmyer, M. A. *Angew. Chem.* **2005**, *117*, 6568-6571; *Angew. Chem. Int. Ed.* **2005**, *44*, 6410-6413.

[101] Kaminsky, W.; Lenk, S.; Scholz, V.; Roesky, H. W.; Herzog, A. *Macromolecules*, **1997**, *30*, 7647-7650.

[102] Kaminsky, W.; Arndt, M. *Metallocene-Based Polyolefins* Scheirs, J.; Kaminsky W. (Eds.), **2000**, Wiley, New York, 91-113.

[103] Niaounakis, M.; Kontou, E. *J. Poly. Sci. Polym. Phys.* **2005**, *43*, 1712-1727.

[104] James, D. E. *Encyclopedia of Polymer Science and Engineering*; Mark, H. F.; Bikales, N. M.; Overberger, C. G.; Menges, G. (Eds.) Wiley-Interscience, New York, **1985** Vol. 6, pp 429-454.

[105] Cran, M. J.; Bigger, S. W. *J. Plast. Film & Shtg.* **2006**, *22*, 121-132.

[106] Jin, H.-J.; Kim, S.; Yoon, J.-S. *J. Appl. Polym. Sci.* **2002**, *84*, 1566-1571.

[107] Starck, P.; Malmberg, A.; Löfgren, B. *J. Appl. Polym. Sci.* **2002**, *83*, 1140-1156.

[108] Quijada, R.; Narvaez, A.; Rojas, R.; Rabagliati, F. M.; Galland, G. B.; Mauler, R. S.; Benabente, R.; Perez, E.; Perena, J. M.; Bello, A. *Macromol. Chem. Phys.* **1999**, *200*, 1306-1310.

[109] Galland, G. B.; Seferin, M.; Mauler, R. S.; Santos J. H. Z. D. *Polym. Int.* **1999**, *48*, 660-664.

[110] Quijada, R.; Scipioni, R. B.; Mauler, R. S.; Galland, G. B.; Miranda, M. S. L. *Polym. Bull.* **1995**, *35*, 299-306.

[111] Quijada, R.; Dupont, J.; Miranda, M. S. L.; Scipioni, R. B.; Galland, G. B. *Macromol. Chem. Phys.* **1995**, *196*, 3991-4000.

[112] Fink, G.; Mülhaupt, R.; Brintzinger, H. H. *Ziegler Catalysts*; Eds. Springer-Verlag: Berlin, **1995**.

[113] Bottomley, F.; Sutin, L. *Adv. Organomet. Chem.* **1988**, *28,* 339-396.

[114] Gilje, J. W.; Roesky, H. W. *Chem. Rev.* **1994** *94*, 895-910.

[115] Hillhouse, G. L.; Bercaw, J. E. *J. Am. Chem. Soc.* **1984**, *106*, 5472-5478.

[116] Bortolin, R.; Patel, V.; Munday, I.; Taylor, N. J.; Carty, A. J. *J. Chem. Soc. Chem. Commun.* **1985**, 456-458.

[117] Párkányi, L.; Sharma, S.; Cervantes-Lee, F.; Pannell, K. H. *Z. Kristallogr.* **1993**, *208*, 335-337.

[118] Manriquez, J. M.; McAlister, D. R.; Rosenberg, E.; Shiller, A. M.; Williamson, K. L.; Chan, S. I.; Bercaw, J. E. *J. Am. Chem. Soc.* **1978**, *100*, 3078-3083.

[119] Hunter, W. E.; Hrncir, D. C.; Bynum, R. V.; Penttila, R. A.; Atwood, J. L. *Organometallics* **1983**, *2*, 750-755.

[120] Rausch, M. D.; Sikora, D. J.; Hrncir, D. C.; Hunter, W. E.; Atwood, J. L. *Inorg. Chem.* **1980**, *19*, 3817-3821.

[121] Moraru, B.; Kickelbick, G.; Schubert, U. *Eur. J. Inorg. Chem.* **2001**, 1295-1301.

[122] Jancik, V.; Pineda, L. W.; Pinkas, J.; Roesky, H. W.; Neculai, D.; Neculai, A. M.; Herbst-Irmer, R. *Angew. Chem.* **2004**, *116*, 2194-2197; *Angew. Chem. Int. Ed.* **2004**, *43*, 2142-2145.

[123] Alt, H. G.; Sanzo, F. P. D.; Rausch, M. D.; Uden, P. C. *J. Organomet. Chem.* **1976**, *107*, 257-263.

[124] Samuel, E.; Rausch, M. D. *J. Am. Chem. Soc.* **1973**, *95*, 6263-6267.

[125] Prust, J.; Most, K.; Müller, I.; Alexopoulos, E.; Stasch, A.; Usón, I.; Roesky, H. W. *Z. Anorg. Allg. Chem.* **2001**, *627*, 2032-2037.

[126] Uhl, W.; Koch, M.; Hiller, W.; Heckel, M. *Angew. Chem.* **1995**, *107*, 1122-1124; *Angew. Chem. Int. Ed. Engl.* **1995**, *34*, 989-990.

[127] Kuhn, N.; Fuchs, S.; Niquet, E.; Richter, M.; Steimann, M. *Z. Anorg. Allg. Chem.* **2002**, *628*, 717-718.

[128] Fronczek, F. R.; Baker, E. C.; Sharp, P. R.; Raymond, K. N.; Alt, H. G.; Rausch, M. D. *Inorg. Chem.* **1976**, *15*, 2284-2289.

[129] Thewalt, U.; Wöhrle, T. *J. Organomet. Chem.* **1994**, *464*, C17-C19.

[130] Erker, G.; Kehr, G.; Fröhlich.R. *Coord. Chem. Rev.* **2006**, *250*, 36-46.

[131] Erker, G.; Kehr, G.; Fröhlich. R. *J. Organomet. Chem.* **2004**, *689*, 1402-1412.

[132] Collins, S.; Ward, D. G. *J. Am. Chem. Soc.* **1992**, *114*, 5460-5462.

[133] Williams, V. C.; Dai, C.; Li, Z.; Collins, S.; Piers, W. E.; Clegg, W.; Elsegood , M. R. J.; Marder, T. B. *Angew. Chem.* **1999***, 111,* 3922-3926*. Angew. Chem. Int. Ed.* **1999**, *38*, 3695-3698.

[134] Stojcevic, G.; Kim, H.; Taylor, N. J.; Marder, T. B.; Collins, S. *Angew. Chem.* **2004**, *116*, 5639-5642; *Angew. Chem. Int. Ed.* **2004**, *43*, 5523-5526.

[135] Kotov, V.V.; Fröhlich. R.; Kehr, G.; Erker, G. *J. Organomet. Chem.* **2003**, *676*, 1-7.

[136] Miyazawa, A.; Kase, T.; Hashimoto, K.; Choi, J-c.; Sakakura, T.; Ji-zhu, J. *Macromolecules* **2004**, *37*, 8840-8845.

[137] Mahanthappa, M. K.; Cole, A. P.; Waymouth, R. M. *Organometallics* **2004**, *23*, 836-845.

[138] Nomura, K.; Fujii, K. *Macromolecules*, **2003**, *36*, 2633-2641.

[139] Nomura, K.; Okumura, H.; Komatsu, T.; Naga, N. *Macromolecules* **2002**, *35*, 5388-5395.

[140] Chirik, P. J.; Bercaw, J. E. *Organometallics* **2005**, *24*, 5407-5423.

[141] Joung, U. G.; Lee, B. Y. *Polyhedron*, **2005**, *24*, 1256-1261.

[142] Arndt, P.; Spannenberg, A.; Baumann, W; Becke, S.; Rosenthal, U. *Eur. J. Inorg. Chem.* **2001**, 2885-2890.

[143] Andrés, R.; Jesús, E. d.; Mata, F. J. d. l.; Flores, J. C.; Gómez R. *Eur. J. Inorg. Chem.* **2002**, 2281-2286.

[144] Coates, G. W. *Chem. Rev.* **2000**, *100*, 1223-1252.

[145] Bochmann, M. *J. Chem. Soc., Dalton, Trans.*, **1996**, 255-270.

[146] Alt, H. G.; Köppl A. *Chem. Rev.* **2000**, *100*, 1205-1221.

[147] Kaminsky, W. *J. Chem. Soc., Dalton Trans.*, **1998**, 1413-1418.

[148] Resconi, L.; Cavallo, L.; Fait, A.; Piemontesi, F. *Chem. Rev.* **2000**, *100*, 1253-1345.

[149] Erker, G. *Acc. Chem. Res.* **2001**, *34*, 309-317.

[150] Erker, G. *Acc. Chem. Res.* **1984**, *17*, 103-109.

[151] Rappé, A. K.; Skiff, W. M.; Casewit, C. J. *Chem Rev.* **2000**, *100*, 1435-1456.

[152] Boffa, L. S.; Novak, B. M. *Chem. Rev.* **2000**, *100*, 1479-1493.

[153] Giannini, U.; Cesca, S. *Tetrahedron Lett.* **1960**, *1*, 19-20.

[154] Mena, M.; Royo, P.; Serrano, R.; Pellinghelli, M. A.; Tiripicchio, A. *Organometallics* **1989**, *8*, 476-482.

[155] Wolczanski, P. T.; Bercaw, J. E. *Organometallics* **1982**, *1*, 793-799.

[156] Nomura, K.; Naga, N.; Miki, M.; Yanagi, K.; Imai, A. *Organometallics* **1998**, *17*, 2152-2154.

[157] Nomura, K.; Hatanaka, Y.; Okumura, H.; Fujiki, M.; Hasegawa, K. *Macromolecules* **2004**, *37*, 1693-1695.

[158] Wang, W.; Fujiki, M.; Nomura, K. *J. Am. Chem. Soc*. **2005**, *127*. 4582-4583.

[159] Nomura, K.; Takemoto, A.; Hatanaka, Y.; Okumura, H.; Fujiki, M.; Hasegawa, K. *Macromolecules* **2006**, *39*, 4009-4017.

[160] Kitiyanan, B.; Nomura, K. *Organometallics* **2007**, *26*, 3461-3465.

[161] Erben, M.; Merna, J.; Hermanová, S.; Cisařová, I.; Padělková, Z.; Dušek, M. *Organometallics* **2007**, *26*, 2735-2741.

[162] Zhang, H.; Nomura, K. *Macromolecules* **2006**, *39*, 5266-5274.

[163] Cheng, X.; Slebodnick, C.; Deck, P.A.; Billodeaux, D. R.; Fronczek, F. R. *Inorg. Chem*. **2000**, *39*, 4921-4926.

[164] Phomphrai, K.; Fenwick, A. E.; Sharma, S.; Fanwick, P. E.; Caruthers, J. M.; Delgass, W. N.; Abu-Omar, M. M.; Rothwell, I. P. *Organometallics* **2006**, *25*, 214-220.

[165] Ramos, C.; Royo, P.; Lanfranchi, M.; Pellinghelli, M. A.; Tiripicchio, A. *Organometallics* **2007**, *26*, 445-454.

[166] Noh, S. K.; Jung, W.; Oh, H.; Lee, Y. R.; Lyoo, W. S. *J. Organomet. Chem.* **2006**, *691*, 5000-5006.

[167] Baird, M. C. *Chem. Rev.* **2000**, *100*, 1471-1478.

[168] Poli, R. *Chem Rev.* **1991**, *91*, 509-551.

[169] Foster, J. P.; Weinhold, F. *J. Am. Chem. Soc.* **1980**, *102*, 7211-7218.

[170] Marks, T. J.; *Acc. Chem. Res.* **1992**, *25*, 57-65.

[171] Jezequel, M.; Dufaud, V.; Ruiz-Garcia, M. J.; Carrillo-Hermosilla, F. ; Neugebauer, U.; Niccolai, G. P.; Lefebvre, F.; Bayard, F.; Corker, J.; Fiddy, S.; Evans, J.; Broyer, J-P.; Malinge, J.; Basset, J-M. *J. Am. Chem. Soc.* **2001**, *123*, 3520-3540.

[172] Yasumoto, T.; Yamagata, T.; Mashima, K. *Organometallics* **2005**, *24*, 3375-3377.

[173] Buil, M. L.; Esteruelas, M. A.; López, A. M.; Mateo, A. C.; Oñate, E. *Organometallics* **2007**, *26*, 554-565.

[174] Wang, C.; Erker, G.; Kehr, G.; Wedeking, K.; Fröhlich, R. *Organometallics* **2005**, *24*, 4760-4773.

[175] Qian, Y.; Huang, J.; Bala, M. D.; Lian, B.; Zhang, H.; Zhang, H. *Chem. Rev.* **2003**, *103*, 2633-2690 .

[176] (a) Saunders, L; Spirer, L. *Polymer*, **1965**, *6*, 635-644: (b) Padmanabhan, S.; Katao, S.; Nomura, K. *Organometallics*, **2007**, *26*, 1616-1626.

[177] Jia, L.; Yang, X.; Stern, C. L.; Marks, T. J. *Organometallics* **1997**, *16*, 842-875.

[178] Nembenna, S.; Roesky, H. W.; Mandal, S. K.; Oswald, R. B.; Pal, A.; Herbst-Irmer, R.; Noltemeyer, M.; Schmidt, H.-G. *J. Am. Chem. Soc.* **2006**, *128*, 13056-13057.

[179] Köpf, H.; Schmidt, M. *Angew. Chem.* **1965,** *21***,** 965; *Angew. Chem. Int. Ed.* **1965**, *4*, 953.

[180] McCall, J. M.; Shaver, A. *J. Organomet. Chem.* **1980**, *193*, C37-C39.

[181] Shaver, A.; Marmolejo, G.; McCall, J. M. *Inorg. Synth.* **1990**, *27*, 65-68.

[182] Ruffing, C. J.; Rauchfuss, T. B. *Organometallics* **1985**, *4*, 524-528.

[183] Shaver, A.; McCall, J. M. *Organometallics* **1984**, *3*, 1823-1829.

[184] Bollinger, C. M.; Hoots, J. E.; Rauchfuss, T. B. *Organometallics* **1982**, *1*, 223-225.

[185] Bottomley, F.; Day, R. W. *Can. J. Chem.* **1992**, *70*, 1250-1259.

[186] Lundmark, P. J; Kubas, G. J.; Scott, B. L. *Organometallics* **1996**, *15*, 3631-3633.

[187] Kubas, G. J.; Wasserman, H. J.; Ryan, R. R. *Organometallics* **1985**, *4*, 2012-2021.

[188] Kubas, G. J.; Ryan, R. R. *Polyhedron* **1986**, *5*, 473-485.

[189] Kubas, G. J.; Ryan, R. R.; Kubat-Martin, K. A. *J. Am. Chem. Soc.* **1989**, *111*, 7823-7832.

[190] Toupadakis, A.; Kubas, G. J.; Burns, C. J. *Inorg. Chem.* **1992**, *31*, 3810-3817.

[191] Kim, C. G.; Coucouvanis, D. *Inorg. Chem.* **1993**, *32*, 1881-1882.

[192] Kubas, G. J.; Ryan, R. R. *J. Am. Chem. Soc.* **1985**, *107*, 6138-6140.

[193] Kubas, G. J. *Acc. Chem. Res.* **1994**, *27*, 183-190.

[194] Nadasdi, T. T.; Huang, Y.; Stephan, D. W. *Inorg. Chem.* **1993**, *32*, 347-356.

[195] Maué, G. P.; Fenske, D. *Z. Naturforsch., B: Chemical Sciences.* **1988**, *43B*, 1213-1218.

[196] Müller, U.; Krug, V. *Angew. Chem.* **1988**, *100,* 277; *Angew. Chem., Int. Ed. Engl.* **1988**, *27*, 293-294.

[197] Howard, W. A.; Parkin, G. *J. Am. Chem. Soc.* **1994**, *116*, 606-615.

[198] Howard, W. A.; Waters, M.; Parkin, G. *J. Am. Chem. Soc.* **1993**, *115*, 4917-4918.

[199] Polse, J. L.; Andersen, R. A.; Bergman, R. G. *J. Am. Chem. Soc.* **1995**, *117*, 5393-5394.

[200] Smith, M. R., III; Matsunaga, P. T.; Andersen, R. A. *J. Am. Chem. Soc.* **1993**, *115*, 7049-7050.

[201] Shriver, D. F.; Drezdon, M. A. *The manipulation of Air-Sensitive Compounds*, 2nd ed., McGraw-Hill, New York, USA, **1969**.

[202] Sheldrick, G. M. *Acta. Cryst.* **1990**, *A46*, 467-473.

[203] Sheldrick, G. M. SHELXS-97 and SHELXL-97. Program for Crystal Structure Refinement, Göttingen University, Göttingen, Germany, **1997**.

[204] Lee, C.; Yang, W.; Parr, R. G. *Phys. Rev. B* **1988**, *37*, 785-789.

[205] Miehlich, B.; Savin, A.; Stoll, H.; Preuss, H. *Chem. Phys. Lett.* **1989**, *157*, 200-206.

[206] Frisch, M. J.; Trucks, G. W.; Schlegel, H. B.; Scuseria, G. E.; Robb, M. A.; Cheeseman, J. R.; Montgomery, J. A.; Vreven, T., Jr.; Kudin, K. N.; Burant, J. C.;

Millam, J. M.; Iyengar, S. S.; Tomasi, J.; Barone, V.; Mennucci, B.; Cossi, M.; Scalmani, G.; Rega, N.; Petersson, G. A.; Nakatsuji, H.; Hada, M.; Ehara, M.; Toyota, K.; Fukuda, R.; Hasegawa, J.; Ishida, M.; Nakajima, T.; Honda, Y.; Kitao, O.; Nakai, H.; Klene, M.; Li, X.; Knox, J. E.; Hratchian, H. P.; Cross, J. B.; Bakken, V.; Adamo, C.; Jaramillo, J.; Gomperts, R.; Stratmann, R. E.Yazyev, O.; Austin, A. J.; Cammi, R.; Pomelli, C.; Ochterski, J. W.; Ayala, P. Y.; Morokuma, K.; Voth, G. A.; Salvador, P.; Dannenberg, J. J.; Zakrzewski, V. G.; Dapprich, S.; Daniels, A. D.; Strain, M. C.; Farkas, O.; Malick, D. K.; Rabuck, A. D.; Raghavachari, K.; Foresman, J. B.; Ortiz, J. V.; Cui, Q.; Baboul, A. G.; Clifford, S.; Cioslowski, J.; Stefanov, B. B.; Liu, G.; Liashenko, A.; Piskorz, P.; Komaromi, I.; Martin, R. L.; Fox, D. J.; Keith, T.; Al-Laham, M. A.; Peng, C. Y.; Nanayakkara, A.; Challacombe, M.; Gill, P. M. W.; Johnson, B.; Chen, W.; Wong, M. W.; Gonzalez, C.; Pople, J. A. *Gaussian 03*, revision C.02; Gaussian, Inc., Wallingford CT, 2004.

[207] Hay, P. J.; Wadt, W. R. *J. Chem. Phys.* **1985**, *82*, 270-283.

[208] Petersson, G. A.; Al-Laham, M. A. *J. Chem. Phys.* **1991**, *94*, 6081-6090.

[209] Petersson, G. A.; Bennett, A.; Tensfeldt, T. G.; Al-Laham, M. A.; Shirley, W. A.; Mantzaris, J. *J. Chem. Phys.* **1988**, *89*, 2193-2218.

[210] Reed, A. E.; Weinhold, F. *J. Chem. Phys.* **1985**, *83*, 1736-1740.

[211] Reed, A. E.; Curtiss, L. A.; Weinhold, F. *Chem. Rev.* **1988**, *88*, 899-926.

[212] Hübler-Blank, B.; Witt, M.; Roesky, H. W. *J. Chem. Edu.* **1993**, *70*, 408-409.

Lebenslauf

Name		Prabhuodeyara M. Gurubasavaraj
Geboren		18th April 1977 in Kottur, India
Eltern		Prabhuodeyara M. Mahabaleshwaraiah (Vater)
		Prabhuodeyara M. Annapurnamma (Mutter)
Staatsangehörigkeit		Indisch

Schulbesuch	1984 − 1991	Primary School (I-IX)
	1991 – 1992	Secondary School Examinations (Class X)
	1992 – 1994	Pre-University Course (class XII)
Studium	1994 – 1997	B.Sc. Gulbarga University, Indien
	1997 – 2000	M.Sc. in Chemie, Gulbarga University, Indien
	2000-2001	M.Phil. in Coordination Chemie, Gulbarga University, Gulbarga, Indien
	2001-2003	Project Asistant, Gulbarga University, Gulbarga, Indien
	2003-2004 Mar	Research Asistant, Indian Institute of Science, Bangalore, Indien
Promotion	2004 Mar − 2007 Oct	Experimentelle Promotionsarbeit im Institut für Anorganische Chemie Göttingen unter der Leitung von Prof. Dr. Dr. h.c. mult. H. W. Roesky

List of Publications:

1**. Organometallics (Article), 2007**, *26*, 3346. **"***Oxygen Effect in Heterobimetallic Catalysis-Zr-O-Ti System as an Excellent Example for Olefin Polymerization.***" P. M. Gurubasavaraj,** H W. Roesky, P. M. V. Sharma, R B. Oswald, V. Dolle, R. Herbst-Irmer, A. Pal

2. **Inorganic Chemistry** (**Article**), **2007**, *46*, 1056. *"Synthesis, Structural Characterization, Catalytic Properties, and Theoretical Study of Compounds Containing an Al-O-M (M = Ti, Hf) Core."* **P. M. Gurubasavaraj**, S. K. Mandal, H. W. Roesky, R. B. Oswald, A. Pal and M. Noltemeyer.

3. **Inorganic Chemistry (Article), 2007,** *46,* 7594. *"Synthesis, Structural Characterization, and Theoretical Investigation of Compounds Containing Al-O-M-O-Al (M = Ti, Zr) Core"*. S. K. Mandal, **P. M. Gurubasavaraj,** H. W. Roesky, G. Schwab, D. Stalke, R. B. Oswald, V. Dolle

4. **Journal of the American Chemical Society 2007,** *129,* 12049. *"Synthesis and Structures of Heteroleptic Sylilenes"* C.-W. So, H. W. Roesky, **P. M. Gurubasavaraj,** R. B. Oswald, M.G. Gamer, P. G. Jones.

5. **Inorganic Chemistry (Article) 2007**, *ASAP. "Oxygen Bridged Hybrid Metallocene-Nonmetallocene Polymetallic Catalysts of Group 4 Metals for Bimodal Activity in Olefin Polymerization: Synthesis, Characterization, and Theoretical Investigation"*.

S. K. Mandal, **P. M. Gurubasavaraj,** H. W. Roesky, G. Schwab, D. Stalke. R. B. Oswald, V. Dolle

6*.* **Journal of Organometallic Chemistry** (**Cotton memorial special issue**) *in Press. "Synthesis, Structural Characterization, Reactivity, of Ethyl Substituted Aluminum Hydroxide and Catalytic Properties of its Derivatives"*. Y. Ying, **P. M. Gurubasavaraj,** H.Ye, Z. Zhang, H. W. Roesky, P. G. Jones

7. **Inorganic Chemistry** (**Article**), **2007,** *(manusctript under preparation), "From Unstable to Stable and Highly Active–Heterobimetallic Half-Metallocene Catalysts for Olefin Polymerization and Co-polymerization: Discussion on Structure/Reactivity Relationship"* **P. M. Gurubasavaraj**, H. W. Roesky, A. Pal and R. Herbst-Irmer